BNL-43186
Informal Report

POLYELECTROLYTE-DIFFUSED ZINC PHOSPHATE CONVERSION COATINGS AND POLYACID COUPLING PRIMERS FOR CORROSION PROTECTION OF STEEL AND ALUMINUM, AND ALKALI-CATALYZED HYDROLYSIS OF POLYIMIDE-BASED MATERIALS

FINAL REPORT

T. Sugama, L. E. Kukacka, N. R. Carciello, J. B. Warren and C. R. Clayton

August 1989

Prepared for the
U.S. Army Research Office
P.O. Box 12211
Research Triangle Park, NC 27709

PROCESS SCIENCES DIVISION
DEPARTMENT OF APPLIED SCIENCE

BROOKHAVEN NATIONAL LABORATORY
UPTON, LONG ISLAND NEW YORK 11973

BNL-43186
Informal Report

POLYELECTROLYTE-DIFFUSED ZINC PHOSPHATE CONVERSION COATINGS AND POLYACID COUPLING PRIMERS FOR CORROSION PROTECTION OF STEEL AND ALUMINUM, AND ALKALI-CATALYZED HYDROLYSIS OF POLYIMIDE-BASED MATERIALS

FINAL REPORT

T. Sugama, L. E. Kukacka, N. R. Carciello, J. B. Warren and
C. R. Clayton*

August 1989

Prepared for the
U.S. Army Research Office
P.O. Box 12211
Research Triangle Park, NC 27709

PROCESS SCIENCES DIVISION
DEPARTMENT OF APPLIED SCIENCE
BROOKHAVEN NATIONAL LABORATORY
ASSOCIATED UNIVERSITIES, INC.

*Department of Materials Science and Engineering
State University of New York, Stony Brook

This work was performed under the auspices of the
U.S. Department of Energy, under contract No. DE-AC02-76CH00016
and supported by the U.S. Army Research Office Program MIPR-ARO-102-89

UNCLASSIFIED

SECURITY CLASSIFICATION OF THIS PAGE (When Data Entered)

REPORT DOCUMENTATION PAGE		READ INSTRUCTIONS BEFORE COMPLETING FORM
1. REPORT NUMBER BNL-43186	2. GOVT ACCESSION NO. N/A	3. RECIPIENT'S CATALOG NUMBER N/A
4. TITLE (and Subtitle) Polyelectrolyte-Diffused Zinc Phosphate Conversion Coatings and Polyacid Coupling Primers For Corrosion Protection of Steel and Aluminum, and Alkali-Catalyzed Hydrolysis of Polyimide-Based Materials		5. TYPE OF REPORT & PERIOD COVERED Final August '85 - ~~July~~ August '89 6. PERFORMING ORG. REPORT NUMBER BNL-
7. AUTHOR(s) T. Sugama, L. E. Kukacka, N. R. Carciello, J. B. Warren and C. R. Clayton		8. CONTRACT OR GRANT NUMBER(s) MIPR-ARO-112-86, ARO-112-87 ARO-103-88 and ARO-102-89
9. PERFORMING ORGANIZATION NAME AND ADDRESS Associated Universities, Inc. Brookhaven National Laboratory Upton, NY 11973		10. PROGRAM ELEMENT, PROJECT, TASK AREA & WORK UNIT NUMBERS N/A
11. CONTROLLING OFFICE NAME AND ADDRESS U. S. Army Research Office Post Office Box 12211 Research Triangle Park, NC 27709		12. REPORT DATE 13. NUMBER OF PAGES
14. MONITORING AGENCY NAME & ADDRESS(if different from Controlling Office)		15. SECURITY CLASS. (of this report) Unclassified 15a. DECLASSIFICATION/DOWNGRADING SCHEDULE

16. DISTRIBUTION STATEMENT (of this Report)

Approved for public release; distribution unlimited.

17. DISTRIBUTION STATEMENT (of the abstract entered in Block 20, if different from Report)

NA

18. SUPPLEMENTARY NOTES

The view, opinions, and/or findings contained in this report are those of the author(s) and should not be construed as an official Department of the Army position, policy, or decision, unless so designated by other documentation.

19. KEY WORDS (Continue on reverse side if necessary and identify by block number)

Zinc phosphate conversion coating
Polyelectrolyte macromolecule
Cold-rolled steel
Corrosion protection
Polyurethane topcoat
Polyacid coupling primer
Adhesion durability
Polyimide
Akali-catalyzed hydrolysis

20. ABSTRACT (Continue on reverse side if necessary and identify by block number)

The segmental adsorption of polyelectrolyte macromolecules either on newly precipitated crystal nuclei or on crystal growth sites during the primary zinc phosphate (Zn·Ph) conversion process on cold-rolled steel surfaces, acts to array a uniformly packed fine crystal topography brought about by the suppression and delay of the crystal growth. This adsorption is due to charge transfer from the Zn atoms in the crystalline conversion coatings to the electron accepting →

DD FORM 1 JAN 73 1473 EDITION OF 1 NOV 65 IS OBSOLETE

UNCLASSIFIED

SECURITY CLASSIFICATION OF THIS PAGE (When Data Entered)

20. ABSTRACT CONTINUED

oxygen portion of functional pendent groups such as carboxylic acid, -COOH, and sulfonic acid, $-SO_3H$, in the polyelectrolytes. The formation of Zn-OOC or $-OSO_2$ complexes yielded by charge transfer reactions at the polyelectrolyte-Zn·Ph crystal interfaces, not only provides better corrosion protection and low hydrogen evolution, but also improves the stiffness and ductility of the normally brittle Zn·Ph layers. For the corrosion resistance of polyelectrolytes diffused electrostatically in the crystal layers, one of specific assignments was that, when the NaOH-dissolution of Zn·Ph is considered, the Zn-O electrostatic bonds at polyelectrolyte-Zn·Ph interfaces are transformed into $Na^{+-}O$ ionic bonds which associate with the salt complexed macromolecules. Another is the intermolecular chemical reactions between the polyelectrolyte polymers existing at the outermost surface sites of the conversion coatings and the organic polymer topcoats. These contributions result in a low cathodic delamination rate for topcoat films from the Zn·Ph surfaces.

When polyitaconic acid [p(IA)] macromolecules are applied as water-soluble primers in polyurethane (PU) adhesive/aluminum adherend joint systems, they interact preferentially with the oxide aluminum to form Al-OOC electrostatic bonds, and with the isocyanate groups in the adhesive to yield polymer-to-polymer chemical bonding. This chemical coupling between the adhesive and adherend acts significantly to promote interfacial adhesive bonds. The arrangement of a near monolayer of p(IA) intermediate film plays a key role in governing the adhesion durability of the joint system and the corrosion resistance of the aluminum upon exposure to corrosive fluids. The bond stability and the corrosion resistance are due primarily to the formation of interfacial reaction products which are less susceptible to hydrolysis.

Polyimide (PI) resins which are produced by an in-situ imidization condensation reaction of polyamic acid (PAA) precursors were evaluated for use as binders in high-temperature performance lightweight material systems. Unfortunately, the presence of alkaline fillers in the system led to strength retrogression at room temperature. Significant mechanical failure was observed upon exposure of the specimens to steam at >150°C. This was found to be due mainly to alkali catalyzed hydrolysis of the functionaries of unreacted PAA adjacent to the filler surfaces and the imide rings of PI matrices. The formation of alkali metal complexed carboxylate salts derived from the hydrolysis resulted in chain session of the polymer, thereby decreasing the mechanical ngth, and making the composites unsuitable for use in aqueous environments.

TABLE OF CONTENTS

TABLE OF CONTENTS cont.

LIST OF TABLES

LIST OF FIGURES

LIST OF FIGURES

LIST OF FIGURES

LIST OF FIGURES

LIST OF FIGURES

SUMMARY

Under U.S. Army Research Office (ARO) sponsorship, Brookhaven National Laboratory (BNL) performed research on three topics:

1) Polyelectrolyte-modified zinc phosphate (Zn·Ph) conversion coatings for the corrosion protection of steel,

2) Water-soluble polyacid coupling primers for improving the corrosion resistance and adherence of polymeric paints, and

3) High-temperature lightweight polyimide material systems.

In the first topic, it was found that insoluble crystalline zinc phosphate (Zn·Ph) conversion coatings can be produced on steel surfaces by immersing a surface-cleaned cold-rolled steel substrate into a BNL-developed phosphating solution containing three components, zinc orthophosphate dihydrate [$Zn_3(PO_4)_2 \cdot 2H_2O$], H_3PO_4, and water. The major phase in the conversion coating derived from this simple phosphating solution is the same zinc phosphate dihydrate as that used in the converting solution. This suggests that the conversion to the Zn·Ph occurs through a dissolution-recrystallization process of the original $Zn_3(PO_4)_2 \cdot 2H_2O$ powders.

The Zn·Ph coatings formed by this process significantly reduce the corrosion rate of steel. When the steel surfaces were treated with zinc phosphating solutions containing polyelectrolyte macromolecules having proton-donating type pendant groups such as carboxylic acid, -COOH, or sulfonic acid, $-SO_3H$, several additional corrosion-protective benefits were accrued. It was determined that the positive surface sites of phosphate crystal embryos at the beginning of the precipitation of Zn·Ph conversion coatings on the steel surface were strongly chemisorbed by the anionically charged segments of the polyelectrolytes. This segmental chemisorption of polyanions either on newly precipitated nuclei or on growth sites during the primary crystallization processes, not only acts to array a uniformly packed fine crystal morphology brought about by the suppression and delay of the crystal growth, but also significantly improves the stiffness and ductility characteristics of the normally brittle Zn·Ph layer. The interfacial reaction products at the

p(AA)-Zn•Ph crystal interfaces were identified to be Zn -OOC complexes formed by a charge transfer reaction between the Zn atoms in the crystalline conversion coatings and the electron-accepting oxygen portions in the p(AA). The resultant Zn-O electrostatic interfacial bond does not seem to greatly affect the rate of alkaline dissolution of the conversion coating layers when they are subjected to NaOH. Normally, breakage of the Zn-O bond results from attack by the reactive Na^+. However, the formation of $-COO^-$ Na^+ salt complexed macromolecules precipitated by transformation of the Zn-O electrostatic bonds into Na-O ionic bonds acts to enhance the corrosion resistance of steel.

The addition of excessive amounts of p(AA) led to a reduction in the protective ability. This is due to the precipitation of a large amount of strengite, $FePO_4 \cdot 2H_2O$, rather than $Zn_3(PO_4)_2 \cdot 2H_2O$.

Enhancement of adhesion with subsequent polymeric finishers was also obtained. This relates directly with the chemical bonds formed at the interface between the functional organic species such as ionic carboxylate and carboxylic acid groups existing at the outermost surface sites of the conversion coating and the polymeric topcoats. For example, the intermolecular chemical reaction between the carboxylic groups of the p(AA) existing at the outermost surface sites of the conversion coating and the isocyanate groups in polyurethane topcoats led to a lower rate of cathodic delamination of the polyurethane film from the substrate. Thus, the beginning of the delamination failure occurs through the conversion coating/steel interface, as compared to that at the polyurethane/conversion coating interface in the polyurethane unmodified coating joint system.

As a result of these findings, BNL developed Zn•Ph technology was selected by Industrial Research Magazine as one of the 100 most significant new technical products of 1987.

Referring to the second topic, it was found that the poly(itaconic acid), p(IA), which contains two functional COOH groups located on the same backbone carbon, has potential for use as a water-soluble intermediate coupling primer for polymer adhesive/Al_2O_3 adherend joint systems. When a p(IA) aqueous solution was contacted with Al_2O_3 surfaces, it was observed that the macromolecules having regularly oriented functional COOH pendent groups were mobile enough

to wet continuously the Al_2O_3 surface sites at which the conditions for interfacial Lewis acid-base reactions are favorable. The interfacial reaction products formed by these acid-base (proton donor-acceptor) reactions were predicted to be acid salts of trivalent Al metals, $R-\overset{O}{\overset{\|}{C}}-O^{-}---^{+}H_2O-Al-$ (on surface). When this Al acid salt was heated to temperatures $\geq$150°C, the Al salt formation was transformed into a Al-OOC bond formation containing electrostatic bonds formed by charge transfer from the Al in Al_2O_3 to the electron-accepting carboxylate oxygen portion, $^{-}$ OOC-, in p(IA). Water was eliminated.

Good bond performance and improved durability in alkaline environments brought about by the use of p(IA) were associated not only with the chemical crosslinking functional groups coupling the hydrated oxide aluminum with the polymer adhesive, but also with the optimum thickness of the intermediate primer layers. The latter means that the p(IA) film should have only enough functional groups to occupy all available -OH and functional groups at the adherend and adhesive interface sites. In fact, the presence of a near monolayer of p(IA) film, produced using a 0.05% concentration in an aqueous medium, played a key role in achieving excellent bond durability in hot alkaline solutions. In other words, the coupling structure of p(IA) in the interfacial regions contributes significantly to the formation of a stable interfacial bond which is resistant to moisture because of transformation of hydrophilic COOH to less hydrolytic reaction products at the interfaces. This directly reduces the corrosion rate of the Al substrate. The presence of additional COOH groups associated with thicker p(IA) layers, contributes to gel-induced primer failures beneath the polymer topcoat.

Although microsphere-filled polyimide (PI) lightweight materials which were characterized by their excellent mechanical properties, low bulk density (<0.35 g/cc), and thermal stability in air at 300°C, appear very attractive for use as high-temperature performance composites, the susceptibility of the imide rings in the PI to hydrothermal reactions led to the degradation of the PI matrix in the systems. Therefore, emphasis in the third topic was placed on understanding the reaction processes and degradation mechanisms of PI polymers which occur at the interfaces between the PI and inorganic pigments in hydrothermal environments at $\geq$150°C. The findings were elucidated as follows:

The extent of the hydrolysis was found to increase as cation releasable fillers were incorporated in the polyamic acid (PAA) precursor of PI. This can be explained by base-catalyzed hydrolysis mechanisms involving the functional groups on the unreacted PAA and the imide groups in the PI. Hydrolysis of the former occurs principally in the interfacial regions between the PAA and the hydrated alkali filler at room temperature, and the latter is initiated by the attack of hydroxide anions on the imide carbon in steam at $\geq$150°C. In these mechanisms, the bond breakage and cleavage of the amide linkages in PAA and the imide rings in PI, brought about by the nucleophilic attack of OH^-, lead to the formation of transitory intermediate compounds containing carboxylate anions and amine compounds. Therefore, such degradation processes not only result in scission of polymer chains, but also lead to the considerable strength retrogression of the PI materials. It is concluded that PI lightweight materials not containing any alkaline fillers may be suitable for use in hot air environments at temperatures up to 300°C, but are questionable for use in high pH hydrothermal environments.

I. INTRODUCTION

In 1985, Brookhaven National Laboratory (BNL), under U.S. Army Research Office (ARO)-sponsorship, initiated basic studies which contribute to three research areas: 1) the chemical modification and process technology of insoluble crystalline zinc phosphate (Zn•Ph) conversion coatings which can be used for the corrosion protection of steel, 2) water-soluble polyacid coupling primers for use in aluminum/polymer joint systems, and 3) high-temperature lightweight polymer systems. Major concepts in each of these areas are described below.

1. Crystalline Zinc Phosphate Conversion Coatings

Large quantities of organic-coated high strength cold-rolled steel plates are presently used by major consuming industries such as automotive and appliance manufacturers. Suppliers and users are becoming more aware that the modification and treatment of steel surfaces prior to application of the organic coatings are most important factors in improving the adhesion and corrosion

resistance of the substrate surfaces. At present, the zinc phosphate (Zn·Ph) pretreatment conversion coatings are typically employed in automotive paint systems.

It has been reported[1] that when the cold-rolled steels are immersed in zinc orthophosphate dihydrate-based phosphating solutions, the resultant crystalline Zn·Ph conversion layer deposited on the steel substrate surface consists of a highly dense configuration of large rectangular-like crystals. The surface topographical features of the Zn·Ph conversion precoat are characterized by a dendritic microstructure array comprised of interlocking rectangular crystals of insoluble zinc phosphate hydrate. The open surface structure of the interlocked crystal layers contributes significantly to the formation of a strong mechanical interlocking reaction with the polymeric topcoat systems, thereby enhancing the magnitude of the adhesive force at the precoat/topcoat interfaces. Although thick Zn·Ph precoats appear to be suitable as a corrosion barrier for the substrate, the fragile characteristics of this bulky crystal structure lead to failure during flexure or other deformation of the substrate. Deformation failures of layers having low stiffness characteristics appear to be directly related to the development of micropores and fissures which reduce the effectiveness of the corrosion-resistant coatings. These characteristics lead to a high oxygen and moisture availability at the substrate surface and progressively promote a cathodic delamination reaction.

Cathodic delamination of polymeric coatings from zinc phosphated steel surfaces is due mainly to alkaline dissolution of the phosphate coating. This is caused by the hydroxyl ions generated by oxygen reduction reactions, $H_2O + 1/2\ O_2 + 2\ e^- = 2\ OH^-$, and the migration of alkali metal cations through the topcoat to the reaction zone for charge balance.[2] Thus, it has been demonstrated that the sodium hydroxide solution dissociates a larger amount of zinc and phosphate ions from the Zn·Ph coating surfaces. Since the OH^- ions which cause delamination at paint/Zn·Ph interfaces form at pores and defects in the Zn·Ph layers, the formation of highly dense, thick, and low porosity conversion coatings should yield inherently slow oxygen reduction kinetics. Thus, an increase in the flexural modulus of the crystalline conversion layer itself is of considerable importance when the physical deformation characteristics of the metal substrate are considered.

The brittle characteristics of the Zn•Ph can be modified by the introduction of polyacrylic acid p(AA) macromolecules into the phosphating solutions.[3]

The incorporation of p(AA), which is generally expressed as a polyelectrolyte macromolecule, was shown to form a highly dense fine crystal topography, suggesting that the crystal formation results in an improvement in the stiffness and ductility characteristics of the normally brittle Zn•Ph layers. The stiff p(AA)-Zn•Ph complex crystal layer and surface not only provide a corrosion barrier on the substrates, but they also possess the ability to promote adhesive bonds at polymeric topcoat-to-complex Zn•Ph adherend joints. The latter is due to the presence of organic functional species at the outermost surface sites of the Zn•Ph films.

As a result, an investigation was conducted to determine how the molecular structures and functional species of polyelectrolytes act to suppress crystal growth of Zn•Ph and improve interfacial bond durability of Zn•Ph-to-polymeric adhesive joints. Moreover, studies were conducted to explore the effects of p(AA) polyelectrolyte macromolecules when they are internally diffused throughout the crystalline Zn•Ph, and on the degree of the alkaline dissolution of coatings. Cathodic delamination studies for polyester-modified polyurethane (PU)-coated Zn•Ph specimens were also performed to determine the role of the intermolecular chemical reaction at PU modified Zn•Ph interfaces in reducing the delamination rates of the PU topcoat from the Zn•Ph.

2. Water Soluble Polyacid Coupling Primers

Oxide treatments for commercially important metals and alloys such as iron[4], aluminum[5,6], and magnesium[7,8], are designed to form fresh metal oxide layers and to eliminate naturally deposited alkaline hydroxide-carbonate contaminant films. One of the most significant features of newly formed metal oxide surfaces is the extremely high susceptibility to hydration. The resultant hydroxyl-rich hydrated oxide surfaces adsorb and strongly retain several molecular layers of bound water.[9-11] When the pitting corrosion of aluminum (Al) and Al alloys is considered, the corrosion occurs in accordance with the following steps:[12]

Step 1 - adsorption of halide on the hydroxylated Al surface;

Step 2 - complexing of Al cation in oxide lattice with halide to form a soluble AlX^{-}_{4}(X : Cl, Br, F as halide) type species;

Step 3 - soluble species diffuse away from the surface, resulting in a thinning of the protective oxide film; and

Step 4 - at sufficiently thinned sites, Al reacts directly with the electrolyte to produce pitting corrosion.

However, the fact that Al oxide surfaces contain these hydrated polar surface groups is fortunate from the standpoint of wetting with polar organic and inorganic liquids.(13)

At present, the pre-treatment of hydroxylated Al surfaces using functional organic and inorganic primer systems prior to the application of polymeric topcoats, is indispensable in providing corrosion protection to Al and Al alloys. It is believed that these protective factors are directly related to the reaction products at the interface between the hydroxyl groups on the surface of the substrate and the functional groups in the primers.

Several investigations have explored the nature of the key interfacial interactions which promote adhesive bonding and improve durability at interfacial contact zones in adherent joint systems in polyurethane (PU) adhesive/p(AA) primer/FPL-etched Al.(14) It was concluded that a near-monolayer thickness of an intermediate p(AA) primer film should be applied to occupy all of the available functional groups at the PU adhesive and Al_2O_3 adherend sites. The primer preferentially interacts with the hydrated Al_2O_3 covering the Al subsurface to form hydrogen bonds, and with the isocyanate groups in the PU to yield polymer-to-polymer chemical bonding. The chemical coupling resulting from the thin p(AA) film significantly promotes interfacial adhesive bonds and improves adhesion durability at the joints.

When the coupling characteristics and interplay of polycarboxylic acids were considered theoretically, it was presumed that poly(itaconic acid) [p(IA)] macromolecules, which have two functional carboxylic acid pendant groups

attached to the same backbone carbon atom, would be a more effective crosslinking material than p(AA) which contains a single functional group. An ideal coupling mechanism for p(IA) primer to connect a hydrated Al_2O_3 adherend and a PU adhesive would be as follows:

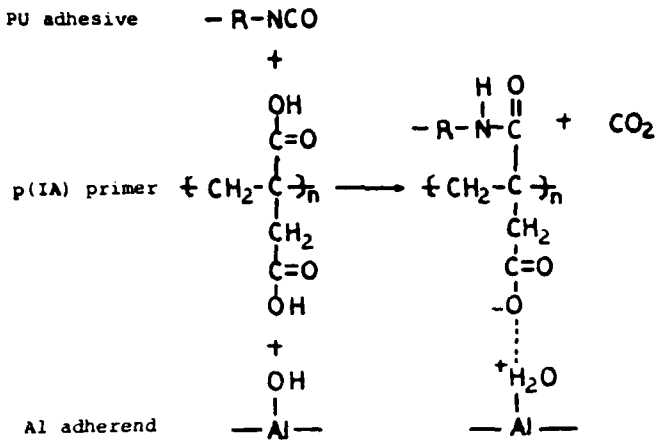

The presence of a p(IA) intermediate monolayer will also improve the adhesion bond and its durability at PU/p(IA)/Al interfacial joints. Therefore, the present study was to investigate the coupling nature and the role of the p(IA) intermediate layer in PU-to-Al joint systems. Emphasis was placed on the interface between the carboxylic acid groups of p(IA) and the PU adhesive or Al adherend. In addition, the nature of the interface produced by intermolecular reactions was studied to determine its role in the corrosion resistance of Al upon exposure to corrosive fluids.

3. High Temperature Lightweight Polyimide Systems

Since polyimide (PI) polymers have high temperature stability, high radiation and chemical resistance, and good mechanical and dielectric properties[15], they are the subject of ever increasing interest for use in microelectronic[16,17] and aerospace applications.[18] Based upon this information, work was performed at BNL to evaluate the potential for the use of PI polymers as a thermally stable matrix in lightweight composite material systems.

The PIs are generally formed by a typical two-stage synthesis[19,20] as shown in Eqs. (1) and (2) below. In this synthesis, solution condensation reactions between carboxylic dianhydride compounds such as benzophenonete-

tracarboxylic dianhydride, benzenetetracarboxylic dianhydride or 3,3',4,4'-benzophenonetetracarboxylic dianhydride, and aromatic diamines such as 1,4-phenylenediamine, 1,3-phenylenediamine or 4,4"-diaminodiphenyl ether et al, are initiated at ambient temperature in organic solvents such as N-methylpyrollidone, bis (2-methyoxyethyl) ether or dimethyl acetamide. These yield a soluble polyamic acid p(AA) precursor [see Eq. (1)]. The PI polymer is then formed through <u>in-situ</u> imidization condensation reactions by means of thermal or chemical dehydration of the PAA polymer [see Eq. (2)].

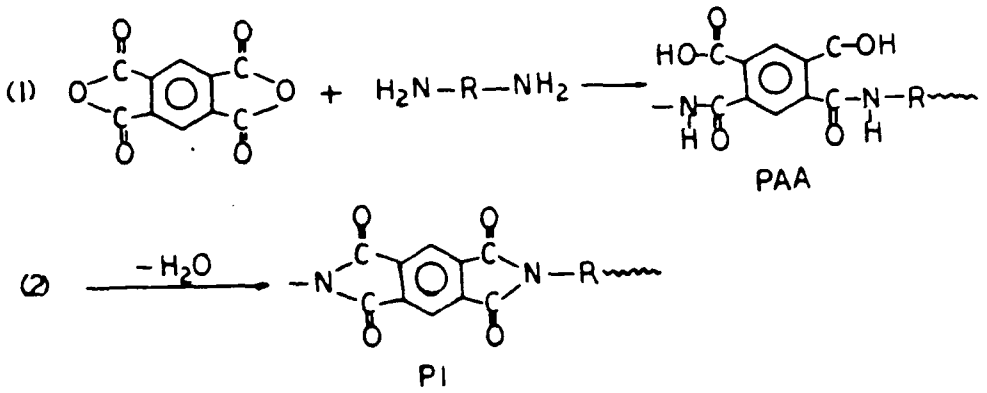

When considering this unique curing process for the formation of PI-filler systems, it was realized that the reactions would have to take place in a slurry consisting of the solvent-based PAA precursor and the lightweight fillers. It was, therefore, predictable that, when moisture was incorporated into the composite slurry, the carboxylic acid, COOH, groups within the PAA might be converted into cation-accepting carboxylate anions, COO^-, prior to transforming the COOH into the imide ring structure of PI. These functional COO^- groups will preferentially react with counterion species such as Na, Ca, Mg, Cu et al.[14].

Hydrated portland cement is a Ca counterion-releasable material. Therefore, it was decided to investigate the effects of the addition of hydrated cement particles to the PAA composite slurries on the interactions at interfaces between the cement hydrate and PAA. The strength developed by the material system as a function of temperature was also determined. Accordingly, our approach to evaluating the applicability of PI polymer-based lightweight materials for use in hydrothermal environments was focused on the following

three subjects: 1) the rate of the in-situ imidization reaction of PAA when the system constituents are in slurry form under hydrothermal environments, 2) hydrothermal stability and degradation of the cured PI systems, and 3) influence of hydrated cement on the mechanical properties of the systems.

In an attempt to accomplish the three objectives described above, fundamental studies commenced in August 1985 and were completed at the end of July 1989. The work emphasized the fundamental understanding of the effects of polyelectrolyte-modified Zn•Ph on the adhesion and corrosion protection of steel; the roles of interfacial intermolecular reactions in adhesion durability and corrosion protection of aluminum using polyacid macromolecules, and the principal factors governing interfacial bond failures between PI and reactive fillers used in lightweight material systems.

II. CHARACTERISTICS OF POLYELECTROLYTE-DIFFUSED ZINC PHOSPHATE CONVERSION COATINGS ON STEEL

In this task, work was conducted on the following three subjects: 1) determinations of how the molecular structure and functional species of polyelectrolytes act to suppress cyrstal growth of Zn•Ph and improve the interfacial bond durability of Zn•Ph to polymeric adhesive joints, 2) the effects of polyelectrolytes on the degree of alkaline dissolution of Zn•Ph coatings, and 3) the role of the intermolecular chemical reactions at polymeric topcoat-modified Zn•Ph interfaces in reducing the cathodic delamination of topcoats from substrates.

A. Materials

The metal substrate used was a high strength cold-rolled sheet steel supplied by the Bethlehem Steel Corporation. The steel contained 0.06 wt% C, 0.6 wt% Mn, 0.6 wt% Si, and 0.07 wt% P. The formulation for the zinc phosphating liquid used in this study consisted of 0.9 to 2.6 wt% zinc orthophosphate dihydrate, 1.8 to 5.1 wt% H_3PO_4, and 97.3 to 92.3 wt% water. These formulations were modified by incorporating a water-soluble polymer at concentrations ranging from 0 to 5.0% by weight of the total solution.

Four polyelectrolytes obtained from Scientific Polymer Products, Inc. were used; polyacrylic acid [p(AA); $\{CH_2\text{-}CH(COOH)\}_n$], polyitaconic acid [p(IA); $\{CH_2C[(COOH)]CH_2OCOH\}_n$], polystyrenesulfonic acid [p(SSA);

$\dagger CH_2\text{-}CH(C_6H_4SO_3H)\dagger_n$], and poly-2-acrylamid-2-methylpropane sulfonic acid [p(AMSA); $\dagger CH_2C[CONH_2C(CH_3)_2CH_2SO_3H]\dagger_n$]. For the purpose of comparison with the polyacid macromolecules, two water-soluble amide type polymers were employed, polyacrylamide [p(AM); $\dagger CH_2\text{-}CH(CONH_2)\dagger_n$] and polyvinylpyrolidone [p(VP); $\dagger CH_2\text{-}CH(C_3H_6CON)\dagger_n$]. These were also obtained from Scientific Polymer Products, Inc. All of these macromolecules had an average molecular weight in the range of 40,000 to 120,000, and they were dissolved in water to prepare a 25% polymer solution.

An array of the macromolecule-Zn·Ph composite conversion layers having crystal dimensions in the order of microns on the substrate surface was prepared in the following way: The metal substrate first was rinsed with an organic solvent to remove any surface contamination with mill oil. A typical auger spectrum for a solvent-cleaned steel surface is shown in Figure 1. The consequent quantitative data indicated that the predominant element at the outermost surface sites of the steel was carbon. Several investigators have reported that the presence of surface carbon impedes the formation of high-quality Zn·Ph coatings.[21-23] Low zinc and phosphorous levels in Zn·Ph deposited on high carbon areas lead to a porous structure and poor bonding to the steel. These characteristics result in a higher availability of oxygen and moisture at the interface between the Zn·Ph and steel, and promote a cathodic delamination reaction. Based upon these features, the quality of the steel surface used in our work upon which the Zn·Ph was deposited, can be categorized as inferior.

After rinsing with the organic solvent, the steel was immersed for up to 20 min in the coating solution described above at a temperature of 80°C. Then, it was placed in an oven at 150°C for 30 min to remove any moisture from the deposited conversion film surface and to solidify the polyelectrolyte macromolecules.

Commercial-grade polyester-modified polyurethane (PU) M313 resin, supplied by the Lord Corporation, was applied as an elastomeric topcoating. The polymerization of PU was carried out by incorporating a 50% aromatic amino curing agent M201. The topcoat system was then cured in an oven at a temperature of 80°C.

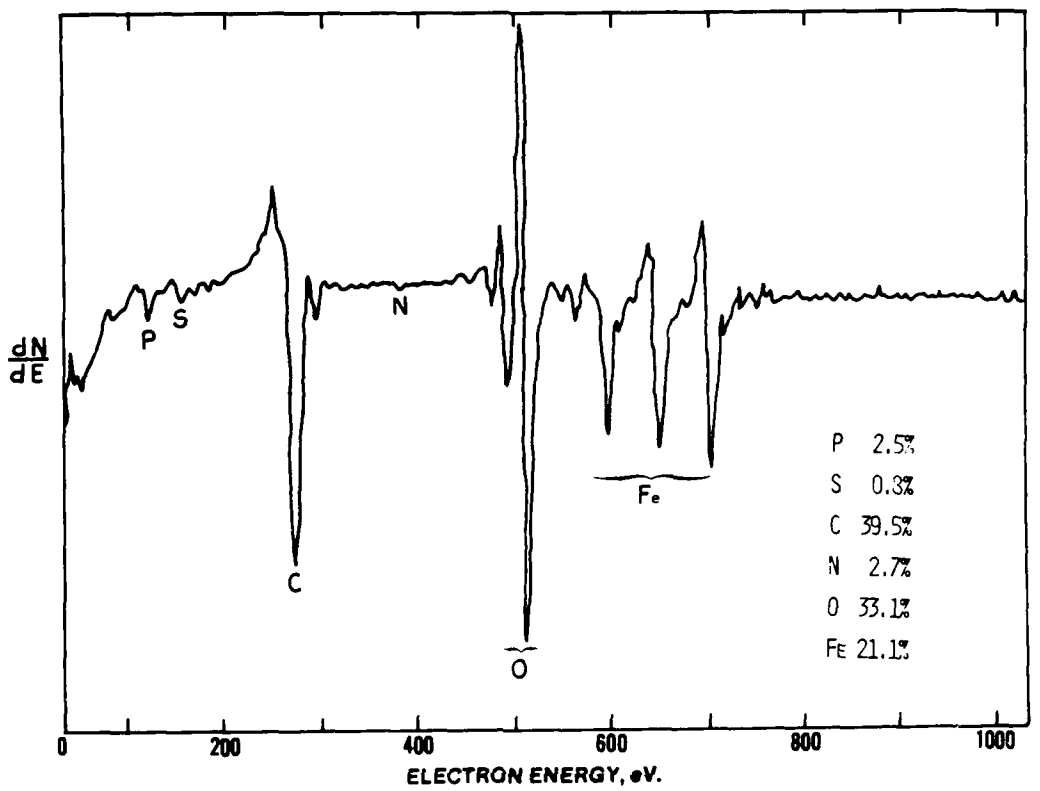

Figure 1. Auger survey spectrum from a solvent-cleaned steel surface.

B. Measurements

An image analysis was conducted of the surface microtopography and the surface chemical components of the polyelectrolyte-modified Zn•Ph coatings using AMR 100 Å scanning electron microscopy coupled with TN-2000 energy-dispersion X-ray spectrometry.

Auger electron spectroscopy (AES) combined with Ar ion sputter-etching was used in depth-composition profiling studies to detect interdiffusion of elemental composition at internal interfaces in the polyelectrolyte-adsorbed Zn•Ph layers. A Perkin-Elmer PHI Model 610 Scanning Auger Microprobe was used.

The electrochemical testing for data on corrosion was performed with an EG & G Princeton Applied Research Model 362-1 Corrosion Measurement System. The electrolyte was a 0.5 M sodium chloride solution made from distilled water and reagent grade salt. The specimen was mounted in a holder and then inserted into a EG & G Model K47 electrochemical cell. The tests were conducted in an aerated 0.5 M NaCl solution at 25°C, and the exposed surface area of the specimens was 1.0 cm^2. The cathodic and anodic polarization curves were determined at a scan rate of 0.5 mV/sec in the corrosion potential range of -1.2 to 0.3 volts.

The conversion products deposited on the treated metal surfaces were identified by X-ray powder diffraction analyses. To prepare the fine powder samples, the deposited conversion layers were removed by scraping the surfaces and were then ground to a size of 325 mesh (0.044 mm).

Electron spectroscopy for chemical analysis (ESCA) was employed for identifying the chemical states and elemental compositions at the surface and interface of p(AA)-Zn•Ph composite layers. The spectrometer used was a V.G. Scientific ESCA 3 MK II. The exciting radiation was provided by a magnesium Kα X-ray source operated at a constant power of 200 W (10 kV, 20 mA). The vacuum in the analyzer chamber of the instrument was maintained at 10^{-9} Torr throughout the experiments.

The cathodic delamination tests for the PU-coated Zn•Ph specimens were conducted in an air covered 0.5M NaCl solution using an applied potential of -1.5 volts vs the standard calomel electrode (SCE) for a period of 6 days. This procedure is described in Reference No. 2. A defect was made using a drill bit with a diameter of approximately 1 mm. After exposure, the specimens were removed from the cell and allowed to dry. The PU coating was removed by cutting, and a delaminated region which appeared as a light gray area adjacent to the defect was detected.

A Perkin-Elmer Model 257 spectrometer was employed for specular reflectance infrared (IR) spectroscopic analysis. To explore the interfacial interaction mechanisms at the polyelectrolyte-to-polyurethane joints, we recorded IR spectra from thin film samples overlaid on reflecting aluminum mirror surfaces.

Peel strength tests of adhesive bonds at the polyurethane topcoat-modified metal substrate interfaces were conducted at a separation angle of ∿180° and a crosshead speed of 5 cm/min. The test specimens consisted of one piece of flexible polyurethane topcoat, 2.5 cm by 30.5 cm, bonded for 15.2 cm at one end to one piece of flexible or rigid substrate material, 2.5 cm by 20.3 cm, with the unbonded portions of each member being face to face. The thickness of the polyurethane topcoat overlaid on the complex crystal surfaces was ∿0.95 mm.

C. Results and Discussion

1. Surface and Subsurface Characteristics

The surface microtopographies of unmodified and 2.0% polyelectrolyte-modified Zn•Ph conversion coatings deposited on steel surfaces were studied by low resolution scanning electron microscopy (SEM). Typical micrographs are shown in Figures 2 and 3. The images for both the unmodified and modified Zn•Ph crystalline films made after immersion of the steel in the zinc phosphating solution for 20 min, reveal interlocking and dense agglomerates of rectangular-like crystals completely covering the substrate surface. The only microscopically discernible difference in the morphology of unmodified and modified crystals is a variation in size of the randomly growing crystals. Figure 2 shows that the crystal size of Zn•Ph converted by the p(AA) and p(SSA) phosphating solutions is notably smaller than that of the unmodified Zn•Ph. A smaller sized crystal was also precipitated when p(IA) macromolecules were included in the phosphating solution (not shown). There were no such alterations in the crystal dimensions of p(AMSA), p(AM), and p(VP)-modified Zn•Ph surfaces (Figure 3). The decreasing crystal size is believed to be due primarily to segmental chemisorption to the precipitated crystal surfaces of functional electrolyte groups such as carboxylic acid (-COOH) and sulfonic acid ($-SO_3H$).

The magnitude of the chemisorption of organic macromolecules on Zn•Ph crystal faces was identified by studying the depth-composition profile in the conversion layers using auger electron spectroscopy (AES) in conjunction with Ar ion sputter-etching. The sputter rate for the depth profiling was ∿1.0 nm/min. The profile obtained in ∿50 min using simultaneous sputtering and analysis permits a rapid identification of layer constituents and structure. The thickness of all of the crystals deposited on the samples tested ranged from ∿40 to ∿10 μm.

CONTROL

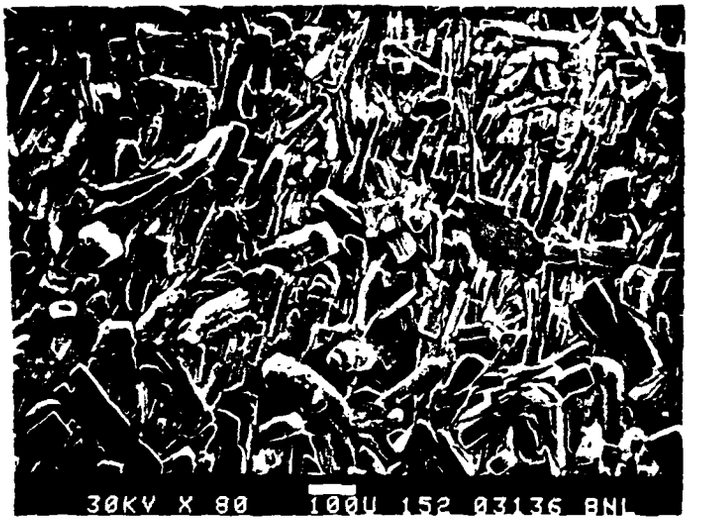

PAA

PSSA

Figure 2. Alteration in the control Zn·Ph crystal size by p(AA) and p(SSA) polyelectrolyte macromolecules.

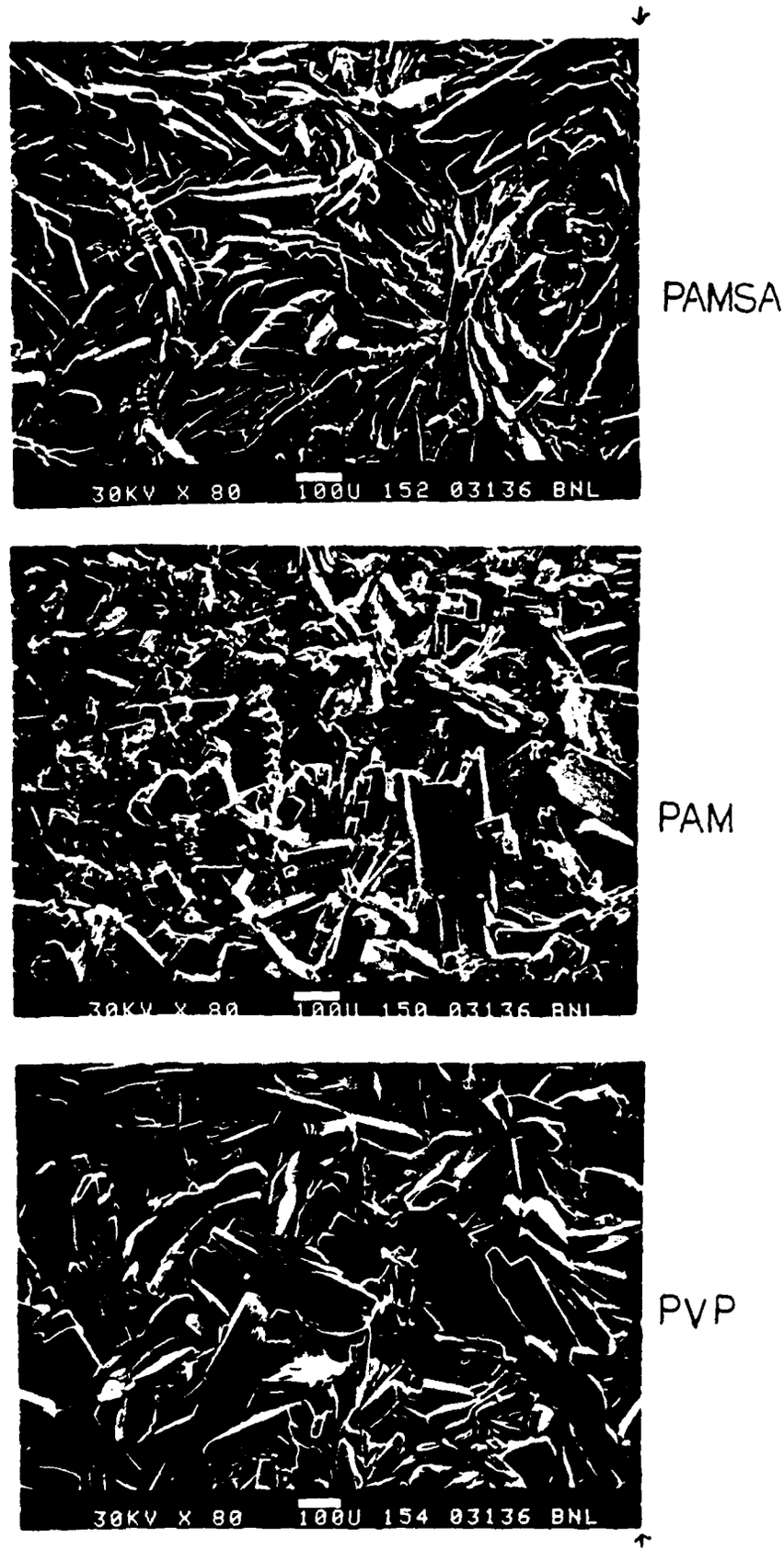

Figure 3. Photomicrographs of p(AMSA), p(AM) and p(VP)-modified Zn·Ph crystal surfaces which suggest that no significant changes in the crystal size occur.

Figures 4 through 6 depict the changes in atomic concentration versus sputter time for the unmodified, p(AA)-, and p(AM)-modified Zn·Ph layers, respectively. In the unmodified Zn·Ph samples (Figure 4), the approximate concentrations of the elements occupying the outermost surface sites were 48% oxygen, 23% zinc, 16% carbon, 9% phosphorous, and 4% iron. The signal intensity for oxygen, the major component at the surface sites, was gradually reduced as the sputtering time was increased until the concentration stabilized at a value of ∿40% after ∿10 min. Similar trends were observed for the carbon and phosphorous concentrations, but the zinc and iron atom concentrations initially increased with sputtering time and then leveled off at a depth of ∿10 nm. This seems to demonstrate the presence of a high quality and less contaminated zinc phosphate hydrate as a major conversion phase in conjunction with phosphophyllite [$Zn_2Fe\ (PO_4)_2 \cdot 4H_2O$] and iron phosphate [$Fe(H_2PO_4)_2$] as minor phases at depths >10 nm. The presence of surface carbon is due to the carbonates resulting from the adsorption of atmospheric carbon dioxide by residual hydroxide in the crystal. The constant value for carbon of ∿4.2% at depths >10 nm may be associated with the contamination of carbon dissociated from the substrate during the conversion reaction processes.

The AES depth profile for the p(AA)-modified Zn·Ph film (Figure 5) shows that carbon and oxygen were the predominant elements at depths up to ∿5 nm from the surface. These reveal the presence of the p(AA) polymer and carbonaceous species. The carbon content slowly decreased with elapsed sputter time until it leveled off at ∿18% at a depth of ∿35 nm. Of particular interest was the constant value of carbon reached after a sputtering time of 35 min, that was much higher than the value of contaminated carbon in the unmodified Zn·Ph layers. Therefore, even though the p(AA)-Zn·Ph composite layer contains a certain amount of carbon contaminant, it appears that the carbon element exisiting at depths >35 nm is due mainly to the p(AA) macromolecules chemisorbed on the crystal faces throughout the conversion layers. The profiles for other elements such as O, Zn, P, and Fe indicate that their concentrations increase monotonically within the first ∿35 nm depth and then stabilize. This depth corresponds to the depth at which the carbon stabilized.

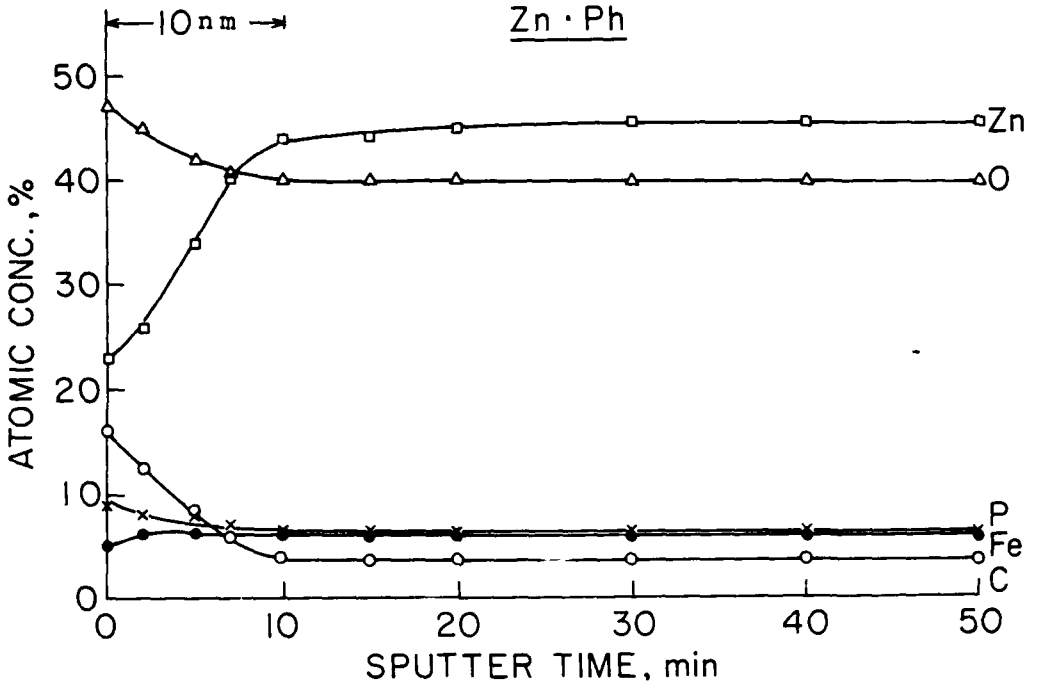

Figure 4. Auger depth profiles for an unmodified Zn·Ph conversion layer.

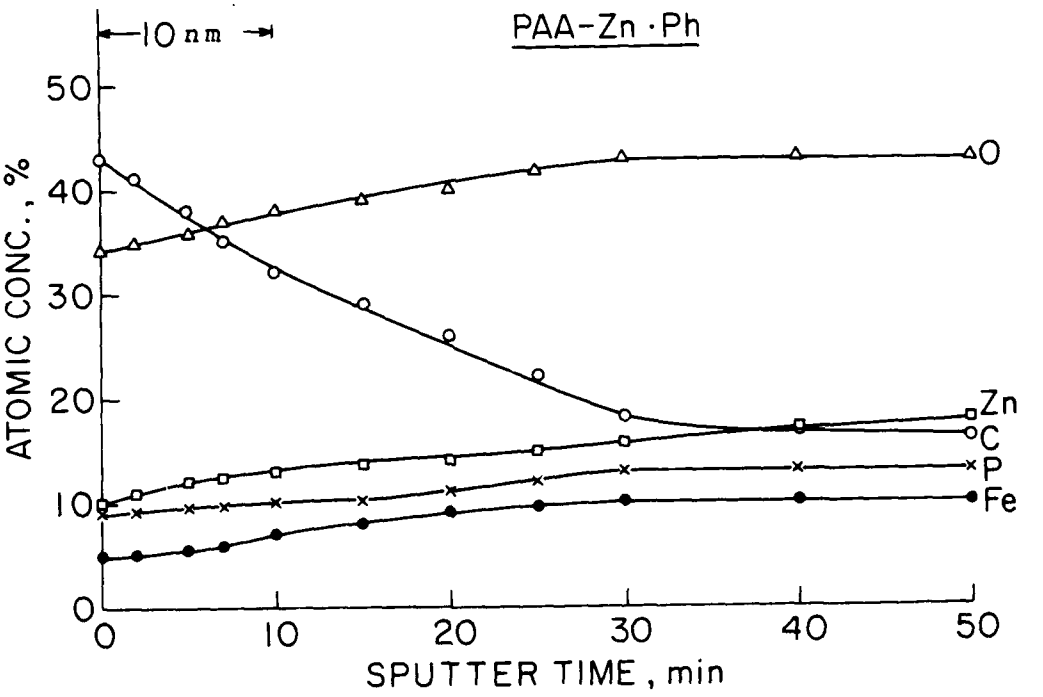

Figure 5. Auger depth profiles for a p(AA)-chemisorbed Zn·Ph layer system.

Although the actual data are not presented in any of the figures, the variations in atomic concentration obtained from the p(IA)- and p(SSA)-modified Zn•Ph conversion surfaces were quite similar to those obtained from the p(AA)-Zn•Ph composites. Accordingly, the profiling structure of Zn•Ph layers modified with functional polyelectrolytes such as p(IA), p(AA), and p(SSA) can be interpreted as follows: 1) highly concentrated polyelectrolyte macromolecules exist throughout the first ∿5 nm of the layer, 2) poorly crystallized zinc and iron phosphate formations caused by chemisorption of the abundant polyelectrolyte are present at depths ranging from 5 to 35 nm, and 3) there is a well-crystallized phosphate phase in the presence of a small amount of polyelectrolyte at depths >35 nm below the surface.

In contrast, the depth-composition profile of the p(AM)-Zn•Ph composite illustrates quite different features (Figure 6). The major difference is the carbon atom profile, in which the carbon concentration at the outermost surface sites is considerably lower than that of the oxygen atom. Furthermore, the carbon concentration is conspicuously reduced with increased sputter time within the first five minutes, but subsequently levels off at a depth of ∿10 nm. This concentration, of ∿4.5%, is 25% less than that measured in the p(AA)-Zn•Ph systems, and is almost equal to that found in unmodified Zn•Ph layers. Therefore, it can be deduced that p(AM), which is a water-soluble macromolecule, does not strongly chemisorb on the superficial and internal crystal faces. The ∿4.5% carbon concentration at depths >10 nm is more likely to be associated with the carbon-contaminated Zn•Ph rather than resulting from chemisorbed organic macromolecules. Since nitrogen can be associated with the presence of pendant-NH_2 groups in p(AM) molecules, this conclusion is supported by the existence of an exiguous amount of N atoms at depths >10 nm. Results similar to those for the p(AM)-Zn•Ph systems were obtained from an AES study of the Zn•Ph modified with p(VP), another water soluble macromolecule. These profiles are not included in this paper. On the other hand, p(AMSA) macromolecules having two pendent groups, electrolyte COOH and non-electrolyte NH_2 groups, combined to the same backbone carbon atom, can be categorized as semi-polyelectrolyte macromolecules. The resulting profile for the semi-polyelectrolyte-modified Zn•Ph system is depicted in Figure 7. When compared to those for the p(AA)- and p(AM)- Zn•Ph systems, the profiles for

O, Zn, P, and Fe atoms which represent the conversion crystal formations, exhibit unusual variations in concentration as a function of sputter time. For example, the signal intensities for O and P atoms slowly increase during the first ∿5 min sputter time, and subsequently decrease with time. On the other hand, the intensities of the Zn and Fe signals progressively grow over the depth range from 0 to 50 nm. The reason for the uncommon features of the profile of these elements is not clear. The carbon depth profile, which relates directly to the presence of p(AMSA) macromolecules, is very similar to that for the p(AM)-Zn·Ph system. Therefore, a semi-electrolyte macromolecule appears to be less susceptible to the chemisorbing activity of the crystal faces.

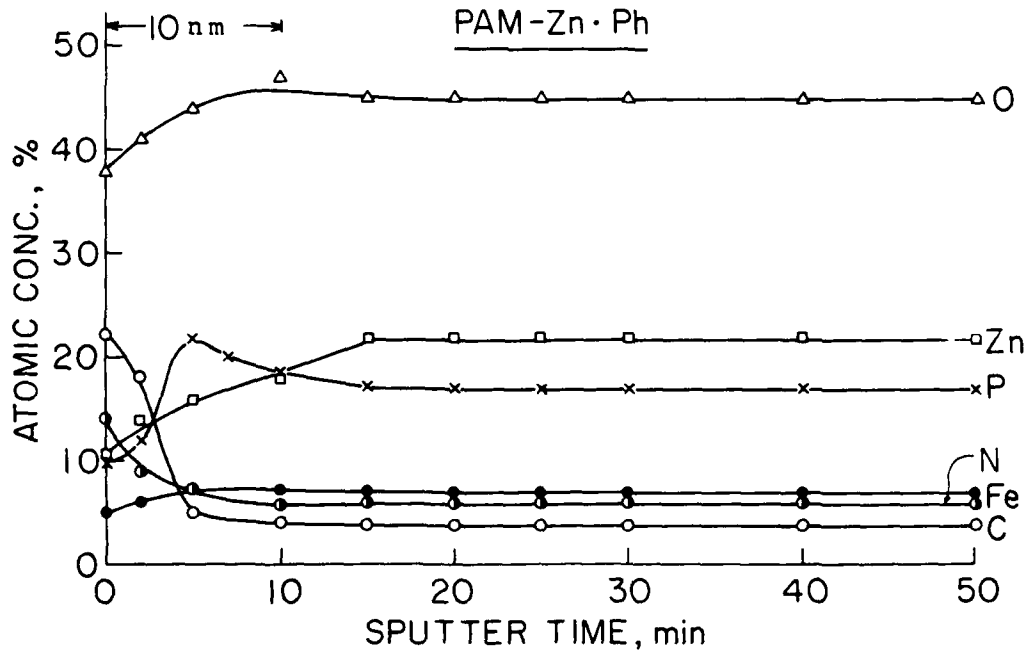

Figure 6. Auger depth profiles for a Zn·Ph layer system modified with a water-soluble p(AM) macromolecule.

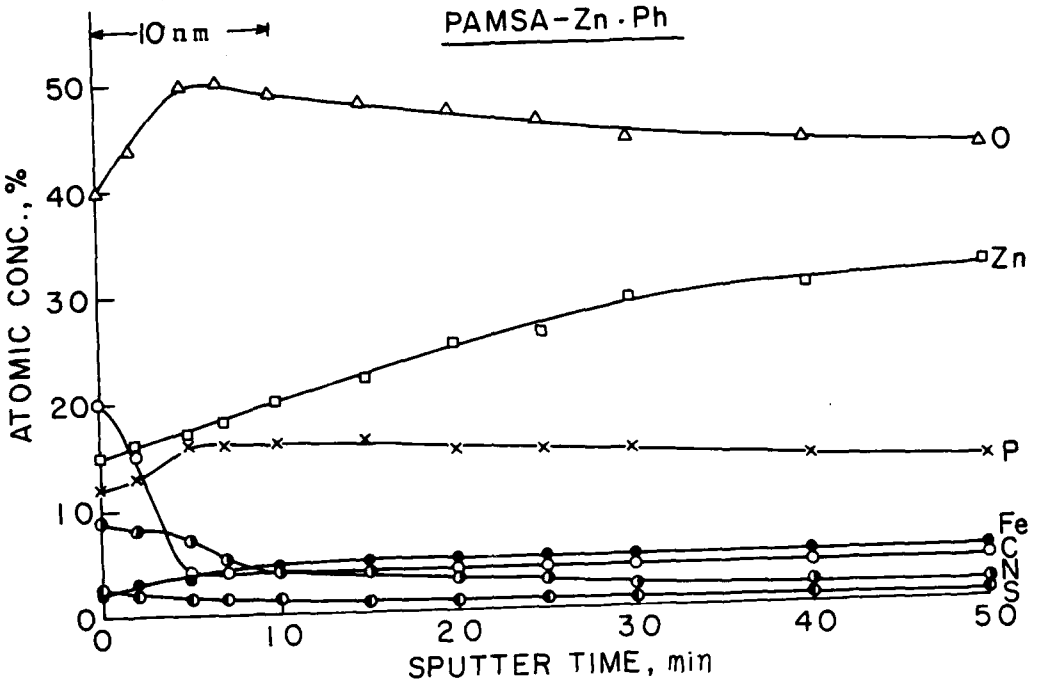

Figure 7. Auger depth profiles for a semipolyelectrolyte p(AMSA)-Zn·Ph composite layer.

In conjunction with the results from the SEM surface survey, it was found that the presence of functional carboxylic acid (-COOH) and sulfonic acid ($-SO_3H$) pendant groups in the polyelectrolytes acts significantly to suppress crystal growth. This is because of the strong chemisorption behavior of these functional groups on the precipitated crystal faces. In contrast, the magnitude in chemisorbing ability of the amide groups such as $-CONH_2$ and -CO-N is apparently very small.

The ESCA survey scan to indentify elements at the outermost surface sites of p(AA)-modified Zn·Ph is shown in Figure 8. Carbon and oxygen atoms appear as major lines, and zinc and phosphorous as minor ones. The chemical states of Zn and P are assigned to the presence of the zinc and phosphorous compounds, and the C is attributed to the organic p(AA) macromolecules. The O atom is related to both the organic compounds and the polyelectrolyte. This suggested that certain areas of the Zn·Ph film surfaces were covered with a thin p(AA) layer no thicker than 5 nm, which corresponds to the escape depth of the magnesium photoelectron. Such areas probably represent the interface regions which are of primary interest in this study.

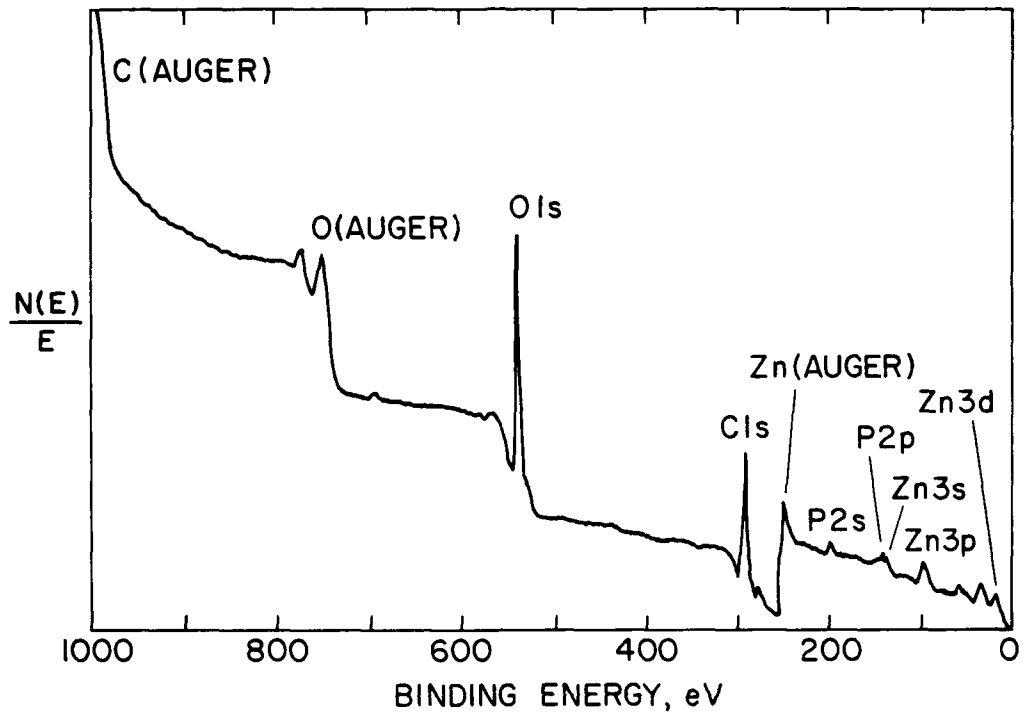

Figure 8. ESCA survey spectrum taken from a p(AA)-complexed Zn•Ph conversion precoating surface.

Another important goal of our work was to obtain knowledge regarding possible interactions between p(AA) and the crystal conversion coating, and then to understand how the interfacial reaction products act to increase the corrosion resistance of Zn•Ph-coated steel. The former was investigated by means of XPS, and it was observed that even when a high concentration of 5% p(AA) was used, the p(AA) film deposited at the outermost surface sites was thin enough to see the photoemission signal from the underlying Zn- and Fe- phosphate compounds. The binding energy (BE) scale in the XPS spectra was calibrated with the C_{1s} of the principal hydrocarbon, "CH_n", peak fixed at 285.0 eV as an internal reference standard.

The C_{1s} core level photoemission spectra for bulk p(AA), and 1% p(AA)- and 5% p(AA)- modified conversion coating surfaces are shown in Figure 9. The C_{1s} region of the bulk p(AA) (Figure 9-a) has two main peaks; 285.0 eV corresponds to the hydrocarbons in the main chain and 288.9 eV ascribes to the carbon originating from the carboxylic acid, COOH, in the p(AA). The spectrum for the 5% p(AA)-modified coating (Figure 9-b) shows a shift in the peak to a lower BE site and the appearance of a new peak at 287.2 eV, as compared to that of the bulk p(AA). The new peak emerging at about 1.7 eV lower BE from the COOH peak, is located between a carbonyl carbon, C=O, at approximately 288.0 eV and a carbon-oxygen single bond at approximately 286.5 eV.[24] For samples containing 1% p(AA) (Figure 9-c), a further shift in the COOH peak toward lower BE was observed.

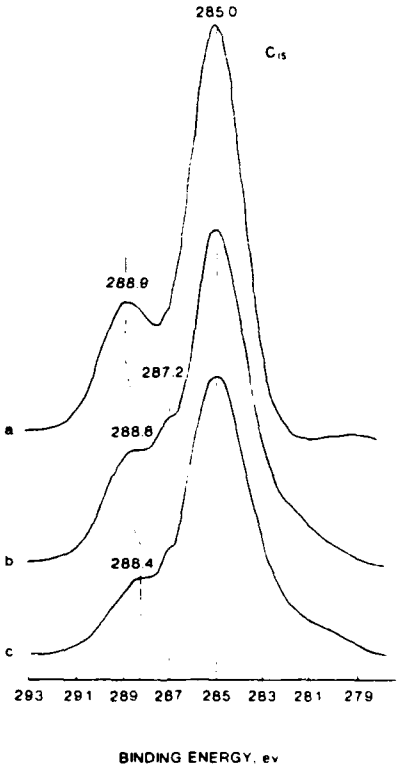

Figure 9. C_{1s} spectra for bulk p(AA) (a), 5% p(AA)-Zn•Ph interface (b), and 1% p(AA)-Zn•Ph interface (c).

Figure 10 shows typical 2p doublet separation spectra for the Zn2p3/2 and 2p1/2 lines from unmodified and modified conversion coatings. The distance separating the 2p3/2 and the 2p1/2 energies for both the unmodified and modified coatings is in the range of 23.7 to 23.5 eV. This means that the presence of p(AA) in the conversion coatings does not change the separation distance. Therefore, these peaks appear to be assigned to zinc originating from the zinc phosphate dihydrate crystal. The main difference between these spectra is the shift of the 2p3/2 and 2p1/2 peaks to higher energy sites when the p(AA) content is reduced. For 5% and 1% p(AA) concentrations, the values of 1022.5 eV (Figure 10-e) and 1022.9 eV (Figure 10-f) for the 2p3/2 core level correspond to increases of 0.1 and 0.5 eV, respectively, compared to unmodified coatings. The reason for the increased Zn2p peak energy, the decrease in BE of the COOH carbon, and the new peak at 287.2 eV for the C_{1s} region, may be charge transfer from the Zn in the crystal coating to the electron accepting oxygen portion in the functional pendent group of p(AA). In fact, the O_{1s} core level (not shown) at the p(AA)/Zn·Ph interfaces indicated the presence of a strong peak at 531.4 eV which ascribes to the formation of COO-metal complexes. Two possible Zn-O bond formations for carboxylate-linked Zn complexes yielded through a mechanism involving charge transfer reactions at p(AA)-Zn·Ph interfaces, are discussed below.

(I)

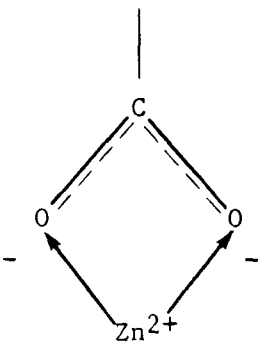

(II)

One of the complex formations is a zinc-oxygen-carbon (Zn-O-C) bond structure (I) which is produced by the reaction of an oxygen atom in the carboxylic anion with a Zn atom. The other (II) may be formed by a charge transferring interaction between both oxygens in the carboxylate group and the Zn atom.

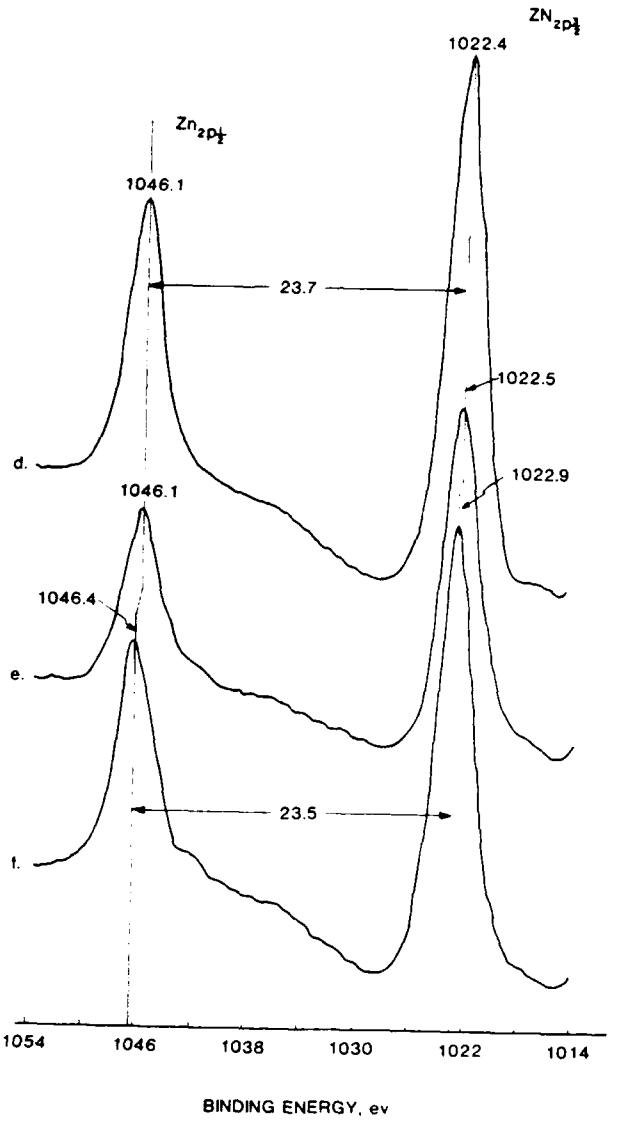

Figure 10. Zn2p separation spectra for unmodified Zn•Ph (d), 5% p(AA)-modified (e) and 1% p(AA)-modified Zn•Ph (f).

On the basis of the assumption that the p(AA)-diffused crystal conversion layer is composed of the hybrid phases of zinc phosphate, iron phosphate, and mixed iron and zinc phosphate compounds, both the relative quantities and the identification of these conversion products were studied with X-ray powder diffraction (XRD). The resultant XRD pattern in the diffraction range of 0.883 to 0.167 nm for the 150°C-dried samples of a layer removed by scraping the surface, is given in Figure 11. These spacings suggest that the major conversion product is zinc phosphate dihydrate, $Zn_3(PO_4)_2 \cdot 2H_2O$.[25] The

presence of hopeite, $Zn_3(PO_4)_2 \cdot 4H_2O$, phosphophyllite, and iron phosphate, which are reported by Ghali and Potvin,[26] could not be clearly identified in the layers derived from the zinc orthophosphate dihydrate-based phosphating solution.

From these results obtained using various analytical techniques, possible conversion mechanisms for polyelectrolyte-chemisorbed Zn·Ph crystal layers are presented schematically in Figure 12. As depicted in the figure, the proposed mechanism consists of four steps. In step A, when the p(AA) electrolyte is introduced into the zinc phosphating liquid system, the divalent zinc cations are readily complexed with the proton-donating-type carboxylic acid groups in the p(AA) molecules. The extent of the complex is dependent upon the charge density of the polymer and the concentration of the counterion.[27] It must, therefore, be assumed in the present work that the p(AA) species are partly dissociated p(AA) molecules to which a number of Zn ions are bound. This amount of ion binding should permit extensive random coiling of poly-

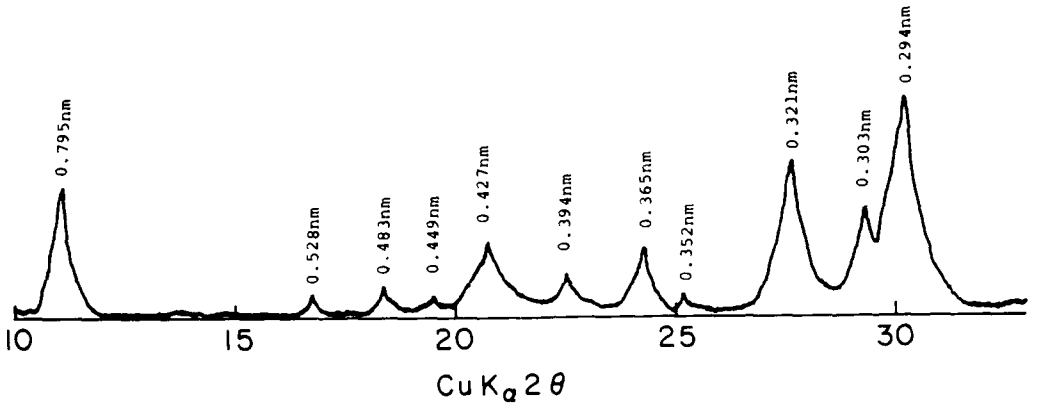

Figure 11. Powder X-ray diffraction pattern of p(AA)-treated Zn·Ph crystal layer.

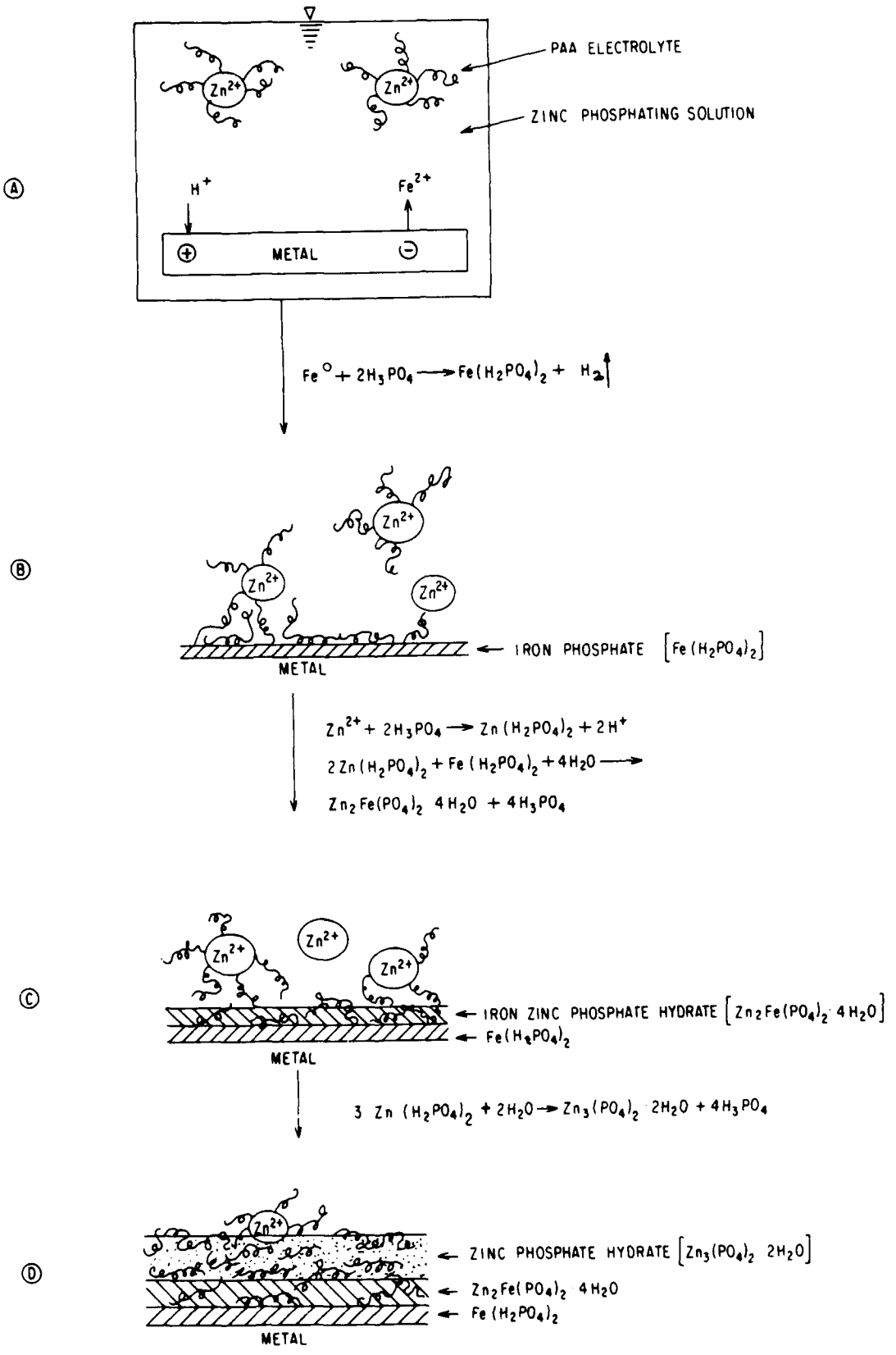

Figure 12. Schematic conversion mechanism of polyelectrolyte-zinc phosphate systems deposited on steel surfaces.

anions. Upon immersion of the metal substrate in the acid medium, the substrate surfaces undergo an electrochemical dissolution reaction. The ferrous ions that migrated electrochemically from the substrate surface at the steel-solution interfaces have a strong chemical attraction with the orthophosphoric acid. This reaction is followed by the precipitation of a thin layer of the first conversion product in terms of iron phosphate, $Fe(H_2PO_4)_2$.[26] The surface of the precipitated iron phosphate is charged positively because of the large number of Fe^{2+} ions adjacent to the iron phosphate cores. The surface cationic strength might be strong enough to chemisorb the polyelectrolyte in preference to that of Zn^{2+} ions (see stage B). It is, therefore, postulated that the most logical surface sites to electrostatically attach the ionized COOH groups would be Fe ions on the precipitated iron compound surfaces. As a result of chemisorption of ionized p(AA) segments, some Zn cations masked with p(AA) macromolecules are released from the p(AA)-Zn complex formations, and then the dissociated Zn^{2+} ions react with the $2H_3PO_4$ to form zinc phosphate, $Zn(H_3PO_4)_2$. Crystalline zinc iron phosphate hydrate, in terms of phosphophyllite, $Zn_2Fe(PO_4)_2 \cdot 4H_2O$, is probably derived from a reaction between the $Zn(H_3PO_4)_2$ and $Fe(H_3PO_4)_2$ in the aqueous media.[28] Even though the newly precipitated phosphophyllite is superimposed on the p(AA)-chemisorbed iron phosphate, the segmental chemisorption to the precipitated crystal surfaces by p(AA) will occur consecutively, as illustrated in step C. As is evident from the AES and XRD studies, the amount of these iron-rich phosphates, which are precipitated at the beginning of the treatment, is much smaller than the zinc phosphate dihydrate, $Zn_3(PO_4)_2 \cdot 2H_2O$, which is the major conversion product of the precoat layers. During the final period depicted in step D, the residual zinc phosphate is converted into zinc phosphate dihydrate.

From the viewpoint of the polyelectrolyte chemisorption process, the strongly ionized segments of p(AA) are electrostatically diffused to the positive surface sites of zinc phosphate dihydrate embryos at the beginning of the precipitation. There is no doubt that the high efficiency of segmental chemisorption of organic macromolecules either on newly precipitated nuclei or on growth sites occurring during the primary crystallization processes, acts significantly to inhibit the rate of crystal growth. The extent of chemisorption is increased with increasing molecular weight of the p(AA). This is

related directly to the decrease in size of the crystal or embryonic crystal. The precipitated crystal morphology and habit are also markedly transformed by a strong chemisorption of p(AA) with an appropriate molecular weight. However, as reported previously,[1] when a molecular weight >250,000 was used, the formed crystals were much smaller than those produced using a lower-molecular-weight p(AA). The incorporation of extremely high-molecular-weight p(AA) completely suppressed the crystal growth by strongly chemisorbing the p(AA) on the embryonic crystal faces. An alternative explanation for the effect of molecular weight on the crystallization rate is that the high magnitude of entanglement in the p(AA)-Zn complex systems results in suppression of the electrostatic diffusion of segments to the cathodic crystal nuclei surfaces. In other words, it is very difficult for the Zn^{2+} ions existing in a tightly coiled configuration of p(AA) chains to migrate as free cations from the complex formations. This phenomenon can be expressed in terms of shielding effects which should occur at the strong ionic attractions of p(AA) with Zn^{2+}. Thus, it is rationalized that the presence of p(AA) having a particular molecular weight which is representative of less chain entanglement, contributes to the great accessibility of segmental diffusion to the crystal surface sites.

2. Corrosion Control

Prior to incorporating the p(AA) macromolecules into the phosphating solutions, the resulting morphological and topographical features and the major chemical compositions for Zn·Ph conversion coatings made using varying water contents while maintaining a constant weight ratio of $Zn_3(PO_4)_2 \cdot 2H_2O$ to H_3PO_4, were explored using the combined techniques of SEM with EDX. Examples of the SEM micrographs and accompanying EDX elemental analyses are shown in Figure 13. From the viewpoint of surface topography, the SEM image of the coating derived from the formulation containing the lowest water concentration (see Figure 13-a) revealed an interlocking structure of 300 μm long plate-like crystals. Microscopic examination of single crystals indicated that the thickness of this conversion layer was approximately 40 μm. However, this value is only approximate because of the assumed uniform single crystals.

a

Formulation:

2.6% $Zn_3(PO_4)_2 \cdot 2H_2O$-5.1% H_3PO_4-92.3% H_2O

Thickness: ~40μm

Element	Intensity Counts/100 sec.	Intensity ratio/Zn
Fe	12072	0.39
Zn	30883	1.00
P	15830	0.51

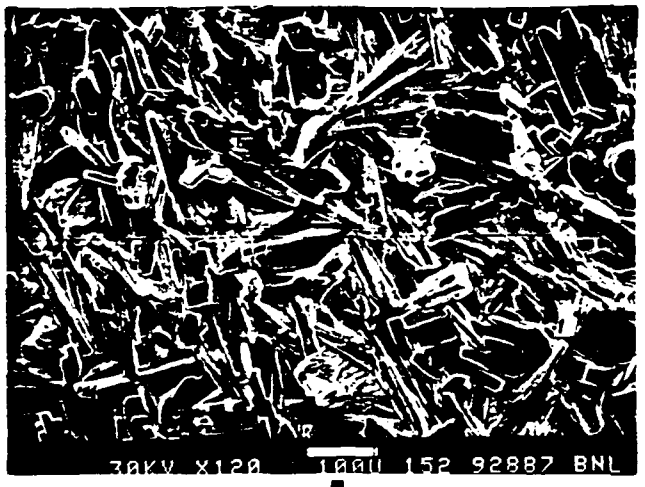

b

Formulation:

1.3% $Zn_3(PO_4)_2 \cdot 2H_2O$-2.7% H_3PO_4-96.0% H_2O

Thickness: ~30μm

Element	Intensity Counts/100 sec.	Intensity ratio/Zn
Fe	18134	0.49
Zn	36843	1.00
P	20107	0.55

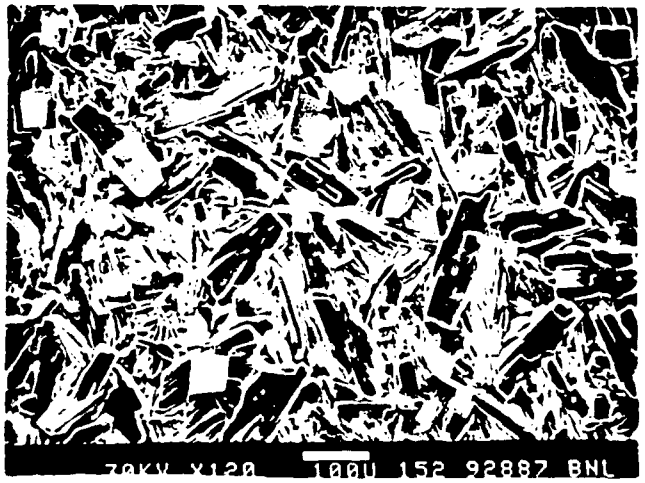

c

Formulation:

0.9% $Zn_3(PO_4)_2 \cdot 2H_2O$-1.8% H_3PO_4-97.3% H_2O

Thickness: ~25μm

Element	Intensity Counts/100 sec.	Intensity ratio/Zn
Fe	17741	0.56
Zn	31883	1.00
P	16918	0.53

Figure 13. SEM images and EDX analyses for conversion coatings derived from zinc phosphating solutions diluted with various amounts of water.

The dimensions of the crystals can be controlled by varying the water content while maintaining a constant $Zn_3(PO_4)_2 \cdot 2H_2O$ to H_3PO_4 ratio. As an example, increasing the water content to 97.3% produced a smaller crystal having a length of approximately 150 μm and a thickness of approximately 25 μm. This is shown in Figure 13-c. EDX intensity count ratios of Fe to Zn elements indicated that this ratio tends to increase with decreased coating thickness. No significant changes in the P to Zn ratio were evident. Hence, thinner conversion coatings appear to contain more Fe than the thicker ones.

The effectiveness of these conversion coatings with various dimensions and Fe/Zn ratios as corrosion protective layers on cold-rolled steel, was determined using electrochemical polarization behavior measurements. These tests were conducted in an aerated 0.5 M NaCl solution at 25°C. Figure 14 shows typical polarization curves of log current density vs potential for a plain steel (blank) and Zn·Ph-coated steels. The shape of the curves presents the transition from cathodic polarization at the onset of the most negative potential to the anodic polarization curves at the end of lower negative potential. The potential axis at the transition point from cathodic to anodic curves is normalized as the corrosion potential, E_{corr}. The figure indicates that all of the conversion coating specimens had an E_{corr} value of about -0.6 V and a current density of approximately 6×10^{-1} $\mu A/cm^2$ in the vicinity of E_{corr}. This seems to suggest that the protective coverage of all of these crystalline coatings is essentially the same.

When compared with those for the blank steel, the striking characteristics of the cathodic curves for the coated steel specimens are as follows: 1) a large reduction in E_{corr} to less negative potentials, 2) a considerably decreased relative current density in the vicinity of E_{corr}, and 3) a lower short-term steady-state current value in the potential region between -1.1 and -1.0 V. As a result, the rate of corrosion of steel in an aerated NaCl solution is believed to be significantly decreased by the presence of the conversion coatings deposited through the dissolution-recrystallization process.

In order to investigate the ability of p(AA)-chemisorbed conversion coatings to provide corrosion protection to steel, p(AA) macromolecules at concentrations of up to 5 wt% were incorporated into a convertible solution consisting of 1.3 wt% $Zn_3(PO_4)_2 \cdot 2H_2O$, 2.7 wt% H_3PO_4 and 96.0 wt% water.

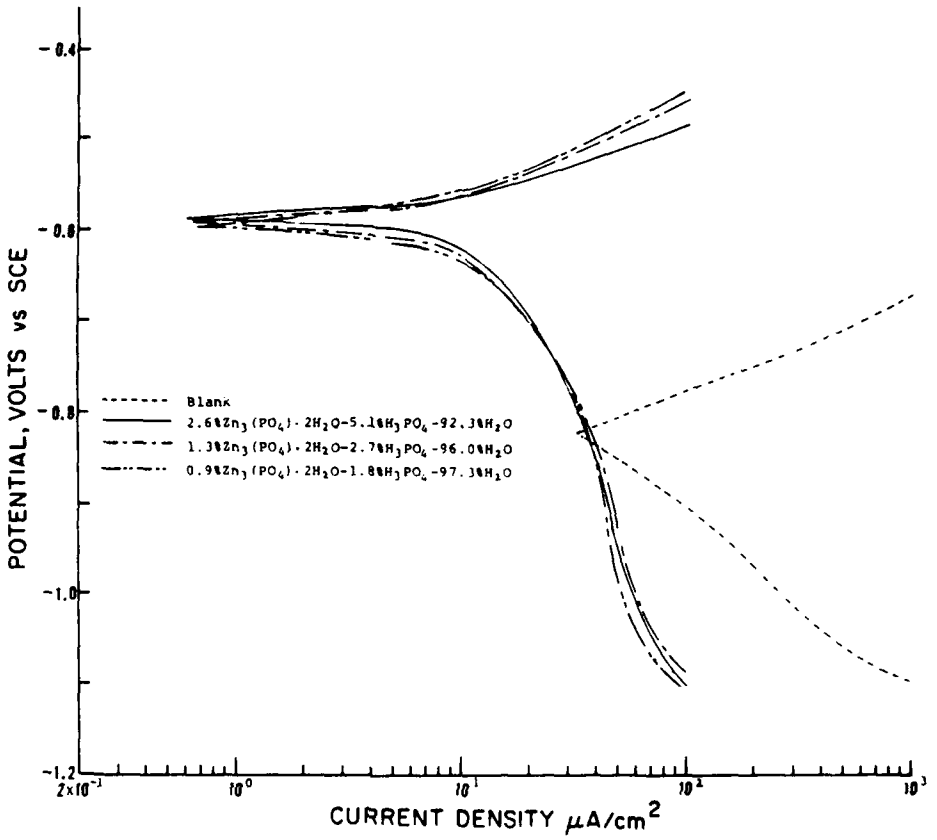

Figure 14. Comparisons of polarization curves for blank steel and steel containing conversion coatings deposited through dissolution-recrystallization processes.

Figure 15 shows SEM microtexture views and associated EDX data for the unmodified, and 1 and 2% p(AA)-modified conversion coatings. It is evident from comparisons of the topographical features of the crystals precipitated on the steel surfaces, that the addition of p(AA) serves to decrease the crystal size. This is due primarily to the chemisorption of p(AA) on the precipitated crystal nuclei faces at the beginning of recrystallization processes, thereby suppressing the crystal growth.[29] The accompanying EDX data indicate that the Fe/Zn ratios for the conversion coatings increase with increased p(AA) concentration. Since the only source of Fe is the steel, the extent of suppression of crystal growth by the p(AA) relates directly to the precipitation rate

d

P(AA): 0%

Element	Intensity Counts/100 sec.	Intensity ratio/Zn
Fe	18134	0.49
Zn	36843	1.00
P	20107	0.55

e

P(AA): 1.0%

Element	Intensity Counts/100 sec.	Intensity ratio/Zn
Fe	19068	0.56
Zn	34050	1.00
P	18387	0.54

f

P(AA): 2.0%

Element	Intensity Counts/100 sec.	Intensity ratio/Zn
Fe	18368	0.60
Zn	30611	1.00
P	17295	0.57

Figure 15. SEM photographs and associated EDX data for unmodified and p(AA)-modified conversion coatings.

of iron-rich phosphate compounds. At a 5% p(AA) concentration, a further increase in the Fe/Zn ratio was obtained (see Figure 16). The surface morphological image shows two discriminable crystal phases: one is that of a reticular crystal network (Figure 16-A) and the other is the plate-like crystal network (Figure 16-B). From the EDX quantitative evaluation, the former is associated with the Fe-rich phosphate crystalline coatings and the latter is from the Zn-rich phosphate compounds. The identification of these different phosphate phases was made using x-ray powder diffraction (XRD) with CuK_α radiation at 50 KV and 16 mA.

X-ray diffraction (XRD) tracings recorded in the diffraction range 0.288 to 0.444 nm for powdered 2% and 5% p(AA)-modified conversion coatings are given in Figure 17. For the 2% p(AA) samples, all of prominent spacing lines in the XRD pattern ascribe to zinc phosphate dihydrate [$Zn_3(PO_4)_2 \cdot 2H_2O$], which is representative of the recrystallization of the starting material dissolved in the phosphating solution. In contrast, the XRD pattern for the 5.0% p(AA) sample has two new spacings at 0.311 and 0.437 nm. These spacings reveal the presence of strengite ($FePO_4 \cdot 2H_2O$).[30] Therefore, the Fe-rich reticular and Zn-rich plate-like crystals which were observed by SEM-EDX analyses, are associated with the formation of $FePO_4 \cdot 2H_2O$ and $Zn_3(PO_4)_2 \cdot 2H_2O$ phases, respectively. Although XRD spacings for conversion coatings modified with lesser amounts of p(AA) are not shown, it is known that insoluble ferric phosphate ($FePO_4$) is present in normal Zn·Ph coating layers on steel surfaces.[31] The precipitation of strengite may occur through the following hypothetical conversion sequences:

$$Fe + 2H_3PO_4 \longrightarrow Fe(H_2PO_4)_2 + H_2\uparrow \qquad (1)$$

$$4Fe(H_2PO_4)_2 + O_2 \longrightarrow 4FePO_4 + 4H_3PO_4 + 2H_2O \qquad (2)$$

$$FePO_4 + 2H_2O \longrightarrow FePO_4 \cdot 2H_2O \ . \qquad (3)$$

Once a dense layer of this insoluble ferric phosphate has been deposited on the steel, further precipitation may be retarded because of the precipitation of $Zn_3(PO_4)_2 \cdot 2H_2O$ as the major conversion layer. This information indicates a large suppression of Zn·Ph crystal growth which occurs as a result of adding high concentrations of p(AA). This results in the production of thinner

Element	Intensity Counts/100 sec.	Intensity ratio/Zn
Fe	46403	1.10
Zn	42388	1.00
P	12130	0.29

Element	Intensity Counts/100 sec.	Intensity ratio/Zn
Fe	19565	0.39
Zn	50792	1.00
P	11870	0.23

g

Figure 16. SEM-EDX analyses of 5% p(AA)-modified conversion coating.

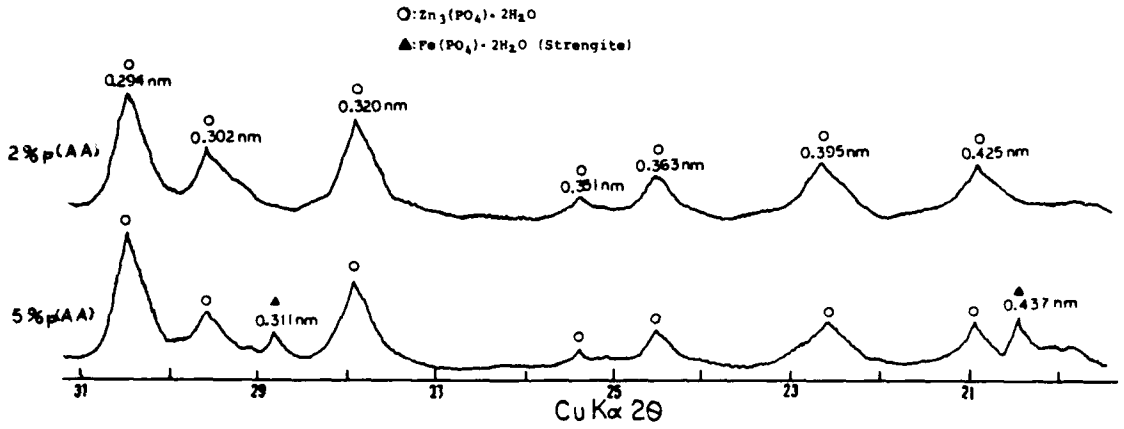

Figure 17. XRD tracings of 2% and 5% p(AA)-modified conversion coatings.

conversion coatings containing a high proportion of ferric phosphate compounds. Thus, the coating thickness and iron content appears to depend on the amount of p(AA). Experimentally, the measured thicknesses for coatings containing 0, 1, 2 and 5% p(AA) were approximately 30, 28, 25 and 20 μm, respectively.

Efforts were made to determine how the proportions of Fe existing in the conversion layers participate in the corrosion protection process. To obtain this information, the polarization behavior of p(AA)-modified conversion specimens in an aerated 0.5M NaCl solution was determined, and the resultant polarization curves were correlated as a function of EDX Fe/Zn ratios for various p(AA) concentrations. These results are given in Figure 18. A comparison of the cathodic polarization areas from the unmodified Zn•Ph and p(AA)-modified Zn•Ph specimens indicates two noteworthy features: (1) the short-term steady-state current value for the modified specimens is lower than that for the unmodified one in the potential region between -1.0 and -1.1 v, and (2) the incorporation of 5% p(AA) resulted in a shift in corrosion potential to a more negative site and an increase in current density at the potential axis. The lower current density for the modified specimens (result No.1 above)

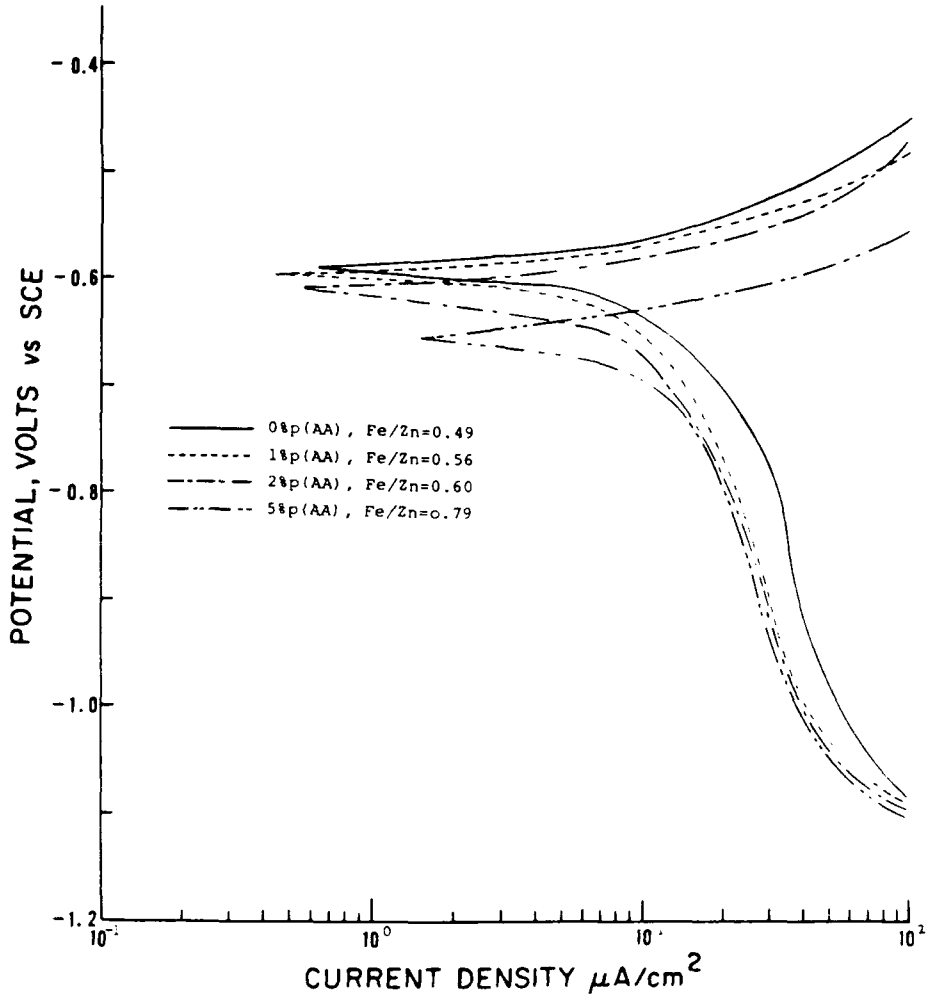

Figure 18. Polarization curves for zinc phosphated steel specimens containing p(AA) concentrations of up to 5% in aerated 0.5M NaCl solutions.

compared to that of the specimen without p(AA), is attributed to a low hydrogen reduction as well as to a less active surface. This confirms that the oxygen reduction reaction is inhibited by the p(AA) macromolecule chemisorbed on the crystal faces. With regards to the second observation, the introduction of 5% p(AA) into the conversion layer seemed to reduce the corrosion-resistive effectiveness. From this observation and the previously discussed SEM-EDX data, it can be concluded that the presence of agglomerated strengite in the $Zn_3(PO_4)_2 \cdot 2H_2O$ layer results in an increase in intrinsic phosphate porosity, thereby giving poor corrosion protection.

3. Alkali-dissolution of Conversion Coatings

The studies were extended further to investigate the influence of these interfacial complex products upon the alkali-dissolution of the conversion coatings. Table 1 indicates the changes in the EDX intensity ratios of P/Zn and Fe/Zn, and E_{corr}, as a function of p(AA) for phosphated steel specimens after exposure to a 0.1M NaOH solution for 1 hr at 25°C. As seen in the table, the P/Zn ratios for all exposed specimens are significantly lower than those for the unexposed specimens. All of the Fe/Zn ratios increased. The former suggests the dissociation of a greater amount of phosphate brought about by the alkaline dissolution of Zn•Ph. Thus, this seems to imply that interfacial reaction products composed of Zn-O-C complexes do not significantly inhibit the alkali-dissolution of conversion coatings. However, the differences in Fe/Zn ratios compared with those from the unexposed samples decreased significantly with increased p(AA) concentrations, thereby suggesting that p(AA) macromolecules diffused electrostatically onto Zn•Ph crystal faces act to decrease the rate of ferrous ion dissociation from the steel.

Table 1. Variations in P/Zn and Fe/Zn Intensity Count Ratios and Corrosion Potential Values, E_{corr}, as a Function of p(AA) Concentration for Phosphated Steel Specimens After Exposure to 0.1M NaOH Solution.

PAA,	Before Exposure			After Exposure		
%	P/Zn	Fe/Zn	E_{corr}, Volt	P/Zn (Difference*)	Fe/Zn (Difference)	E_{corr}, Volt
0	0.55	0.49	-0.592	0.26 (-52.7%)	0.72 (+46.9%)	-0.620
1	0.54	0.56	-0.595	0.24 (-55.6%)	0.75 (+33.9%)	-0.540
2	0.57	0.60	-0.610	0.23 (-59.7%)	0.79 (+31.7%)	-0.521
5	0.55	0.74	-0.651	0.25 (-54.6%)	0.89 (+20.3%)	-0.480

*Difference compared with that of unexposed specimen; difference, % = [(ratio of exposed specimen - ratio of unexposed specimen)/ratio of unexposed one] x 100.

The E_{corr} values for specimens after exposure to NaOH were determined from the polarization curves in aerated 0.5M NaCl solutions. To investigate the variation in Na atom percentages as a function of p(AA), the surfaces of the exposed specimens were also examined using XPS. As noted in Table 1, the E_{corr} values for all the exposed specimens containing p(AA) shifted to less negative positions, as compared to those for the unexposed ones. The largest shift was observed for specimens modified with 5% p(AA). Figure 19 gives comparisons between the C_{1s} spectrum features of 1% p(AA)-modified Zn·Ph before (Figure 19-j) and after (Figure 19-k) exposure to NaOH solutions. The most striking features in the spectrum of the exposed samples were the shift in the carboxyl carbon, $-\underset{\underset{O}{\|}}{C}-O-$, peak to a higher BE site, and a decrease in intensity of the peak at 287.2 eV, while maintaining the same position of hydrocarbons at 285.0 eV. In conjunction with the increase of 0.3 eV in the BE of carboxyl carbon,

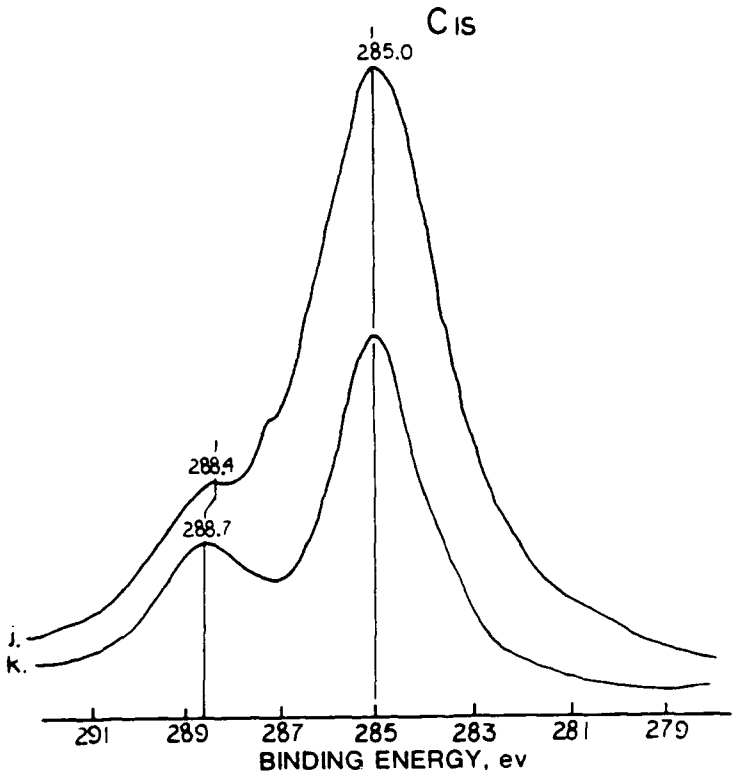

Figure 19. C_{1s} spectra for 1% p(AA)-modified Zn·Ph before (j) and after (k) exposure in 0.1M NaOH solution.

there was a corresponding decrease in the BE in the Zn2p3/2 region for the sample subjected to NaOH exposure (see Figure 20-m), as compared with that of the unexposed sample (Figure 20-1). The excitation of the new line at 1020.4 eV for the exposed samples is assigned to the formation of new Zn-based compounds brought about by the alkali-dissolution of the conversion coating. This seems to suggest that during the exposure to the NaOH solution, Na ions act to promote the breakage of the Zn-OOC electrostatic bonds. The breakage may be related to an elemental substitution of Zn for Na. However, the corresponding Na_{1s} core level spectra have not yet been clearly resolved because of a very noisy exciting peak feature.

To obtain information regarding the transformation of Zn-OOC into a Na-OOC bond structure, infrared (IR) spectroscopic analyses were performed. However, direct observations that could be used for the clarification of the interaction structure at the interface were very difficult to make using IR. Thus, to create a resemblant reaction model that would yield a product that was detectable using IR, a mixture of 50 wt% p(AA) and 50 wt% $Zn_3(PO_4)_2 \cdot 2H_2O$ was prepared for use in the IR study. The mixture was allowed to evaporate in a vacuum oven at 150°C, and the residue was then exposed in 0.1M NaOH for 1 hr. After the exposure, the powdered samples were incorporated into KBr pellets for IR analysis. For comparison purposes, IR spectra for the unexposed mixture and the $Zn_3(PO_4)_2 \cdot 2H_2O$ powder were also determined. These spectra for frequency ranges from 2000 to 1350 cm^{-1}, are given in Figure 21. As seen in Figure 21-a, the spectrum of the $Zn_3(PO_4)_2 \cdot 2H_2O$ powder indicates the presence of a strong band near 1610 cm^{-1} which can be assigned to the crystallized water in Zn•Ph. The spectrum for the p(AA)-$Zn_3(PO_4)_2 \cdot 2H_2O$ composite sample (Figure 21-b) indicated the C=O in carboxylic acid at 1710 cm^{-1} and the main chain CH_2 of saturated methylene at 1440 cm^{-1}, in addition to crystallized water at 1610 cm^{-1}. The NaOH-exposed composite produced a dramatic change in the spectrum. Two new sharp bands appeared at 1550 and 1410 cm^{-1} (see Figure 21-c). The formation of bands at these frequencies and the decrease in the C=O peak intensity at 1710 cm^{-1} indicate the formation of Na^{+-}OOC-salt complexes.(32)

On the basis of the above information, the following statements can be made regarding the function of p(AA) in reducing the dissociation of Fe and improving the protection of the conversion coatings when subjected to NaOH.

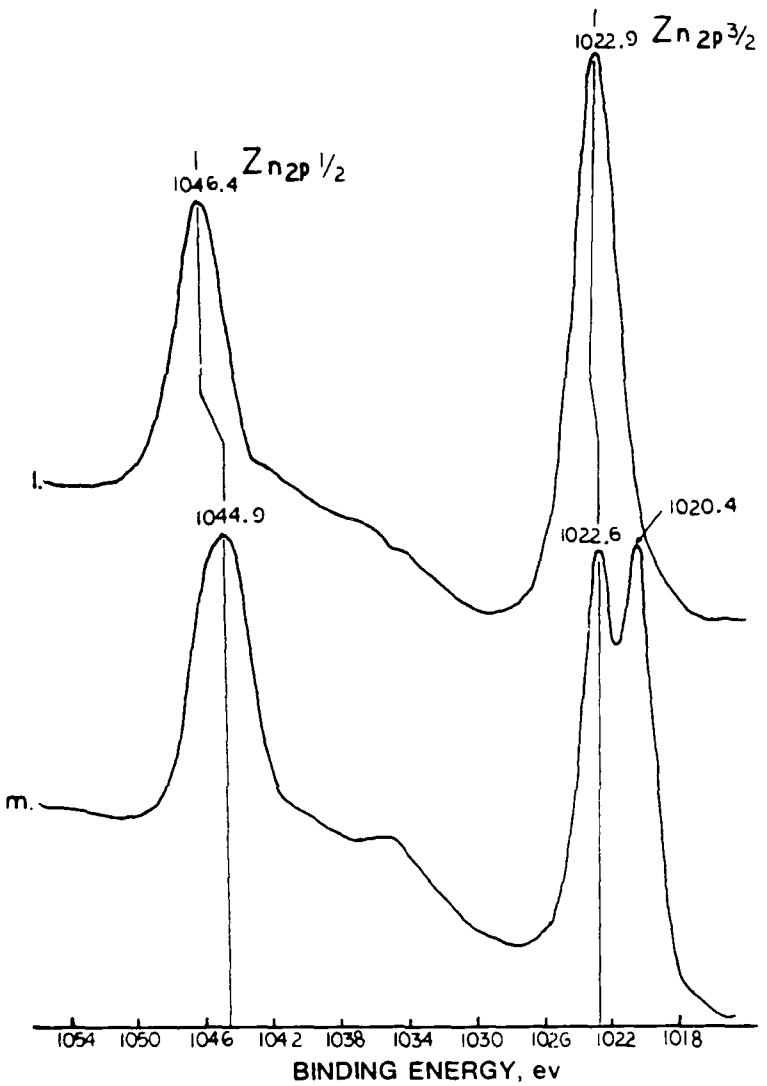

Figure 20. Zn2p regions for unexposed (l) and NaOH - exposed p(AA)-Zn·Ph (m).

When the p(AA)-modified conversion coatings come in contact with a NaOH solution, the reactive Na^+ ion will break the Zn-OOC electrostatic bonds in the interfacial reaction products to form a $-COO^-$ Na^+ salt complex which contains an ionic bond. This transformation from a Zn-O electrostatic bond to a Na-O ionic bond can be expressed as follows:

$$-COO-Zn- + 2NaOH \longrightarrow -COO^{-}\ Na^{+} + NaO-Zn- + H_2O$$

It can therefore be assumed that the precipitation of a salt complexed macromolecule formed by an ionic reaction between the carboxylic anion and the Na^{+} cation during the progression of the alkaline dissolution of the conversion layers can serve as a barrier to the ferrous ion dissociation from the steel. This reflects on the corrosion resistance of the steel.

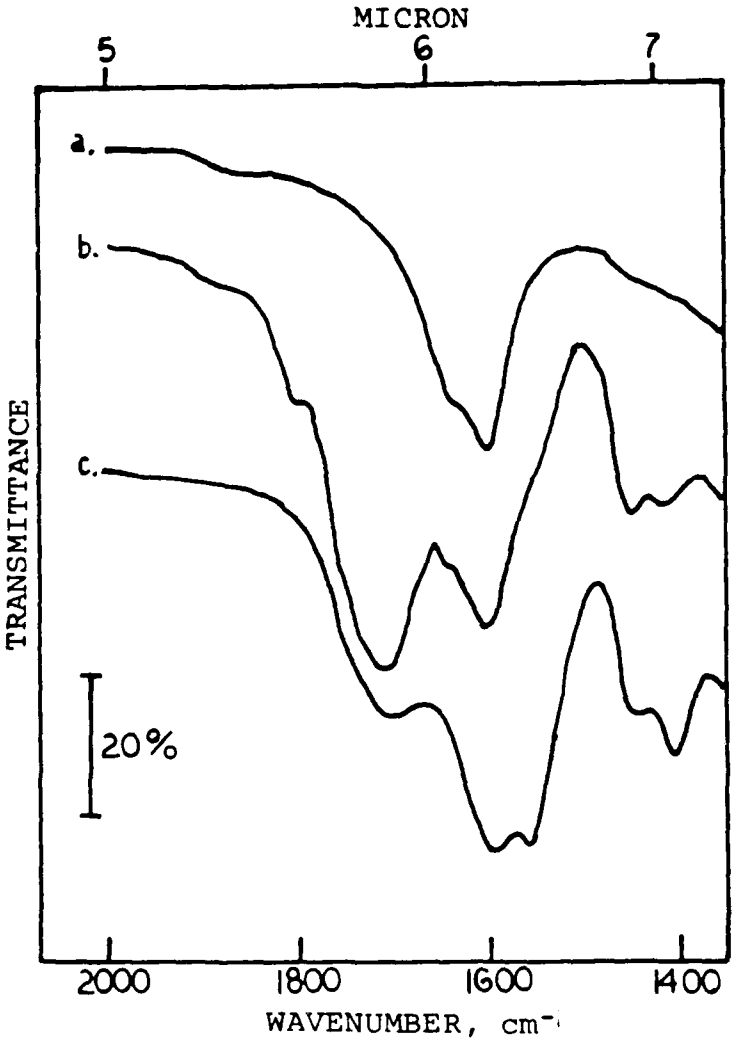

Figure 21. Infrared spectra for $Zn_3(PO_4)_2 \cdot 2H_2O$ powder (a), p(AA)-$Zn_3(PO_4)_2 \cdot 2H_2O$ composite (b) and composite subjected to NaOH exposure (c).

4. Adhesion

The presence of the functional organic groups at the outermost surface sites of the conversion coatings serves to promote the adhesive force between the organic polymer topcoat and the crystal precoat. Therefore, the adhesive ability of the polymer-Zn·Ph composite surface was evaluated from the 180°-peel strength of polyurethane (PU) topcoat films overlaid on the composite surfaces. In Figure 22, test results are given that show the variations in peel strength at PU-to-p(AA), p(IA), p(SSA), p(AMSA), p(VP), and p(AM)-modified and unmodified Zn·Ph interfacial joints. The degree of improvement in adhesive bonds at PU-modified Zn·Ph interfaces appears to depend mainly on the species of the functional groups existing at the surface sites of the Zn·Ph. The PU/p(AA) and p(IA)/Zn·Ph joint systems exhibited a great enhancement of peel strength as the concentration of these polyelectrolytes was increased.

In this series, the highest strength value of 7.1 kg/cm was attained at the adhesive joint between the PU and the 1.5% p(AA)-Zn·Ph composite. This superior bond force corresponds to an improvement of 11 times over that measured for the PU-to-unmodified Zn·Ph joints. The intrinsic adhesion observed at PU-to-single Zn·Ph joints is attributed to a mechanical interlocking bond that anchors the polymer as a result of the penetration of PU liquid resin into the open spaces and surroundings of the rectangular-like Zn·Ph crystals. The p(IA)-Zn·Ph composites also displayed a highly reactive surface, although the maximum peel strength was only 50% of that from the p(AA)-Zn·Ph. The modification of Zn·Ph by p(SSA) and p(AMSA) macromolecules resulted in considerably smaller increases in peel strength. In contrast, the interfacial bond strengths for the surfaces of p(VP)- and p(AM)- Zn·Ph composite systems were not enhanced by the addition of these macromolecules.

It is useful to assess the interfacial bond mechanism responsible for the great enhancement in polymer-polymer adhesion. To gain this information, specular reflectance IR analyses were made. The samples were prepared by spincasting the PU resin onto polyelectrolyte and non-polyelectrolyte-coated aluminum mirrors at 4000 rpm. A PU film with 10^4 nm thickness was overlaid

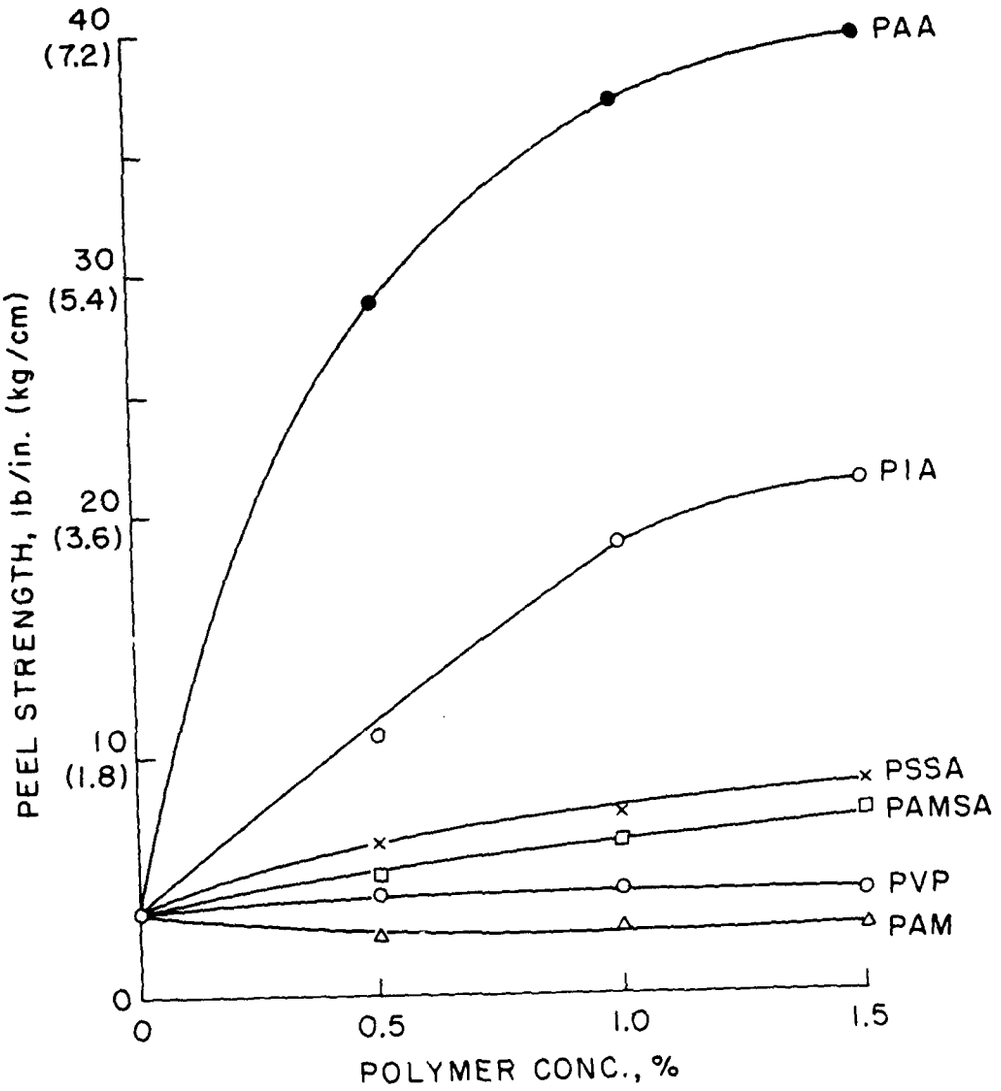

Figure 22. Changes in the 180°-peel strength at PU-to-modified Zn·Ph joints as a function of polyelectrolyte and non-polyelectrolyte macromolecule concentrations.

on the films. The resultant IR spectra, shown in Figure 23, were recorded in the frequency range of 1900 to 1400 cm^{-1}. The spectrum from the PU-coated aluminum mirror in the absence of polyelectrolyte exhibited absorption bands at about 1715, 1590, and 1530 cm^{-1}. These indicate the C=O in amide I, the phenyl, and the C=O in amide II, respectively. Interestingly, spectra obtained from samples having a p(IA) layer showed the formation of new bands at 1680 and 1630 cm^{-1} which can be assigned to newly formed amide I and II groups. Although not shown, the intensity of this new peak rises conspicuously as the p(IA) concentration is increased, whereas that of the isocyanate, N=C=O, at 2260 cm^{-1} tends to decrease. This fact proves that isocyanate groups in PU polymer adjacent to the p(IA) macromolecules can form chemical bonds with the carboxylic acid of p(IA). This interfacial chemical reaction of isocyanate with carboxylic acid induces the formation of the amide I and II.

An IR spectrum quite similar to that for the PU/p(IA) interface was obtained for the PU/p(AA) boundary regions. Therefore, it is believed that the chemical intermolecular reaction is a very important mechanism which greatly enhances the adhesive strength between PU and p(AA) or p(IA) having a carboxylic acid side group. On the other hand, no obvious signs of chemical intermolecular reactions were identified on the IR spectra at the interface of PU/p(SSA), p(AM), and p(VP) joints. The spectra do not show the growth of any new bands or any marked shifting of frequencies in the range of 1900 to 1400 cm^{-1}. Thus, the reason for the slight increase in peel strength of the p(SSA)-modified system may be the result of interdiffusion of PU molecules in the absence of strong chemical interactions.

5. Cathodic Delamination

The effect of p(AA) macromolecules existing at the outermost surface sites of the modified Zn·Ph coatings on the resistance to the cathodic delamination of the polymeric topcoat from the Zn·Ph, was also investigated. In these studies, a polyester-modified polyurethane (PU) topcoat was applied to modified Zn·Ph specimens. The cathodic delamination tests for the PU-coated Zn·Ph specimens were conducted in an air covered 0.5M NaCl solution using an applied potential of -1.5 volts vs SCE for up to 6 days. A defect was made using a drill bit with a diameter of approximately 1 mm. After exposure, the specimens were removed from the cell and allowed to dry. The PU coating was removed by

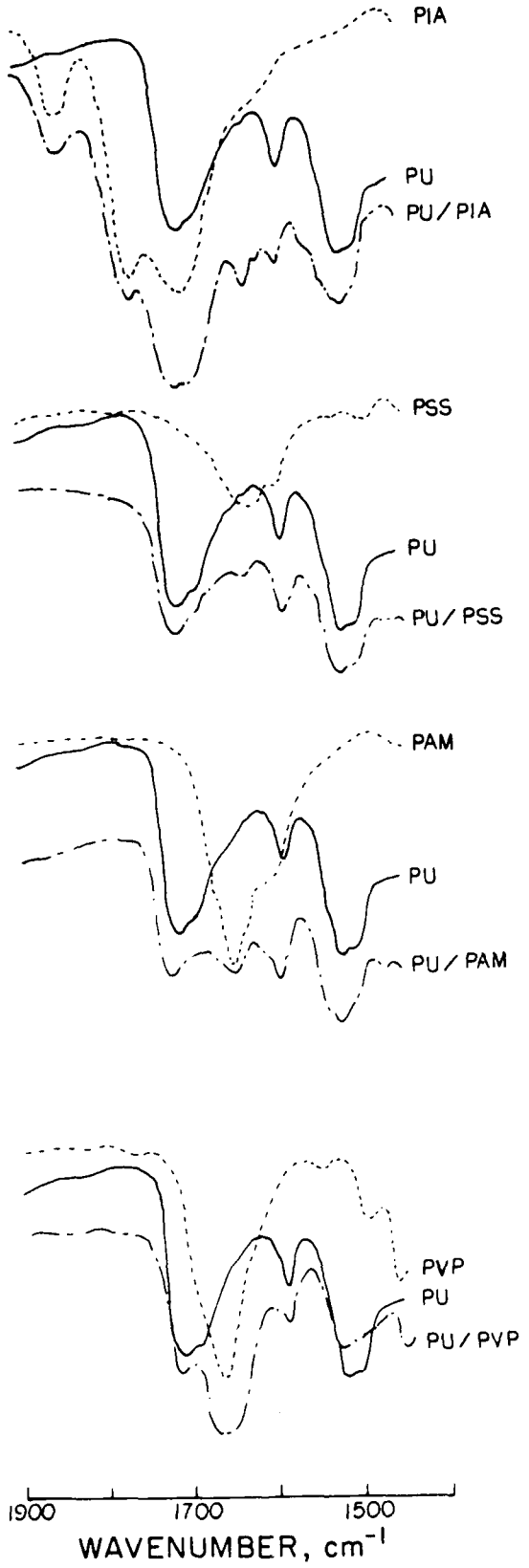

Figure 23. Specular reflectance IR spectra at the interface of PU/p(IA), p(SSA), p(AM), and p(VP) joints.

cutting, and a delaminated region which appeared as a light gray area adjacent to the defect, was detected. Since the 0.5M NaCl electrolyte releases a high concentration of Na^+ ions, the ionic reaction between the OH^- ions generated by the oxygen reduction reaction and the Na^+ ions that migrate through the PU topcoat, can lead to a high NaOH concentration beneath the PU layers.(33) These test results are reported in Table 2. The PU to-blank steel joint systems exhibited considerable delamination of the PU after exposure for only one day. In contrast, the presence of a conversion coating as an intermediate layer in the PU/steel joint system significantly reduced the rate of cathodic delamination. Further improvement was obtained using the p(AA)-modified conversion coating systems. As seen in the table, the delamination rates for the 6 day-exposed specimens decrease with increased p(AA) concentrations ranging from 1 to 5%.

To elucidate the reasons for the above results, the failed interfaces delaminated by the cathodic reaction after exposure for 6 days, were examined using SEM-EDX combined techniques. Both the backside of the PU topcoat and the conversion coating side of the cathodically delaminated PU/unmodified and/5% p(AA)-modified Zn•Ph interfaces were subjected to an inspection of the failure locus. The quantitative data provided by EDX spectra contain the intensity counts per 100 sec of the selected elements and the elemental ratio of an individual element-to-zinc peak counts. The energy regions of the primary lines of Si, P, Cl, Fe and Zn that were used to determine the intensity counts were 1700 to 1850, 1950 to 2100, 2544 to 2706, 6306 to 6519, and 8525-8750 eV, respectively. It should be noted that the line near 900 eV is the primary line of Na overlapped in a secondary Zn line.

Figure 24 shows SEM micrographs and EDX analyses of substrate surface sites after delamination of the PU film from a PU/unmodified Zn•Ph joint system. As seen in the middle photograph on the figure, the SEM topographical image reveals the existance of two discernible areas. Site C represents an area approximately 1300 μm in diameter surrounding a defect and the other, site D, is at the edge of delaminated PU. The top photograph which is an enlargement of site C, discloses that almost all of the crystalline conversion coating surrounding the defect was dissolved by the cathodic reaction occurring in this area beneath the PU film. EDX data from this region indicate the presence of large amounts of Fe and Zn, and small amounts of Si, P and Cl. The Si

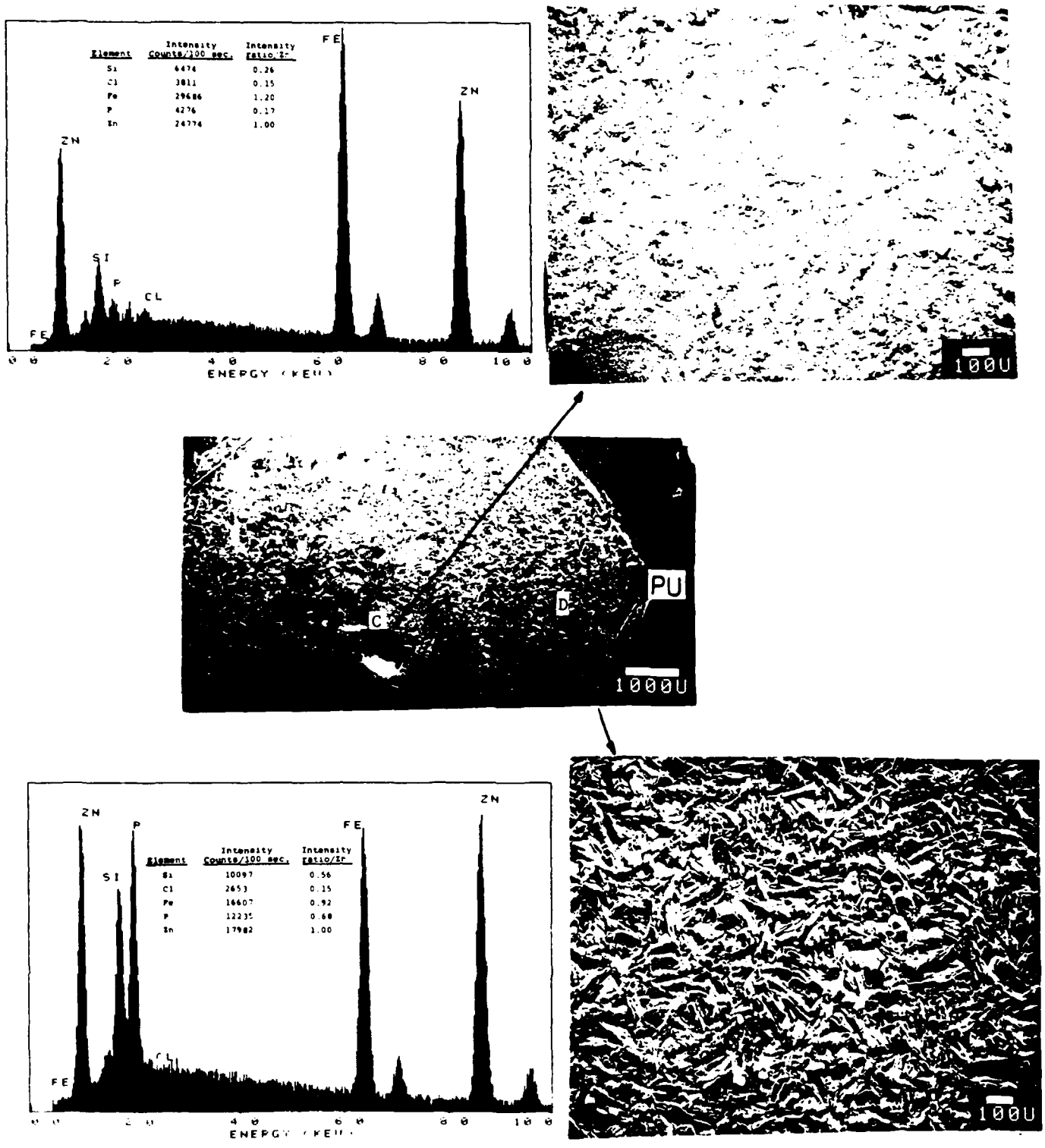

Figure 24. SEM micrographs and EDX analyses near a defect (C) and at the delaminated front (D) of a conversion coating site after removal of the PU film from the PU/unmodified Zn•Ph joint system.

Table 2. Comparison Between the Delaminated Areas of Polyurethane-Coated Steel, Unmodified Zn•Ph, and p(AA)-Modified Zn•Ph Panels Exposed to 0.5M NaCl Solution.

p(AA), %	Delaminated Area, mm^2		
	1 Day	3 Day	6 Day
PU/Steel Joint	113	1256	---
0	0.8	4.9	19.6
1	0.2	2.5	10.8
2	0.2	0.9	7.1
5	0.2	0.9	4.9

originates from the silica flour used as a filler in the PU top coat, and therefore, it infers that a small amount of PU remained on the dissolved coating surface. When compared with the P/Zn ratio for the coating before exposure, the conspicuously lower ratio of 0.17 indicates that a majority of the P atoms was removed from the conversion coating adjacent to the defect. The P seems to have been replaced by Fe which came from the substrate. Hence, the corrosion product formed by the dissolution of the crystal coating was composed of Fe-rich zinc compounds.

The lower portion of Figure 24 shows SEM-EDX results from the site D area. It is apparent from the SEM microstructure features and the high P/Zn and Fe/Zn ratios, that the crystal coating in the region remained on the substrate surface, and that the remaining crystals had a normal zinc phosphate layer containing a large amount of Fe.

A similar analysis was performed for a substrate beneath a film which had delaminated from a PU/5% p(AA)-modified phosphate joint system. These results are given in Figure 25. Again, the delaminated surface appears to have two distinct regions. The first, site E, is an area adjacent to a defect, and the second (site F) is at a delaminating front. The EDX data for site E show mostly Fe associated with very small amounts of P and Zn. This indicates that most of the p(AA)-modified coating was removed from the substrate during the process of delamination.

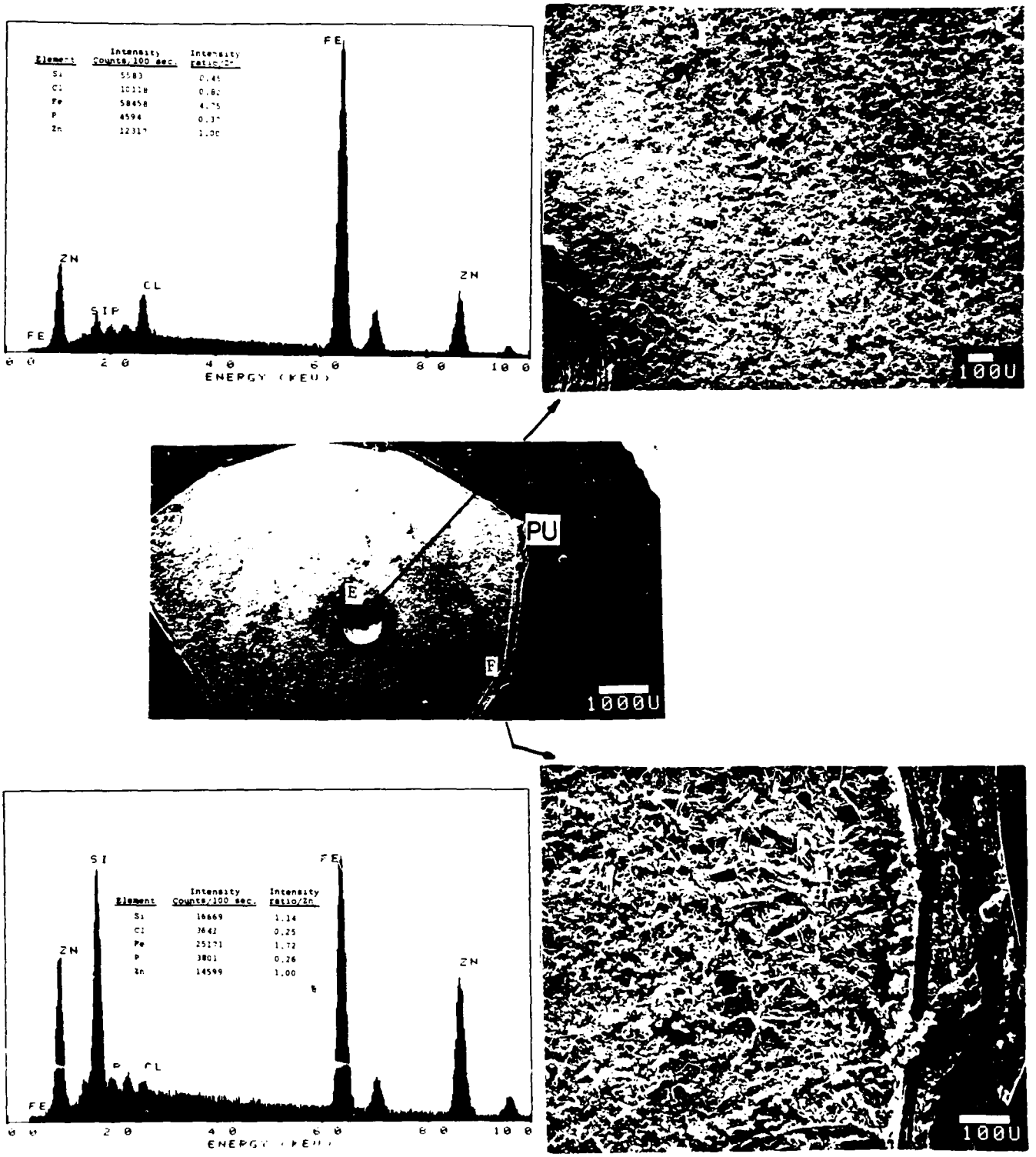

Figure 25. SEM microprobe and EDX analysis near a defect (E) and at the delaminated front (F) of a p(AA)-modified conversion coating after removal of the PU from the PU/5% p(AA)-modified Zn•Ph joint system.

Comparison with the count intensity for the Si line from a region near the defect on the unmodified phosphate surface [see Figure 24 (top)], reveals a weaker line, thereby indicating that the amount of residual PU present is less than that on the unmodified substrate surface. The second area (see bottom SEM-EDX data) was characterized by the presence of a crystalline coating comprised of Fe-rich Zn compounds containing a small amount of P. The total area of these remaining crystals at the delaminating front was found to be much smaller then that observed for the delaminated unmodified one. This relates to the higher bonding forces generated at the interface between the PU and the p(AA)-modified coating.

The backsides of PU films delaminated from unmodified and p(AA)-modified conversion coating surfaces are shown in the SEM images of Figure 26 along with EDX results recorded near a defect. For the former (see top figure), EDX indicates that the predominant element is Si. Other elements present, but with low peak intensities, are P, Fe and Zn. In contrast, the chemical composition of the PU removed from the p(AA)-modified substrate was different. Referring to the SEM-EDX data at the bottom of Figure 26, one of the differences was the presence of Na indicated by the most intensive Na-Zn mix line near 900 eV. The existence of a high Na level is due to migration of Na ions to the p(AA) diffused in the crystal layer in order to form the neutral Na-complex p(AA). In addition, the Si/Zn and Fe/Zn ratios were lower and higher, respectively, than those for the interfacial top coat in the PU-unmodified phosphate joint systems. This information, in conjunction with the SEM images which revealed a rough surface texture for the delaminated PU films, suggests that the amount of the modified crystal coatings which is transferred to the PU sites is relatively larger than that at the PU-unmodified coating interfaces.

The results from the cathodic delamination mechanism studies of the PU/unmodified phosphate joint system are in agreement with those obtained by Leidheiser.[2] Namely, the hydrogen evolution which takes place and the defect lead to blistering of the PU film during the first stage of a delamination process, and then an oxygen reduction reaction at some point away from the defect occurs as the dominant cathodic reaction. The NaOH solution produced by the reaction between the OH^- generated by the oxygen reduction and the migrated Na^+ then acts to dissolve the conversion coatings at the PU/conversion coating

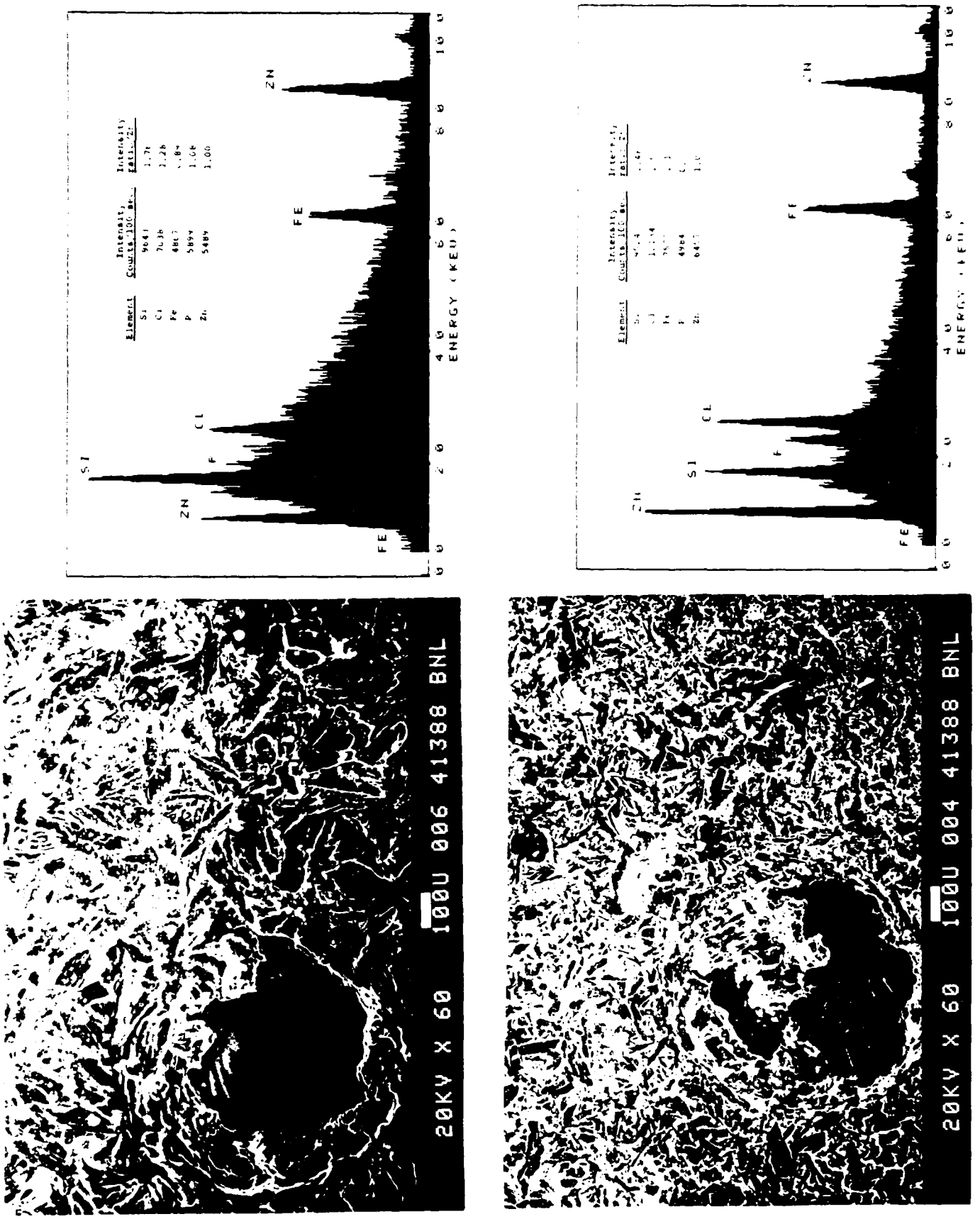

Figure 26. SEM-EDX of adhesive side of PU film delaminated from unmodified (top) and 5% p(AA)-modified Zn·Ph substrates (bottom) near defects.

interfaces. There is no doubt that the high pH environment generated at the leading edge of the delaminated regions results in the dissolution of the conversion coatings which promotes significantly the extent of the cathodic delamination area of PU topcoat from the conversion coating. However, our earlier paper[34] reported that the PU film adjacent to the metal surface in the presence of NaOH is susceptible to hydrolysis. Therefore, the high extent of the delamination areas which are represented by the remaining portions of the conversion crystals on the substrate after delamination of the PU films, seems to verify that the cathodic failures are not only due to the alkaline dissolution of conversion coatings, but also hydrolysis of the interfacial PU film.

On the other hand, in the PU/p(AA)-modified coating joint systems, the major reason for reducing the rate of delamination is the intermolecular chemical reactions between the carboxylic acid groups of p(AA) existing at the outermost surface sites of the conversion coating and the isocyanate groups of PU. The interfacial reaction product formed through the interaction mechanism given below could result in a lower susceptibility to hydrolysis of the particular isocyanate which is essentially hyrolyzed to substitute the primary amine in the presence of NaOH.[35,36]

$$-R\text{-}NCO + HOOC\text{-}R- \longrightarrow -R\text{-}NH\text{-}CO\text{-}O\text{-}CO\text{-}R- \longrightarrow -R\text{-}NH\text{-}CO\text{-}R- + CO_2$$

The above statements suggest that the initial failure in this joint system occurs at the conversion coating/steel interface, in contrast with the PU/conversion coating interfacial regions for the PU-unmodified coating joint systems.

D. Conclusions

The following generalizations can be drawn from our results.

1. The precipitation of a dense crystalline conversion coating on cold-rolled steel by a dissolution-recrystallization process using zinc orthophosphate dihydrate as a starting material, considerably reduced the corrosion rate of steel in an aerated NaCl solution.

2. In deposition processes for polyelectrolyte-Zn·Ph complex conversion precoats on high-strength cold-rolled steel surfaces, the positive surface sites of multiple phosphate crystal embryos at the beginning of the precipitation were strongly chemisorbed by the anionically charged segments of polyelectrolytes having functional carboxylic acid and sulfonic acid pendant groups. The electrostatically segmental chemisorption of polyanions either on newly precipitated nuclei or on growth sites during the primary crystallization processes acts to suppress and delay the crystal growth. In contrast, the magnitude of susceptibility of pendant amide groups to chemisorption on crystal growth sites was very small.

3. When modified with p(AA) electrolyte macromolecules, the conversion coatings yield low hydrogen evolution as well as a less active surface.

4. The precipitation of a large amount of strengite, $FePO_4 \cdot 2H_2O$, formed by adding an excessive amount of p(AA), seems to result in a less effective protective coating.

5. The interfacial reaction products at the p(AA)-zinc phosphate interfaces, were identified to be Zn-OOC complexes yielded by a charge transfer reaction between Zn atoms in the crystalline conversion coating and the electron accepting oxygen portions of the p(AA).

6. The resultant Zn-O electrostatic interfacial bond did not significantly reduce the rate of alkaline dissolution of conversion coatings subjected to NaOH exposure, because of the breakage of the Zn-O bond by the attack of reactive Na^+.

7. The formation of $-COO^- Na^+$ salt complexed macromolecules precipitated by transformation of Zn-O electrostatic bonds into Na-O ionic bonds, improves the corrosion resistance of steel.

8. The intermolecular chemical reaction between the carboxylic groups of the p(AA) existing at the outermost surface sites of the conversion coating and the isocyanate groups in polyurethane topcoats led to a lower rate of cathodic delamination of the polyurethane film from the substrate. Thus, the beginning of the delamination failure occurs

through the conversion coating/steel interface, as compared to that at the polyurethane/conversion coating interface in the polyurethaneunmodified coating joint system.

III. POLYITACONIC ACID COUPLING PRIMERS FOR ADHESIVE BONDING AND CORROSION CONTROL OF ALUMINUM

A. Materials

The aluminum used in the experiments was 2024-T3 clad aluminum (Al) sheet containing the following chemical constituents: 92 wt% Al, 0.5 wt% Si, 0.5 wt% Fe, 4.5 wt% Cu, 0.5 wt% Mg, 0.1 wt% Cr, 0.25 wt% Zn, and 0.15 wt% other. The oxide etch of the Al was prepared in accordance with a well known commercial sequence called the Forest Products Laboratory (FPL) process. As the first step in the preparation, the surfaces were wiped with acetone-soaked tissues to remove any organic contamination. They were then immersed in chromic-sulfuric acid ($Na_2Cr_2O_7 \cdot 2H_2O$: H_2SO_4 : Water = 4 : 23 : 73 by weight) for 10 min at 80°C. After etching, the oxide surfaces were rinsed with deionized water at 25°C, and subsequently dried for approximately 15 min at 50°C. The poly (itaconic acid) was supplied by Polysciences, Inc. For comparative purposes, we employed three other water-soluble polymers, poly(styrenesulfonic acid) [p(SSA)], poly(acrylamide) [p(AM)], and poly(vinylpyrrolidone) [p(VPD)]. All of these polymeric macromolecules, having an average molecular weight in the range of 40,000 to 120,000, were dissolved in water to prepare a 0.05 to 1.0% solution. These polymer films were deposited on the FPL-etched Al surfaces in the following way. First, the adherend was dipped for 5 min into the macromolecule aqueous solutions that were kept at 25°C. After wetting the hydrated Al_2O_3 surface with the macromolecule solution, the adherends were dried in an oven at 150°C for 1 hr to transform the macromolecule from solution to a solid film. The thickness of the primer film deposited on the adherend surfaces was then determined by auger electron spectroscopy (AES), as described earlier.[14] The average thickness of the films prepared using macromolecule concentrations of up to 1.0% ranged approximately from 1 to 50 nm. With all of the polymers that we used, a concentration of <0.1% produced a film of <4 nm in thickness. The use of a 0.05% macromolecule concentration produced a near-monolayer thickness.

Commercial-grade polyester-based polyurethane (PU) M313 resin, supplied by the Lord Corporation, then was applied as an elastomeric topcoating. The polymerization of the silica-filled PU was carried out by incorporating a 50% aromatic amine curing agent, M201. The topcoat system was then cured in an oven at 80°C.

B. Measurements

Identifications of the failure locus occurring at the interface of adhesive/primer/adherend joint systems and the Al-p(IA) interfacial reaction mode were made on the basis of the peak areas, determination of binding energies, and peak heights deduced from X-ray photoelectron spectroscopy (XPS). The spectrometer used was a V.G. Scientific ESCA 3 MK II. The exciting radiation was provided by an aluminum Kα X-ray source operated at a constant power of 200 W (10 kV, 20 mA). The vacuum in the analyzer chamber of the instrument was maintained at 10^{-9} Torr throughout the experiments.

The image of the surface microtopography for p(IA)-covered Al surfaces was conducted with an AMR 100-Å scanning electron microscope (SEM).

A Perkin-Elmer Model 257 spectrometer was used for specular reflectance infrared (IR) spectroscopic analyses. To detect the changes in the molecular structure of p(IA) and to identify the interfacial interaction mechanisms of PU-p(IA) joints, IR spectra were obtained for samples overlaid on the reflective Al surfaces.

Peel strength tests of adhesive bonds at the polyurethane topcoat-modified aluminum substrate interfaces were conducted at a peel angle of $\sim$180° and a crosshead speed of 5 cm/min. The test specimens consisted of one piece of flexible polyurethane topcoat, 2.5 by 30.5 cm, bonded for 15.2 cm at one end to one piece of flexible or rigid substrate material, 2.5 by 20.3 cm, with the unbonded portions of each member being face to face. The polyurethane topcoat overlaid on the complex crystal surfaces was $\sim$0.95 mm thick.

In an attempt to gain information regarding the effectiveness of the interfacial reaction products as a corrosion protective layer on FPL-etched Al surfaces, the polarization behavior of Al surfaces in p(IA)/Al and PU/p(IA)/Al joint systems was determined.

The electrochemical testing for data on corrosion was performed with an EG & G Princeton Applied Research Model 362-1 Corrosion Measurement System. The electrolyte was a 0.5 M NaCl solution made from distilled water and reagent grade salt. The specimen was mounted in a holder and then inserted into a EG & G Model K47 electrochemical cell. The tests were conducted in an aerated 0.5 M NaCl solution at 25°C, and the exposed surface area of the specimens was 1.0 cm^2. For these tests, the PU topcoat on the 3.5-nm thick p(IA)-coated Al and uncoated Al surfaces was applied by spin-coating at 4000 rpm. The thickness of the deposited PU film was approximately 500 nm.

C. Results and Discussion

1. p(IA)-Etched Al Interfaces

ESCA survey scans of unetched and FPL-etched aluminum surfaces are shown in Figure 27. The spectrum for the as-received aluminum substrate indicates the presence of an intense C_{1s} peak and a strong oxygen (O_{1s}) peak. The former is mainly ascribed to the residual organic solvent which was used to remove organic contamination from the substrate surfaces. Small silicon peaks (Si_{2p} and Si_{2s}) were also identified. The Al peak intensity was too weak to be detected on the survey scan. Thus, the unetched surface appeared to be overlaid with a removable thin film consisting of oxidized silicon and carbon contaminants. These poorly adhered contaminants are easily removed by immersion in a chromic acid solution. The ESCA spectrum for the FPL-etched substrate surface is characterized by an intense oxygen signal, the appearance of Al, Ca, and Cu peaks, and a conspicuous reduction in the carbon and silicon peak intensities, as compared with those from the unetched surfaces. The presence of calcium can be interpreted as another contaminant which is present beneath the oxidized Si and C films.[37] Although not shown in the figure, a weak peak intensity at around 1074 eV indicated the presence of a small amount of Na.

The number of hydrated polar surface groups on the oxide films increases with etching time. It is also known that the presence of exceedingly thick oxide or hydroxide layers results in a decrease in surface structure strength and a poor adhesive bond in aluminum-to-polymer joints.[38]

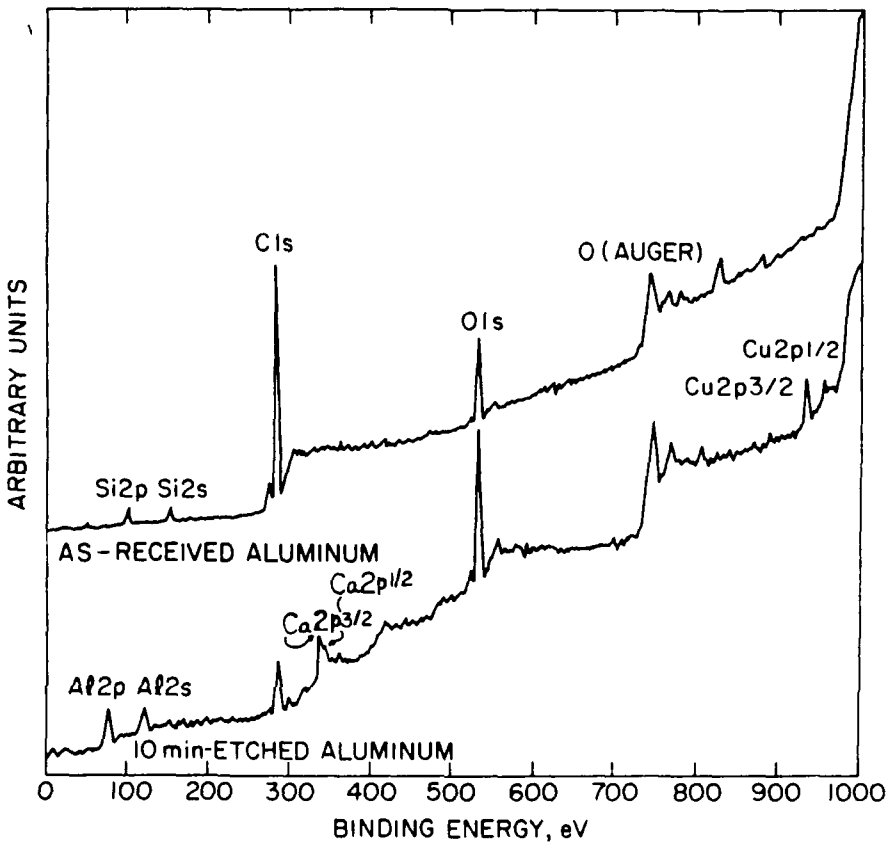

Figure 27. ESCA survey-scan spectra for the surfaces of unetched and 10-min-FPL-etched aluminum.

In order to study the concept concerning intermolecular reactions in the p(AA)-to-etched aluminum joints, samples were prepared in accordance with the following procedure: The 10-min-etched substrates were dipped for 5 min into a 0.05% p(IA) aqueous solution at a temperature of 25°C. After wetting the surfaces with the p(IA) solution, the substrates were placed in an oven at 150°C for 1 hr to remove water. The p(IA)-coated substrate surfaces were then immersed for 1 hr in a deionized water-filled ultrasonic bath at 50°C to remove the washable p(IA) macromolecules. Any residual p(IA) that remained on the substrate surface was subsequently dried for 1 hr in a vacuum oven at 150°C and

stored in a desiccator prior to performing the ESCA analysis. Since the adhesion is a fundamental local phenomenon involving only a few atom layers of adherend and adhesive, the resultant data from the ESCA studies should contribute toward an understanding of the chemical interaction behavior and role at the p(IA)-hydrated oxide film interface and, in part, define the ability of the p(IA) polymer to function as a primer coating.

Although the actual data are not presented in any of the figures, preliminary examinations of wide scan ESCA spectra for residual p(IA) surfaces revealed Al_{2p} peaks of substantial intensity. This suggested that certain areas of the hydrated oxide film surfaces were covered with a thin, no thicker than 5 nm, p(IA) layer which corresponds to the escape depth of the aluminum photoelectrons. Such areas probably represent the interface regions which are of primary interest in this study of the intermolecular reaction at the interface between the p(IA) and the hydrated surfaces.

Figure 28 shows the C_{1s} and Al_{2p} core level spectra for the p(IA)-coated Al_2O_3 surfaces. In the C_{1s} region, the spectrum (Figure 28-a) of the bulk p(IA) indicates the presence of two different carbon species in the binding energy (BE) range of 290.0 - 284.0 eV. The predominant peak at 285.0 eV was calibrated with the contribution of the hydrocarbon-type carbon. The component at 289.2 eV can be assigned to carbon originating from the carboxylic acid, COOH, in p(IA). In the spectrum (Figure 28-b) for the p(IA) at the p(IA)-Al_2O_3 interface regions, attention was given to the peak shifting of COOH to a lower BE site. Conversely, the Al peak (Figure 28-d) for Al_2O_3 at the interfaces shifted to a higher BE site, as compared to that of the Al_2O_3 itself (Figure 28-c). Although not shown in the figure, the O_{1s} core level indicated the presence of a peak at 531.7 eV which ascribes to the formation of COO-metal complexes. These data indicate that the charge transfer from the Al in Al_2O_3 to the electron-accepting carboxylate oxygen portion, $^-OOC-$, in p(IA) occurs at the interfacial boundary. As a result, a possible interfacial bond transition is as follows:

$$\underset{\text{R-C-O}^-\text{----}^+\text{H}_2\text{O-Al-(on surface)}}{\overset{\text{O}}{\parallel}} \xrightarrow[-\text{H}_2\text{O}]{\Delta\text{H}} \underset{\text{R-C-O}\longleftarrow\text{Al-(on surface)}}{\overset{\text{O}}{\parallel}}$$

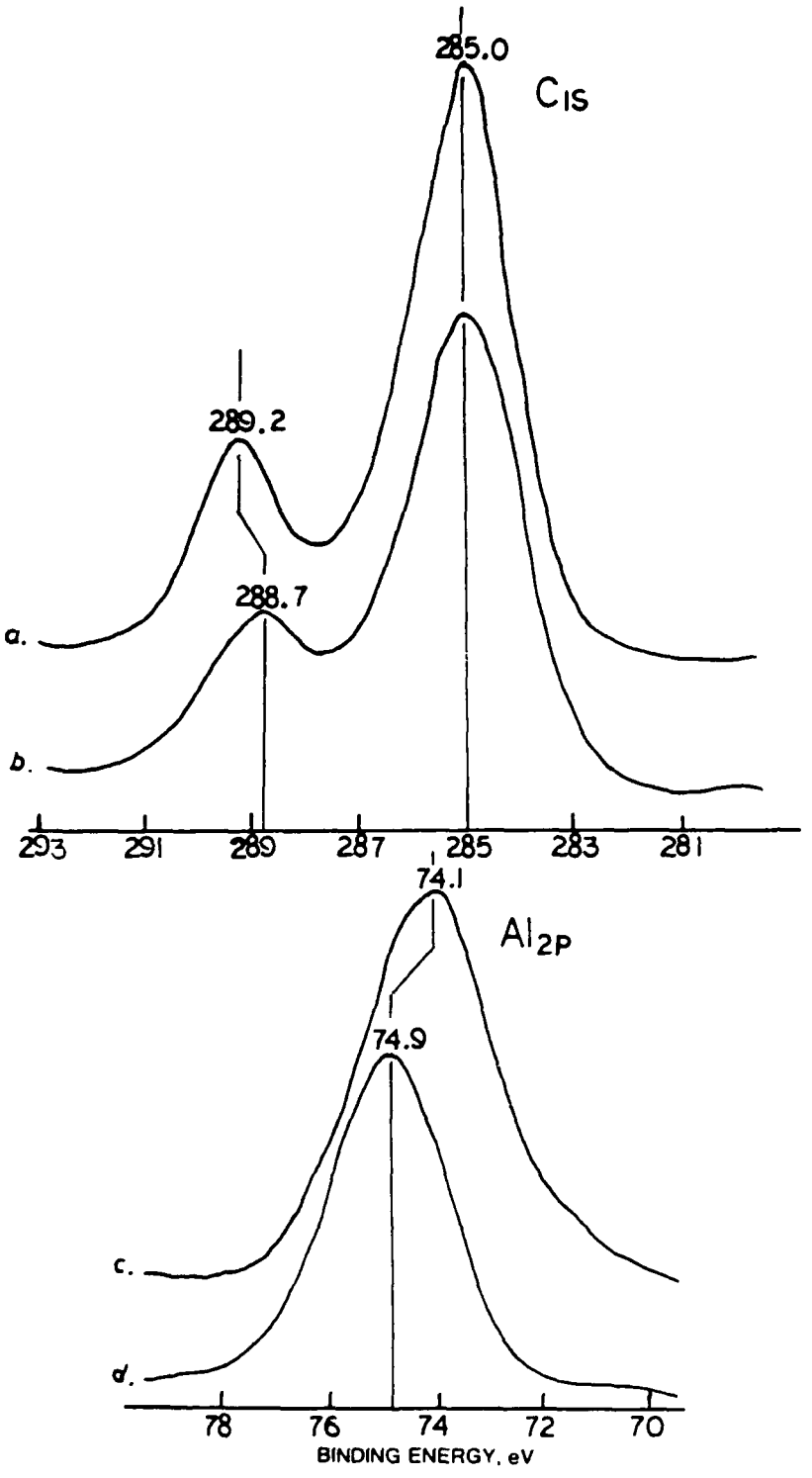

Figure 28. C_{1s} and Al_{2p} regions of bulk p(IA) surface (a), Al_2O_3 surface (c), and the p(IA)-Al_2O_3 interfaces (b and d).

This reaction could play an essential role in improving the interfacial bond forces and in converting the hydrophilic nature of COOH and OH groups into less hydrophilic interfacial reaction products. Further, the interface structure produced by the chemical interaction could be responsible for the stability of adhesive bonds with this pretreatment, especially in a wet environment.

Figure 29 shows the images of uncoated and 0.1% p(IA)-coated 10-min-etched aluminum surfaces. The morphological feature of the etched surface (Figure 29A) exhibits crater-like pits having a wide range of diameters that vary from 0.25 to 2.25 μm. As reported by Smith,[39] the fresh sharp metal ridges surrounding each pit with 10 to 20 nm of oxide or hydroxide would give a highly reactive surface nature. When the reactive surfaces are left in the atmosphere, the active metal ridges instantly react with moisture. The topographical image of a 0.1% p(IA)-coated surface (Figure 29B) was characterized by a continuous layer of a thin p(IA) film coating the entire surface of the large and small pits.

2. Adhesion Durability

The PU-coated adherend specimens were exposed to a 0.1 M NaOH solution at 80°C for 30 hr. All of the edges on the adhesive/primer/ adherend joints were left unprotected to evaluate the susceptibility of the interfacial bonding to the hot alkaline solution. This evaluation was made on the basis of data obtained from 180° peel-strength tests performed before and after exposure. Figure 30 shows some of the data, expressed as a function of the macromolecule concentration of the aqueous solution applied to the etched Al surface. Each value in the figure represents the average of three measurements made for each concentration of primer.

After peel-testing, the Al_2O_3 adherend surface sites were examined to identify the locus of adhesive failure. This was accomplished by comparing the XPS peak areas, which then were converted into elemental concentrations by means of the differential cross sections for core-level excitation.[40,41] The internally generated C_{1s}, Al_{2p}, Si_{2p}, S_{2p}, N_{1s}, O_{1s} and Na_{1s} peak areas were used to obtain the atomic percent ratios. The high-resolution spectrum of the C_{1s} region also was investigated to obtain further information on the

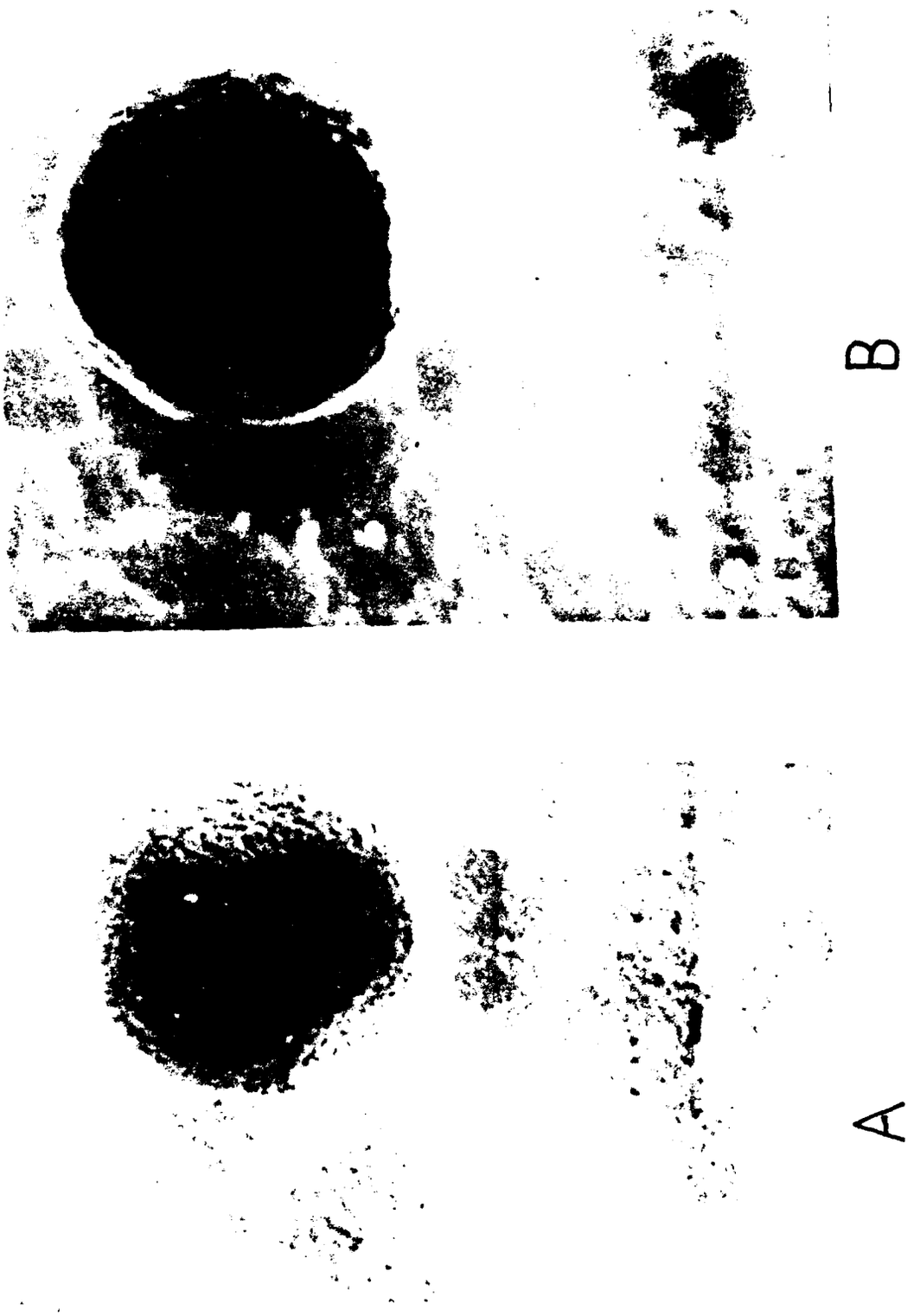

Figure 29. Comparison of micrographs between (A) a 10-min-etched aluminum surface and (B) a 0.1% p(IA)-coated surface.

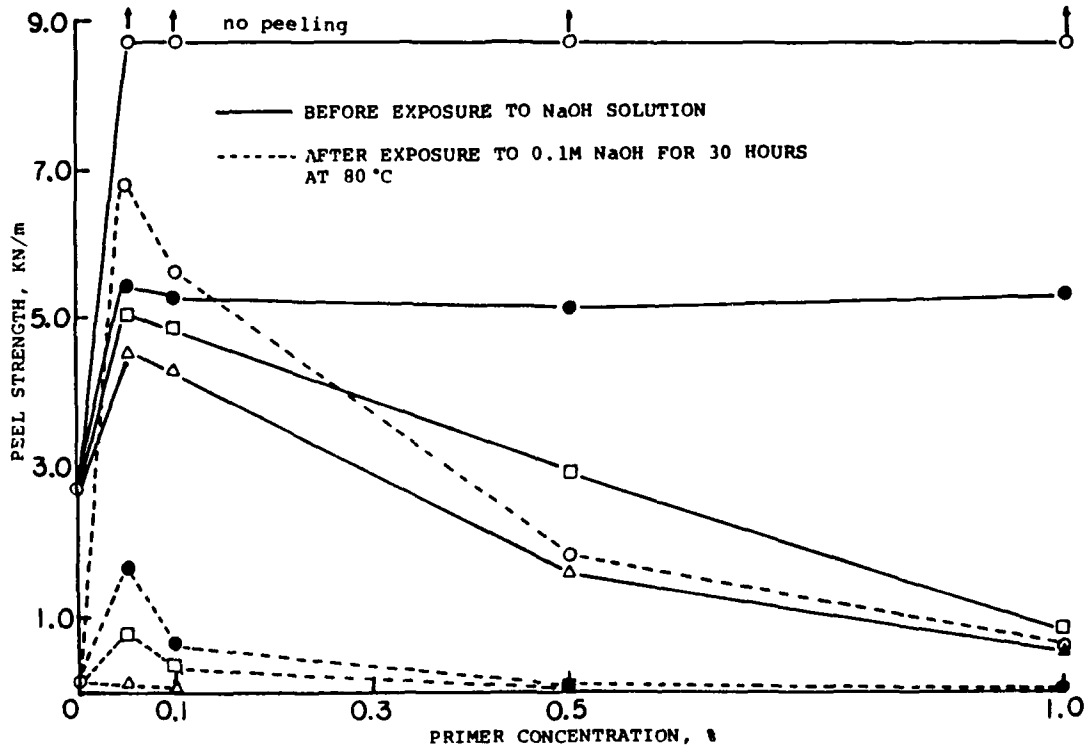

Figure 1. Peel strength as a function of primer concentration for the PU/p(IA)/Al (o), p(VPD)/ (●), /p(AM)/ (□), and /p(SSA)/ (△) joint systems before and after exposure for 30 hr to hot alkali at 80°C.

Figure 30. Peel strength as a function of primer concentration for the PU/p(IA)/Al (o), p(VPD)/ (●), /p(AM)/ (□), and /p(SSA) (△) joint systems before and after exposure for 30 hr to hot alkali at 80°C.

mode of failure. Since all of the adhesive and primer materials used have hydrocarbon-type carbon ($\gtrless$C-H and $\gtrless$C-C$\lessgtr$) as a main component of their macromolecules, the binding energy (BE) for the predominating C_{1s} signal was referred to hydrocarbon. Therefore, the BE was set at 285.0 eV, a value standardized by several investigators. These data were then correlated directly with the peel strengths.

The resultant quantitative data and the XPS spectra for the C_{1s} region of the peeled Al_2O_3 interfaces, before and after exposure to the hot alkaline solution, are given in Table 3 and Figures 31 to 34. For unexposed PU/Al_2O_3 specimens that did not have an intermediate primer layer, (the controls), the peel strength was 2.68 kN/m (Figure 30), and the atomic percent ratios of Al/C, Si/C, N/C, and O/C for the peeled Al_2O_3 interfaces were 0.31, 0.08, 0.04, and 0.70, respectively, (Table 3). The presence of Si is associated with the

Table 3. XPS analyses of Al_2O_3 surfaces removed from PU adhesive, before and after exposure to 0.1 M NaOH at 80°C for 30 hr.

		Atomic percent ratio					
Joint System	Exposure to NaOH	Al/C	Si/C	S/C	N/C	O/C	Na/C
PU/Al_2O_3	Before	0.31	0.08	0.0	0.04	0.70	0.0
	After	0.50	0.16	0.0	0.07	0.79	0.03
PU/0.05%p(IA)/Al_2O_3	After	0.12	0.08	0.0	0.05	0.42	0.02
PU/1.0% p(IA)/Al_2O_3	After	0.02	0.10	0.0	0.04	0.31	0.0
PU/0.05%p(VPD)/Al_2O_3	Before	0.29	0.06	0.0	0.06	0.45	0.0
	After	0.45	0.13	0.0	0.05	0.60	0.0
PU/0.05%p(AM)/Al_2O_3	Before	0.23	0.06	0.0	0.05	0.45	0.0
	After	0.28	0.10	0.0	0.05	0.46	0.0
PU/1.0%p(AM)/Al_2O_3	Before	0.0	0.04	0.0	0.26	0.41	0.0
PU/0.05%p(SSA)/Al_2O_3	Before	0.31	0.04	0.03	0.05	0.56	0.0
	After	0.34	0.12	0.01	0.07	0.80	0.02

silica flour used as a pigment in the PU adhesive. Therefore, it is reasonable to conclude that the failure occurring at the PU-Al_2O_3 joints is probably due to a mixed mode of cohesive (in the PU) and adhesive failure. The latter failure mode can be recognized from the expression of pronounced peak intensity of Al and the presence of Al_2O_3 at 73.7 eV in the Al_{2p} region. The spectrum for the C_{1s} region (Figure 31-a) displays the typical features of a PU signal which could be resolved into components situated at 285.0, 286.5, and 288.8 eV. Published data indicate that the major carbon peak at 285.0 eV includes contributions from the aliphatic CH_2 carbon and the aromatic carbon, since these two peaks appear at approximately the same position.[42,43] The shoulder at 286.5 eV can be assigned to diphenylic carbons joined to O and N, such as $\geq\underline{C}$-O- and $\geq\underline{C}$-N$<$, and the small peak at 288.8 eV is due to the carbonyl carbons.

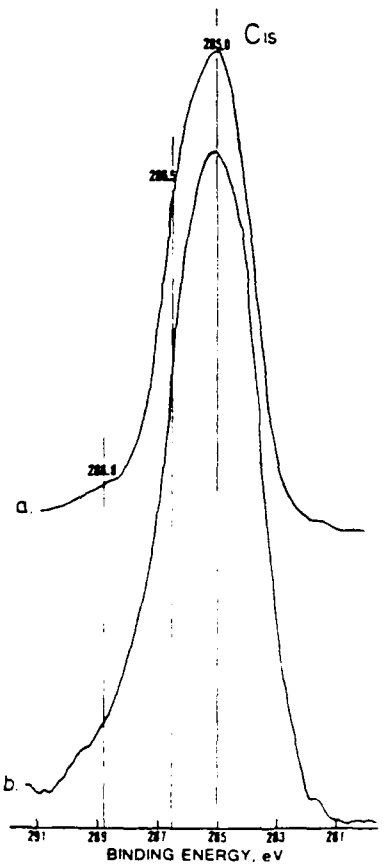

Figure 31. C_{1s} spectra of peeled Al_2O_3 surfaces from PU/Al_2O_3 joints before (a) and after (b) exposure. Integrated intensity ratio of C(C-N and C-O)/C(CH_2) (a) 0.52; (b) 0.29.

After exposure to hot alkali, the strength of the control specimens dropped dramatically, to a value of 0.05 kN/m, a reduction of 98%. Also, a partial separation of the PU film from the Al_2O_3 surface occurred. The XPS analysis of the interface indicated the presence of significant amounts of Al, Si, and O on the peeled Al_2O_3 surface sites. These data, shown in Table 3, indicate that the failure probably occurred at the interface between the PU and the Al_2O_3. After exposure, the features of the C_{1s} region, as compared with those for the unexposed control, are characterized by a stronger peak which represents the hydrolytic disintegration of PU at the interface (Figure 31-b). In the presence of NaOH, despite substituting the ester for the acid portion, the principle product yielded by the hydrolysis of both isocyanate and urethane groups in PU coatings is the primary amine,[36,44]

$$- NCO + H_2O \longrightarrow - NHCOOH \longrightarrow - NH_2 + C$$

$$- NHCO_2-R + H_2O \longrightarrow -NH_2 + CO_2 + ROH.$$

Thus, this becomes more readily apparent from a consideration of the integrated intensity ratios between the C (C-N and C-O) peak at 286.5 eV and the C (CH_2) peak at 285.0 eV. The resultant C(C-N and C-O)/C (CH_2) intensity ratio for the exposed interfaces was much lower than that for the unexposed one (Figure 31). Therefore, we believe that the polyurethane adjacent to the Al_2O_3 surface is very susceptible to hydrolysis. This fact is consistent with the high Si/C ratio, thereby indicating that a large amount of the SiO_2, which is used as a pigment in the PU, is left on the Al_2O_3 surfaces.

The peel strength of the unexposed control specimens was increased by more than three times when a p(IA) intermediate primer layer was applied (Figure 30). No peeling occurred when a primer concentration of only 0.05% was used, and a strength of at least 8.7 kN/m was attained. Thus, the application of p(IA) primer to the Al_2O_3 surface results in strong adhesive bonding in PU/Al_2O_3 joint systems.

As denoted in Figure 30, the durability of the exposed p(IA)-primed joint systems was strongly dependent upon the p(IA) concentration. The deposition of a thin p(IA) film (approximately 1 nm thickness) derived from the addition of

a 0.05% solution, resulted in a reduction in strength of only 22% after 30 hr exposure to 0.1 M NaOH at 80°C. The addition of 0.5% p(IA) which corresponds to a film thickness of approximately 8.5 nm, resulted in approximately 80% retrogression in strength. Further retrogression was noted when a 1.0% concentration (50 nm thickness) was used. Based upon these observations, it is important to understand why a p(IA) film of near-monolayer thickness is more effective in improving the durability of adhesion than a thicker film. We attempted to resolve this question, primarily on the basis of information obtained from XPS analyses. Referring to Table 3, the Si/C, N/C and O/C ratios for the exposed 0.05% p(IA) systems have values similar to those for the unexposed PU/Al_2O_3 control systems. In addition, the C_{1s} region (Figure 32-c) clearly shows the signal intensities of the carboxylic acid carbons of p(IA) at 288.9 eV. Therefore, it is reasonable to assume that cohesive failure of PU/0.05% p(IA)/Al_2O_3 joints after exposure occurs in the mixed region of PU

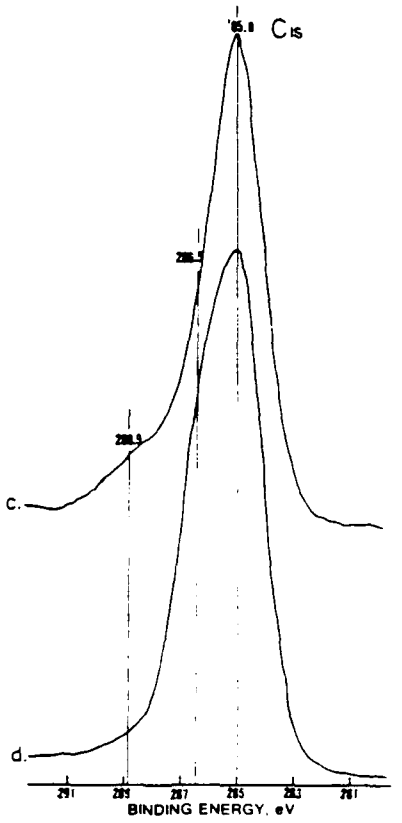

C_{1s} peaks of Al_2O_3 surface removed from PU/0.05% p(IA)/Al_2O_3 (c) and /1.0% p(IA)/ (d) joints after exposure. Integrated intensity ratio of C (C-N and C-O)/C (CH_2): (c) 0.38; (d) 0.66.

Figure 32. C_{1s} peaks of Al_2O_3 surfaces removed from PU/0.05% p(IA)/Al_2O_3 (c) and /1.0% p(IA)/ (d) joints after exposure. Integrated intensity ratio of C(C-N and C-O)/C(CH_2):(c) 0.38; (d) 0.66.

and p(IA). In contrast, the presence of a thick p(IA) film, produced with a 1.0% concentration, resulted in a lower Al/C ratio. This may mean that the locus of failure was not at the Al_2O_3 surface. Referring to Figure 32-d, the features of the C_{1s} regions for this surface indicate the presence of a shoulder at 286.5 eV that closely resembles that from the unexposed PU/Al_2O_3 joint system (Figure 31-a). Hence, the cohesive failure occurred within the PU layer adjacent to the PU-p(IA) mixed layer.

This conclusion was further supported by comparisons of the C (C-N and C-O)/C (CH_2 and $\geqslant$C-C$\leqslant$) ratios for 0.05 and 1.0% p(IA) joint systems. As seen in Figure 32, the ratio for the 1.0% p(IA) joint system is markedly higher than that for the 0.05% system. Since the free COOH groups in the p(IA) primer were neutralized by Na+ ions in the NaOH solution, the possible reason for the significant decrease in peel strength resulting from a thick p(IA) intermediate layer is the transformation of the p(IA) macromolecule which contains abundant residual COOH groups, into Na-neutralized p(IA) complexes. This leads to the conversion of the primer from a solid to a gel, leading to increased water absorption, penetration, and swelling at the interfacial regions, and ultimately, failure. Therefore, the poor durability of the adhesion bonds is due to failure of the primer.

From these observations, we conclude that the formation of a thin film of a near-monolayer thickness is much less susceptible to hydrolysis because of the reduced presence of free hydrophilic groups in the intermediate layers. In such a case, most of the COOH groups in the monolayers will react chemically with the available reactive groups occupying the outermost interfacial sites on the PU and Al_2O_3, and the progression of this interfacial reaction will transform a hydrolytically unstable interface to a stable one.[14] Producing this transformation at the interfaces is the most important factor in achieving long-term bond durability in chemically aggressive environments.

In comparison, p(VPD), p(SSA), and p(AM) primers are less effective than p(IA) primers for unexposed joint systems. For p(VPD) systems, the use of a primer concentration of 0.05% increased the strength by approximately 90%, and this value appeared to be independent of concentration (Figure 30). Quantitative XPS data from the failed surface at 0.05% p(VPD) concentration indicated a high Al/C ratio and a relatively low Si/C ratio (Table 3). In the C_{1s}

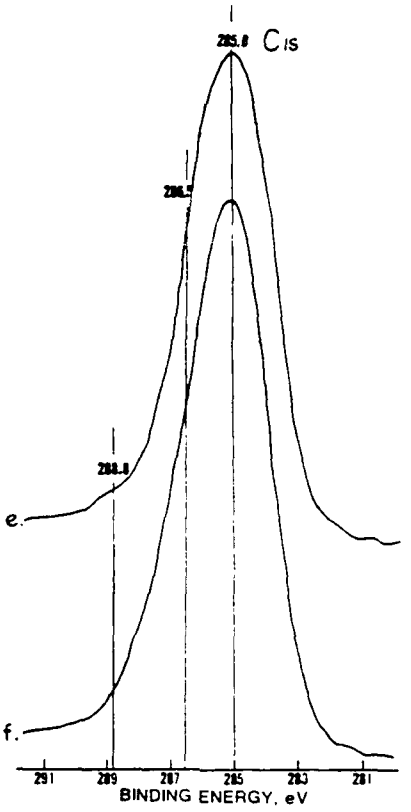

Figure 33. XPS spectra of C_{1s} region for peeled PU/0.05% p(VPD)/Al_2O_3 systems before (e) and after (f) exposure. Integrated intensity ratio of C(C-N and C-O)/C(CH_2): (e) 0.34; (f) 0.19.

region (Figure 33-e), the peak assignment at 288.8 eV is associated with the C=O of PU and the C=O in the pyrolidone, 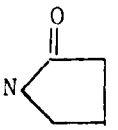 . These data suggest that the failure was not a cohesive one through the PU-p(VPD) mixed layer, but one that occurred near the Al_2O_3 surface. Therefore, one possible explanation is that the magnitude of the interfacial bonding between the Al_2O_3 and the p(VPD) primer is less than that for the PU-to-p(VPD) interfacial bond.

This weak bonding resulted in a noticeable reduction in strength upon exposure to hot alkali. The results from XPS-analyses of peeled Al_2O_3 sites from the exposed 0.05% p(VPD) systems, showed enhanced ratios of Al/C, Si/C and O/C. There were also more intensive C_{1s} peaks (Figure 33-f) and a lower C (C-N and C-O)/C (CH_2) ratio, as compared with those from the unexposed sample.

These findings clearly verify that the failure mode is an adhesive one, through the Al_2O_3/mixed polymer interface. In addition, the interfacial mix polymer layer appeared to be hydrolytically disintegrated; this high susceptibility of the mixed layer results from the inability of the hydrophilic groups in p(VPD) and PU to chemically interact. The relationship between the peel strength and p(VPD) concentration also shows that the rate of reduction in strength increases with an increase in primer concentration. This trend is quite similar to that for the p(IA)-primed joint systems.

For the p(AM) and p(SSA) joint systems, the strengths of the unexposed specimens depend upon the concentration of primer. Figure 30 shows that increases in strength were attained when concentrations of up to 0.05% were used, but further additions resulted in reductions in strength. In the case of the unexposed 0.05% p(AM) system, the ratios of Al/C, Si/C and N/C at the peeled Al_2O_3 surfaces exhibited values similar to those from the 0.05% p(VPD) system. In addition, the shoulder at approximately 288.0 eV in the C_{1s} region (Figure 34-g) indicates the existence of the carbonyl carbon of p(AM). Thus, the failure probably proceeded near the Al_2O_3/mixed layer interface, a mode similar to that for the 0.05% p(VPD) system. The reason for the loss of strength with increased thickness of primer was ascertained from investigations of the atomic ratio and the C_{1s} peak feature of the 1.0% p(AM) system. The XPS data showed a large deficiency of Al and a low ratio of Si/C, thereby implying that the failure occurs through the p(AM) intermediate layer. This information was supported further by comparisons of the C_{1s} peak features from samples containing 1.0 and 0.05% concentrations of p(AM). As shown in Figure 34-h, the typical C_{1s} doublet peak indicates a large amount of p(AM) remains on the Al_2O_3 surface sites, thereby, indicating the weakness of the primer film.

The failed surface for the exposed 0.05% p(AM) system was characterized by increased Al/C and Si/C ratios, low intensity shoulder peaks at 288.0 and 288.8 eV in the C_{1s} region (Figure 34-i), and a low C (C-N and C-O)/C (CH_2) ratio. This information is consistent with the exposed PU/0.05% p(AM)/Al_2O_3 joint system having a failure mode similar to that for the exposed 0.05% p(VPD) system.

The p(SSA) primer systems had characteristics similar to those of the p(AM) primer. Specifically, the bond strength of the unexposed joint system containing a 0.05% p(SSA) layer was significantly reduced by exposure to hot

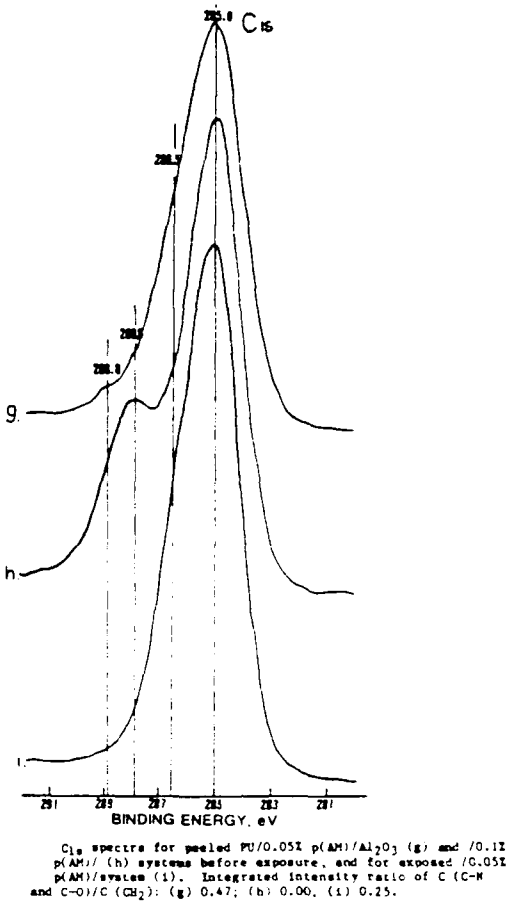

Figure 34. C_{1s} spectra for peeled PU/0.05% p(AM)/Al_2O_3 (g) and /0.1% p(AM)/(h) systems before exposure and for exposed /0.05% p(AM)/system (i). Integrated intensity ratio of C(C-N and C-O)/C(CH_2): (g) 0.47; (h) 0.00; (j) 0.25.

alkali. This noticeable loss of adhesion at the joints can be explained from the XPS inspections of the failed surface. The resulting data (Table 3) indicate a high Si/C and a low S/C ratio, and suggest that failure results from hydrolysis-induced dissolution of the PU-p(SSA) mixed layer adjacent to the Al_2O_3 surface. We note that the sulfur, detected as a S/C ratio, appears to be coming from the sulfonic acid groups of p(SSA).

On the basis of all of these results, it appears that the application of a near monolayer thickness of a p(IA) macromolecule primer will most significantly improve the adhesive bonding and durability of the bond.

It is worthwhile to assess the interfacial bond mechanism responsible for the great enhancement in polymer-polymer adhesion. In an attempt to gain the above information, specular reflectance IR analysis was employed. The samples for these studies were prepared by spin-casting at 4000 rpm the PU resin onto the p(IA)-primed aluminum substrates. The resultant IR spectra, as shown in Figure 35, were recorded in the frequency range 2500-1390 cm^{-1}. The spectrum from the PU resin-coated aluminum in the absence of p(IA) primer film exhibited absorption bands at about 2260, 1715, 1592, and 1525 cm^{-1}. According to literature data, these indicate the isocyanate, -N=C=O, the carbonyl, C=O, in amide I, the phenyl and the carbonyl in amide II, respectively.(45) Interesting spectra were obtained from the PU resin/p(IA) joint systems recorded as a function of the p(IA) concentration. Of particular interest was the appearance of new bands at 1680 and 1630 cm^{-1}, which can be assigned to newly formed amide I and II. The intensity of these new peaks increased conspicuously as the p(IA) concentration was increased, whereas that of the isocyanate in PU resin at 2260 cm^{-1} tended to decrease. This seems to prove that the -N=C=O groups in PU adjacent to the p(IA) macromolecules can form a chemical bond with the carboxylic acid of p(IA). According to the literature,(36) this interaction mechanisms is given below.

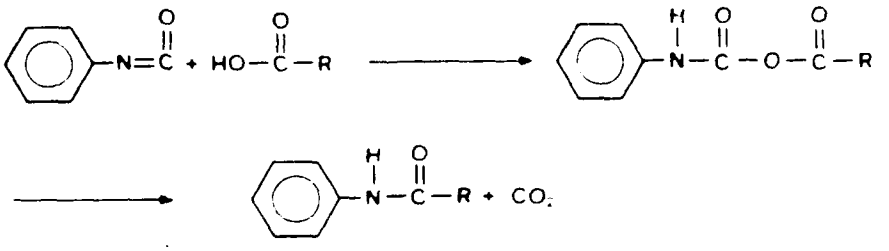

It is believed that this intermolar chemical reaction is a very important mechanism which greatly enhances the adhesive strength and the bond durability of PU/p(IA)/aluminum joints.

3. Corrosion Control

In an attempt to gain information regarding the effectiveness of the interfacial reaction products as a corrosion protective layer on FPL-etched Al surfaces, the polarization behavior of Al surfaces in p(IA)/Al and PU/p(IA)/Al

joint systems was determined. The tests were conducted in a deaerated 0.5 M NaCl solution at 25°C. For these tests, the PU deposition on the 3.5-nm thick p(IA)-coated Al and uncoated Al surfaces was applied by spin-coating at 4000 rpm. The thickness of the deposited PU film was approximately 500 nm. Figure 36 shows the typical polarization curves of log current density vs potential for the FPL-etched Al, p(IA)/etched Al, PU/etched Al, and PU/p(IA)/etched Al systems. From the shape of the curves, the potential axis at the transition point from cathodic to anodic is normalized as the corrosion potential, E_C. The anodic polarization side of all specimens was characterized by a rapid increase in the current density at a certain voltage expressed in terms of the critical pit initiation potential, E_{CI}.(46)

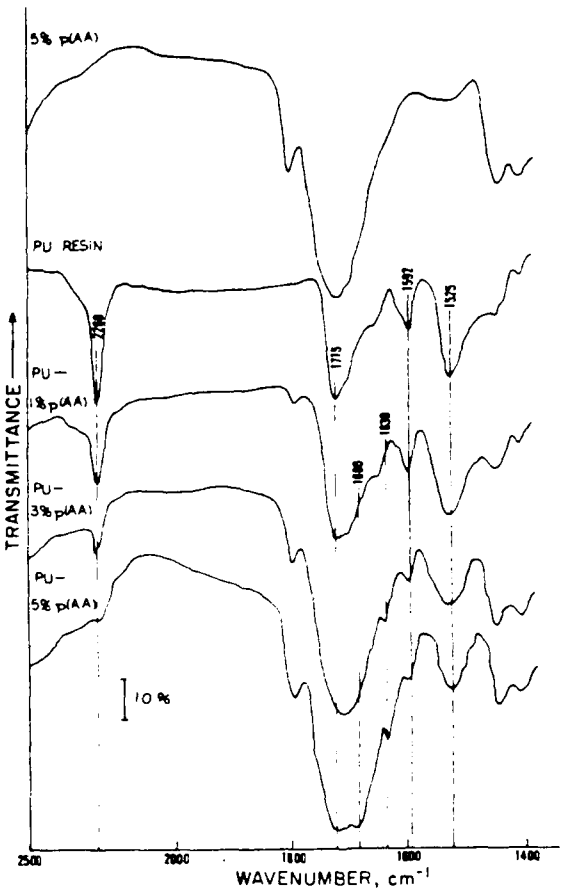

Figure 35. Infrared spectra of PU-p(IA) interfaces.

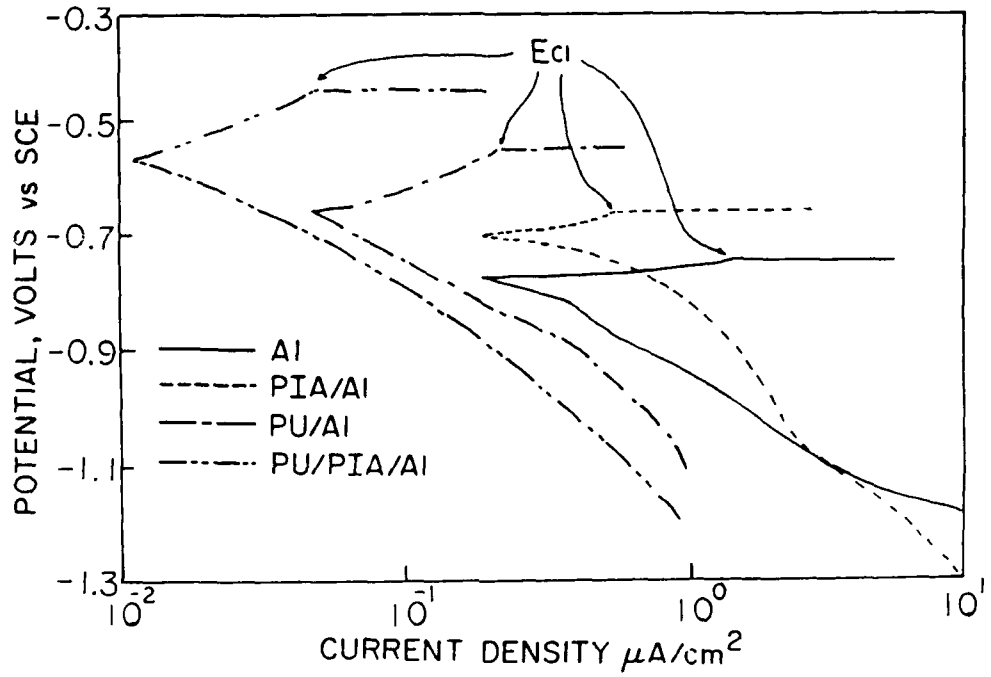

Figure 36. Polarization curves for uncoated, p(IA), PU-, and PU-p(IA)-coated aluminum immersed in deaerated 0.5 M NaCl solution at 25°C.

For the etched-Al surface specimens, noteworthy features of the curve are the E_C of -0.75 V, the current peak of 1.2×10^{-1} $\mu A/cm^2$, and the E_{CI} of -0.73 V. A reduction in E_C and E_{CI} to less negative potentials was achieved with the thin p(IA) film overlaid on the Al surface. A possible interpretation for this is that the magnitude of susceptibility to the colloidal nature of hydrated Al_2O_3 was reduced by the formation of hydrogen bonding between the hydroxyl groups of Al_2O_3 hydrates and the COOH groups of PIA. This suggests that the hydrogen bond-based interfacial reaction products have an ability to protect Al surfaces from aggressive corrosive fluids.

On the other hand, an overlay of PU on the Al adherend with ıA) primer resulted in a notable reduction in E_C, E_{CI}, and the relative current density at E_C, because of the thick (approximately 500 nm) coating. A further reduction in these elements to less negative potential and current density was obtained with the multiple layer PU/p(IA)/Al systems.

From the above results, it is apparent that the mechanisms and nature of the reaction products formed in the interfacial region are important factors in protecting Al substrates from corrosion.

D. Conclusions

When hydrophilic macromolecules were applied as an intermediate coupling primer for PU/Al_2O_3 joint systems, the resulting strength of the bond and its adhesive durability in hot alkali depended primarily on the hydrophilic pendant groups and the thickness of the primer macromolecules. p(IA), which contains two functional COOH groups located on the same backbone carbon, appears to have the greatest potential as a water-soluble primer. The deposition of a near-monolayer thickness of p(IA) significantly reduces the susceptiblity of the interfacial regions to hydrolysis, thereby improving the durability of the bonds of PU/p(IA)/Al_2O_3 joint systems. After exposure to hot alkali, the locus of failure of this system occurs cohesively in a mixed region of p(IA) and PU through which the crack propagates.

The use of a monolayer thickness of other macromolecule primers which contain functional $-SO_3H$, $-\overset{O}{\overset{\|}{C}}-NH_2$ and 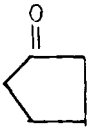 pendant groups is less effective in improving the adhesive bond and the durability. In addition, the intermolecular reaction products contribute significantly to reduce the corrosion rate of Al substrates.

IV. HIGH-TEMPERATURE LIGHTWEIGHT POLYIMIDE SYSTEMS

A. Materials

A commercially available polyamic acid (PAA) varnish product, supplied by Mitsui Toatsu Chemical Inc. of Japan, was used in this study. This PAA precursor was derived from a solution condensation between 3,3'-diaminobenzophenone,

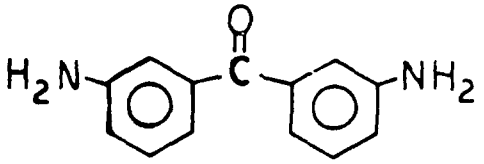

and 3,3', 4,4'-benzophenonetetracarboxylic dianhydride,

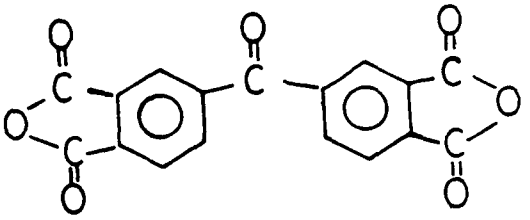

in a bis (2-methoxyethyl) ether (BME) solvent. Since the viscosity of this varnish was too high to fully wet the surface of the lightweight fillers, additional BME solvent was added to the varnish. After adjusting to the appropriate viscosity, the resultant PAA component was composed of 40 wt% varnish and 60 wt% BME solvent.

The lightweight filler used was composed of pressure-resistant hollow alumina silica microspheres having an average particle size of approximately ~125 μm and a bulk density of 0.4 g/cc. They were supplied by Fillite U.S.A., Inc. The chemical components in the microspheres were 55 to 60% SiO_2, 30 to 37% Al_2O_3 and 4% Fe_2O_3.

Type I portland cement was used to produce the partially hydrated cement grains for use as Ca counterion-releasable materials. The cement was exposed to an atmosphere of 80% relative humidity at 24°C for 1 hr prior to mixing with the PAA solution.

A lightweight material slurry consisting of 65 wt% PAA solution and 35 wt% microspheres was used to prepare control specimens. Hydrated cement particles in concentrations of 2, 5, and 8% by weight of the total slurry mass were then added to the PAA-microsphere mixed slurries, which were then cast into glass test tubes, 3.5 cm diam by 7.0 cm long, for subsequent determinations of the compressive strength. The test tubes were stored in air or steam for 24 hr at temperatures up to 400°C before the compressive strength tests were conducted. The densities of the slurries containing 0, 2, 5, and 8 wt% hydrated cement were 0.81, 0.83, 0.87 and 0.91 g/cc, respectively, and the bulk densities for the 300°C-air cured specimens containing 0, 2, 5 and 8 wt% cement were 0.35, 0.39, 0.44, and 0.47 g/cc, respectively.

B. Measurements

Thermogravimetric analysis (TGA) and infrared (IR) spectroscopy were used to follow the PAA solution $\longrightarrow$ PI solid transition resulting from the in-situ imidization condensation of PAA and for determining the onset temperature of thermal decomposition of PI polymers. TGA measurements were made at a heating rate of 10°C/min in flowing N_2 using a DuPont Model 951.

The chemical states and possible interactions at the interfaces between the PI and the hydrated cement or microsphere surfaces were explored using the combined techniques of x-ray photoelectron spectroscopy (XPS) and IR.

C. Results and Discussion

A TGA curve for a PAA solution consisting of 40 wt% varnish and 60 wt% BME solvent is given in Figure 37. Over the temperature range 25° to 650°C, three distinct regions are indicated. The first occurs at temperatures between 25° and 280°C and is characterized by a weight loss of approximately 70%. This significant weight reduction is probably due to volatilization and vaporization of the BME solvent and the water by-product yielded by the in-situ imidization reaction of the PAA precursor upon heating. The magnitude of the weight loss indicates that the as-received PAA varnish product contained approximately 10% BME solvent, since the remaining 60% is associated with the additional BME used to dilute the varnish. In the second region, between 280° and 510°C, the curve levels off, thereby suggesting that the PI polymers have excellent thermal stability in N_2 gas. Beyond 510°C, thermal decomposition of the PI seems to occur.

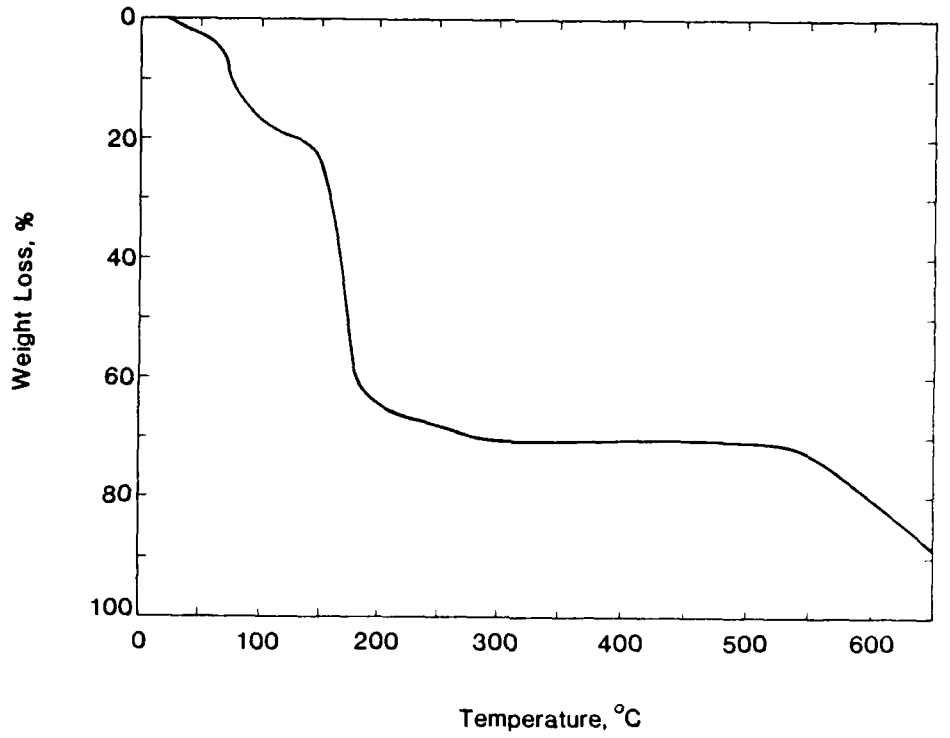

Figure 37. TGA curve for PAA solution.

The above data are supported by the results from IR analyses which are given in Figure 38. For use in this examination, thin film samples were prepared by placing the PAA solution onto NaCl plates and then spinning at 1000 RPM for 10 sec. This was followed by curing for 2 hr in air at temperatures of 100°C, 200°C or 280°C. Compared to that for the BME solvent (Figure 38-a), the assignments of the main IR absorption bands for the PAA solution (b) are as follows; the vibrations of amide amine and amide carbonyl within PAA at 3450, 1660, 1550 and 1300 cm^{-1}, the CH vibrations of the methylene and methyl in BME at 2890 and 1450 cm^{-1}, the C-O-C ether vibrations in BME at 1200 and 1100 cm^{-1}, the aromatic C=C stretching vibrations in PAA at 1600, 1585, and 1490 cm^{-1}, and the carbonyl stretching in COOH ot PAA at 1730 cm^{-1}. The spectrum for the 100°C-treated sample (curve c) is characterized by the appearance of new bands at 1770, 1360 and 710 cm^{-1}, a shift of the C=O peak from 1730 to 1710 cm^{-1}, and the marked decrease in peak intensities at 3450, 1660, 1550 and 1300 cm^{-1} which reveals the amide groups in PAA. The reason for the decreased

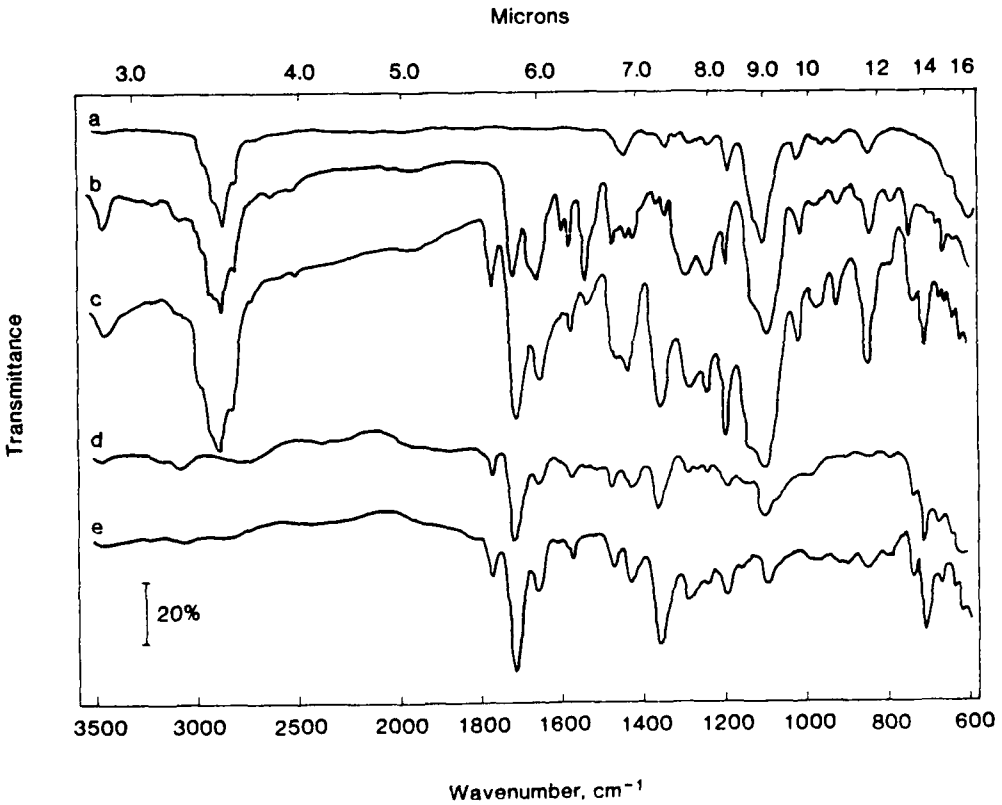

Figure 38. Infrared spectra for (a) BME solvent, (b) PAA solution, (c) 100°C-heated (d) 200°C-heated and (e) 280°C-heated films.

amide peak intensities is the progression of the imidization reaction between the amide and the carboxylic acid groups within PAA. Thus, the new peaks and the shifted peak appear to be ascribed with the C-N and C=O stretching in the imide rings as a result of PI formation.[47-50] However, the strong peaks at 2890, 1450 and 1100 cm^{-1} indicate that a large amount of BME solvent was still present within the film. Almost all of the solvent remaining in the film seemed to be decomposed or volatilized at a temperature of 200°C. This is indicated by the disappearance and significant diminution of these bands on absorption spectrum (d). This spectrum also indicates the further decay of amide peak intensities, suggesting that the rate of the imidization reaction significantly increased at 200°C. For the film treated at a temperature of 280°C, the presence of weak amide peaks on spectrum (e) indicates that a small fraction of unreacted PAA still remained within the cured PI film. This is reflected on the band at 1710 cm^{-1} which reveals the imide carbonyl and the carboxylic acid carbonyl in the residual PAA.

At 510°C which was determined by TGA to be the onset temperature for the thermal degradation of PI, the spectrum (not shown) exhibited a slight reduction in the intensities of the imide bands at 1770, 1360 and 710 cm^{-1}.

On the basis of the fundamental knowledge obtained regarding the thermal imidization process and thermal degradation of PI polymer, the curing characteristics for microsphere-filled lightweight PI cementitious specimens upon exposure to hot air and steam environments, were then investigated. In this work, the PI specimens were precured in air at 80°C for 10 hr and then exposed for 24 hr in either air or steam at temperatures up to 400°C. Compressive strength measurements were then made.

Figure 39 shows the compressive strength of the specimens as a function of post-heating temperature. As expected, the strength of specimens exposed to hot air increases with temperature between 80° and 300°C. At 300°C, the strength was more than three times that of 80°C-precured specimens. Beyond 300°, the strength decreased slowly. In contrast, no strength improvement was obtained for the steam-cured specimens. Beyond 150°C, the steam-exposed specimens exhibited significant strength reductions, as compared to that of the 80°C-precured one. Further increases in steam temperature to 250°C resulted in severe hydrothermal disintegration of the specimens and the strengths were too low to be measured. These results indicate that the curing of in-situ condensation-type polymers should be conducted in dry air conditions to avoid interruption of the intramolecule dehydration reactions caused by the adsorption of moisture by the amide and carboxylic acid functionaries in the PAA.

Experiments were also performed in which the PI cementitious materials were cured and post-heated in air prior to exposure to hydrothermal environments. For use in these tests, PI specimens, with and without partially hydrated cement grains, were prepared and oven heated in the following sequence: 24 hr at 80°C $\longrightarrow$ 10 hr at 150°C $\longrightarrow$ and 24 hr at 300°C. After curing, the specimens were exposed for 24 hr to steam at temperatures of 150°, 200°, 250° and 300°C. Compressive strength measurements were then made to evaluate the hydrothermal stability and to investigate the influence of the inclusion of hydrated cement on the mechanical properties of the materials.

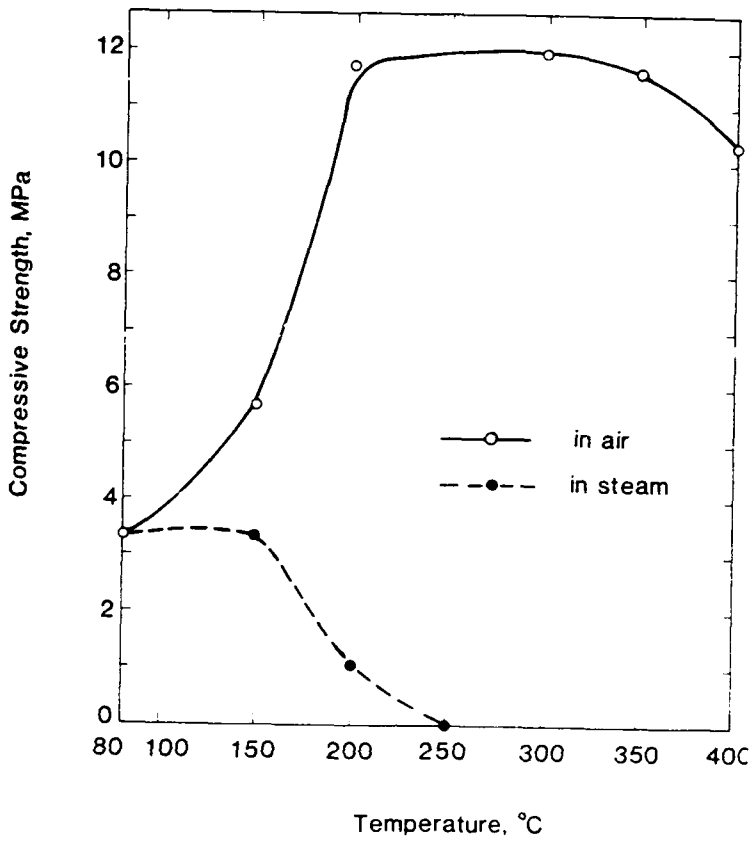

Figure 39. Changes in compressive strength of 80°C air-precured PI specimens after exposure to air or steam at temperatures up to 400°C.

These test results are shown in Figure 40. As is evident from the figure, the compressive strengths for the unexposed specimens at 25°C varied with the concentration of cement hydrate added to the PAA slurry; namely, the strength decreased with increased cement hydrate content.

In an attempt to determine the cause of this effect, the interfaces between the hydrated cement and the PI polymer were explored using XPS. For the XPS studies, discs, 12 mm in diameter and 0.5 to 1 mm thick, of the hydrated cement were made by pressing the cement powders at 100 MPa. The discs were then dipped for 20 sec into 5 wt%, 1 wt%, and 0.5 wt% PAA solutions. After wetting the disc surfaces with the PAA, the samples were dried in an oven at

300°C for 5 hr to convert the PAA solution into solid PI films. Preliminary examinations of wide scan XPS spectra for the cement discs coated with $\leq$1.0 wt% PI which corresponds to $\leq$1.0 wt% PAA, revealed the presence of a doublet Ca2p peak of substantial intensity. This suggests that certain areas of the cement surfaces were covered with a thin layer of PI polymer, no thicker than 5 nm, which associates the escape depth of aluminum photoelectrons. For all samples, the binding energy (BE) scale in the XPS spectra was calibrated with the C_{1s} of the principal hydrocarbon-type carbon, "CH_n", peak fixed at 285.0 eV as an internal reference standard.

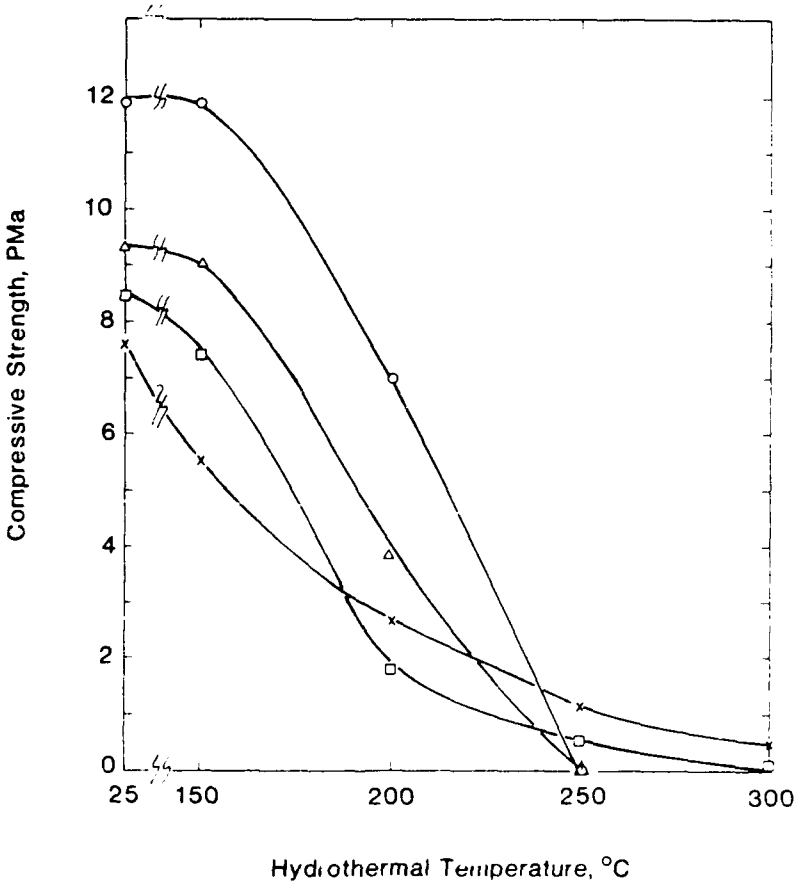

Figure 40. Compressive strength vs hydrothermal temperature for PI specimens containing 0% (o), 2% (Δ), 5% (□) and 8% (x) cement.

The C_{1s} core level photoemission spectra for bulk PI and the 5 wt%, 1 wt%, and 0.5 wt% PI-covered cement surfaces and interfaces are shown in Figure 41. The C_{1s} region for the bulk PI polymer (Figure 41-a) contains three resolvable peaks situated at 285.0, 286.1, and 288.8 eV. According to the literature,[51] the major carbon peak at 285.0 eV includes contributions from the aromatic carbon, the component at 286.1 eV can be assigned to phenylic carbons joined to N, and that at 288.8 eV to carbonyl, C=O, carbons. As evidenced by the lack of a component at 289.4 eV in the C_{1s} region, no free carboxylic acid, COOH, groups which relate directly to the presence of the PAA precursor, were observed on the bulk PI polymer surfaces. In Figure 41-b, the

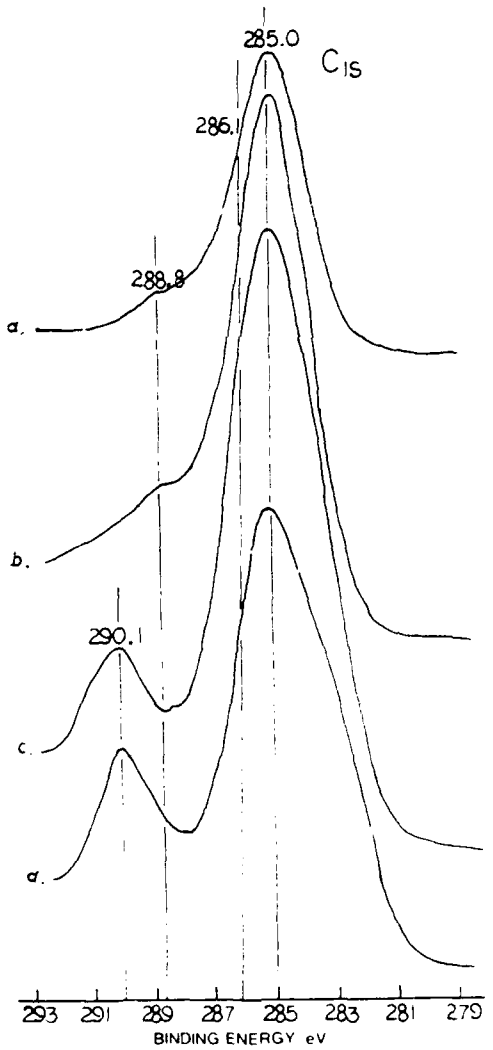

Figure 41. XPS C_{1s} regions for (a) bulk PI, (b) 5% PI-, (c) 1% PI- and (d) 0.5% PI-covered cement samples. Integrated intensity ratio of C (COO) and C (): (c) 0.22; (d) 0.35.

features of the spectrum for a cement pellet surface covered with 5 wt% PI polymer which is recognized as a thick coating, are similar to those of the bulk PI surface. An interesting spectral feature was observed when a thin 1.0% PI film was deposited on the hydrated cement substrate. As seen in Figure 41-c, this spectrum is characterized by the presence of a prominent peak at 290.1 eV and a considerably decayed intensity for the carbonyl carbon peak at 288.8 eV. At a lower coverage of 0.5% PI, the peak intensity of BE at 290.1 eV was increased further (see Figure 41-d). Since the latter is assigned to the carboxyl, COO, carbon components,[52] it is believed that a large number of COO groups are present in the interfacial regions. This becomes more readily apparent from a consideration of the integrated intensity ratio between the C (COO) peak at 290.1 eV and C (-  -) at 285.0 eV. The resultant (C (COO)/C (-  -)) intensity ratio for the 0.5% PI/cement interface was higher than for the 1.0% PI-covered cement (Figure 41). Figure 42 shows the Ca2p3/2 regions for the hydrated cement substrate surface and the 0.5% PI/cement interface. The BE value for the main Ca2p3/2 peak for the cement surfaces (Figure 42-e) was 347.3 eV, which can be ascribed to calcium silicate hydrate species. When the cement substrate was covered with a thin film of 0.5% PI, the Ca2p3/2 region for the PI/cement interface exhibited a new peak at 347.7 eV. This is at a BE 0.4 eV higher than that for the cement peak. This new peak is indicative of the formation of a COO-Ca complex[53] produced at the interface. In contrast, no specific changes in the spectral features were observed in the Si2p regions (Figure 43). Thus, it is reasonable to assume that the carboxylic acid and amide functionaries in the PAA adjacent to the hydrated cement, preferentially react with the transitional Ca ions liberated from the cement and not with the Si. The hydrated cement surfaces have a strong alkaline nature, and it is well known[32] that when carboxylic acid comes in contact with hydroxide anions, OH^-, the reduction of the hydrogen-oxygen bond in the COOH forms the carboxylate anion, COO^-. After loss of the proton, the remaining COO^- group becomes a counterion acceptor which reacts with transitional Ca^{2+} ions. On the other hand, information regarding the amide-cement interaction mode was gained by examination of the N_{1s} core level regions (see Figure 44). The high resolution N_{1s} signal (Figure 44-i) for the bulk PI polymer surface indicates a single peak at 400.4 eV which is due to the imide nitrogen in the

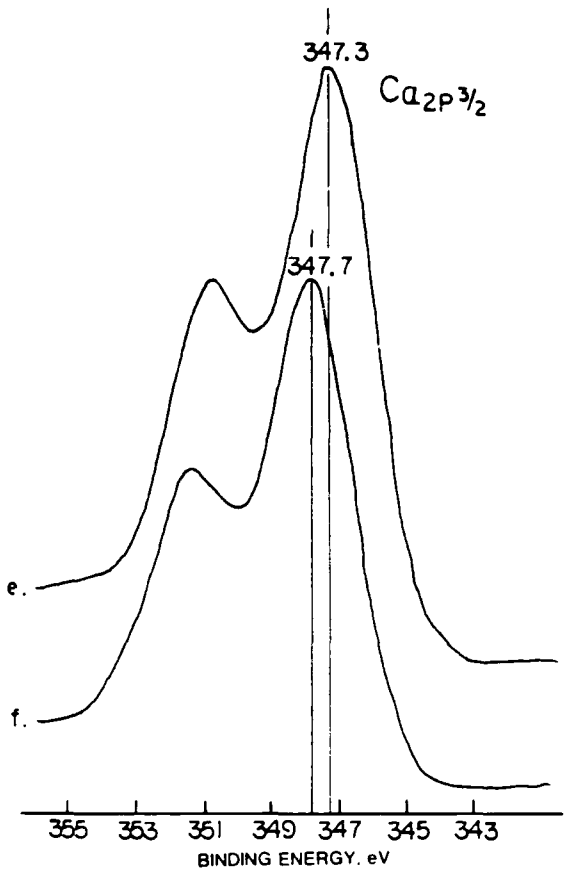

Figure 42. Ca2p3/2 spectra for (e) hydrated cement and (f) 0.5% PI/cement samples.

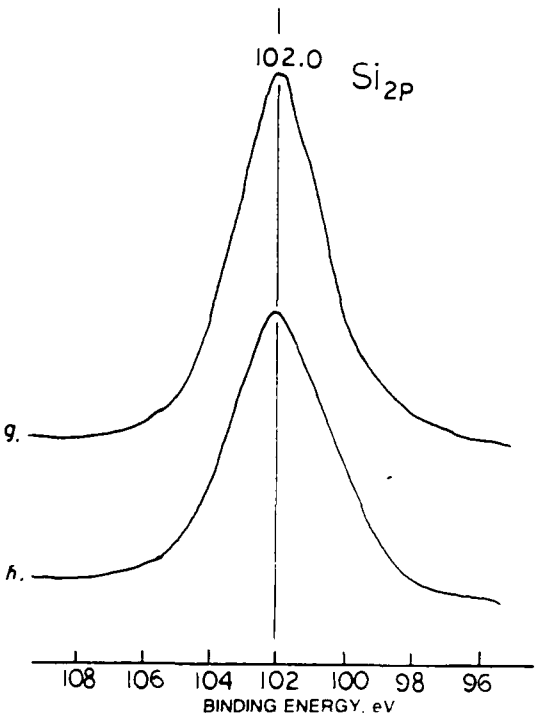

Figure 43. Si2p spectra for (g) hydrated cement and (h) 0.5% PI/cement samples.

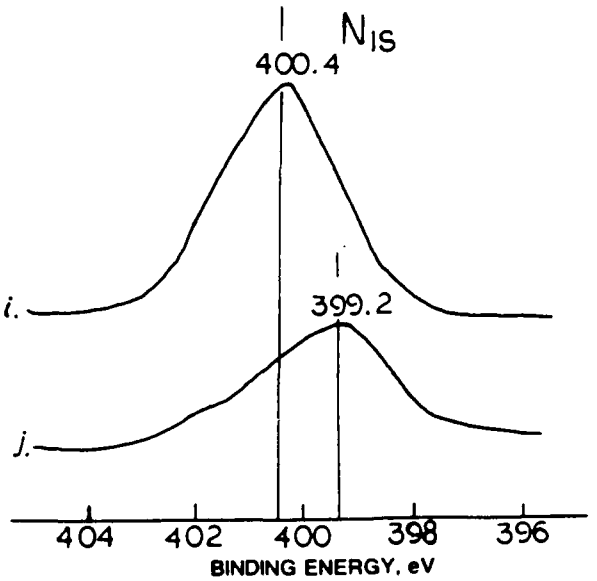

Figure 44. N_{1S} spectra for (i) bulk PI and (j) 0.5% PI/cement samples.

PI. In comparison, the spectrum (Figure 44-j) at the PI/cement interface exhibits a predominant peak at 399.2 eV in addition to the weak peak of the imide at 400.4 eV. Since the BE of the amide nitrogen in PAA is commonly located at 401.4 eV,[54] this principal peak is more likely to be associated with the amino, $-NH_2$, nitrogen joined to the phenyls[55] rather than that of the unreacted amide in the PAA. The results suggest that when the amide groups in the PAA are contacted with hydrated cement, they are transformed into carboxylate anions, COO^-, through the alkali-catalyzed hydrolysis mechanism of amides which are susceptible to reaction with hydroxide anions. This mechanism can be addressed as follows:

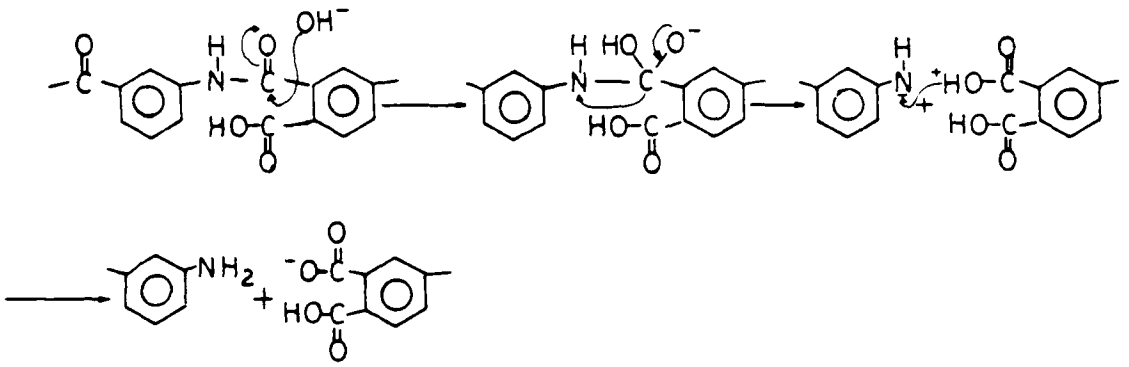

As seen above, the PAAs undergo bond breakages of the amide linkage caused by nucleophilic attack of the OH^- ion on the amide carbon. This breakage leads to the formation of a base soluble intermediate compound containing a carboxylate anion and a base insoluble amine compound. As mentioned previously, the carboxylic acid groups which are one of the other functionaries in the PAA are readily converted into carboxylate anions in alkali environments. Therefore, these carboxylate anions quickly react with the calcium cations from the cement and then form Ca-bridged 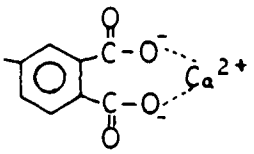 carboxylate complexes. The formation of Ca-carboxylate complexes not only disturbs the intermolecule imidization reaction of PAA, but also leads to session of the linear polymer chains, resulting in lower molecular weight species. This results in the formation of a gel at the interfaces, thereby leading to a weak PI-cement boundary layer. From the above information, it can be conclusively drawn that

when the PAA precursor comes in contact with alkaline substrates, the alkali-catalyzed hydrolysis of PAA acts to promote mechanical failure at the interfaces in PI systems. Hence, the poor strength development in the PI specimens is not surprising, and it becomes less as the proportion of hydrated cement is increased.

Let us return to the compressive strength-hydrothermal temperature relations summarized in Figure 40. As predicted, the extent of strength reduction after exposure of specimens to steam at 150°C increases as the amount of cement in the composites is increased. Although the PI specimens prepared without the inclusion of the cement filler exhibited very little strength loss upon exposure at 150°C, considerable retrogression was observed at 200°C. At 250°C, the strength of the cement-free specimens was too low to be measured. Since a certain amount of unreacted PAA is likely to be present in the specimens, the cause for the hydrothermal degradation of the cement-free PI composites can be explained on the basis of the hydrolysis of the imide rings in the PI polymer structures and of amide linkages in the PAA, as reported previously by several investigators.[56,57] This mechanism is as follows:

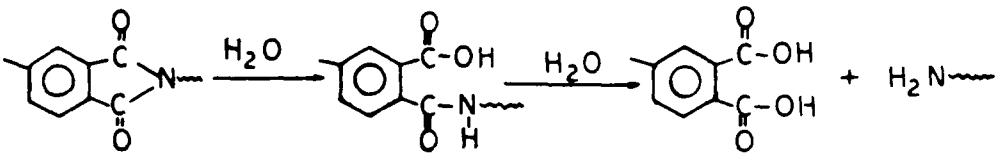

imide amic acid acid amine

For the cement-filled PI specimens at $\geq$250°C, the extent of retrogression seems to decrease with increased cement content. In fact, the 8 wt% cement-filled specimens at 300°C displayed a compressive strength of 0.5 MPa, compared with the no measurable strength for the cement-free specimens at $\geq$250°C.

Figure 45 compares the IR spectra for 8.0 wt% cement-filled PI composite samples before and after exposure to steam at 300°C. Over the frequency range 1900 to 1300 cm^{-1}, the spectrum for the exposed samples (Figure 45-b) indicates severe alkali-catalyzed hydrolysis of the imide rings in the PI, and the hydration products of cement yielded in the composite phases. The former is evident

from the carboxylate anion peaks at 1560 and 1420 cm^{-1} in conjunction with the disappearance of the major peaks at 1770, 1710 and 1360 cm^{-1} which reveal the formation of the imide ring in the PI and the carboxylic acid in the residual PAA. The presence of cement hydration products in the composite can be detected by the noticeable peak at 1635 cm^{-1} which represents the bending vibration of crystallized water.

On the basis of the open literature to date,[58-60] the alkali-induced hydrolysis of PI may occur through the following modified mechanism:

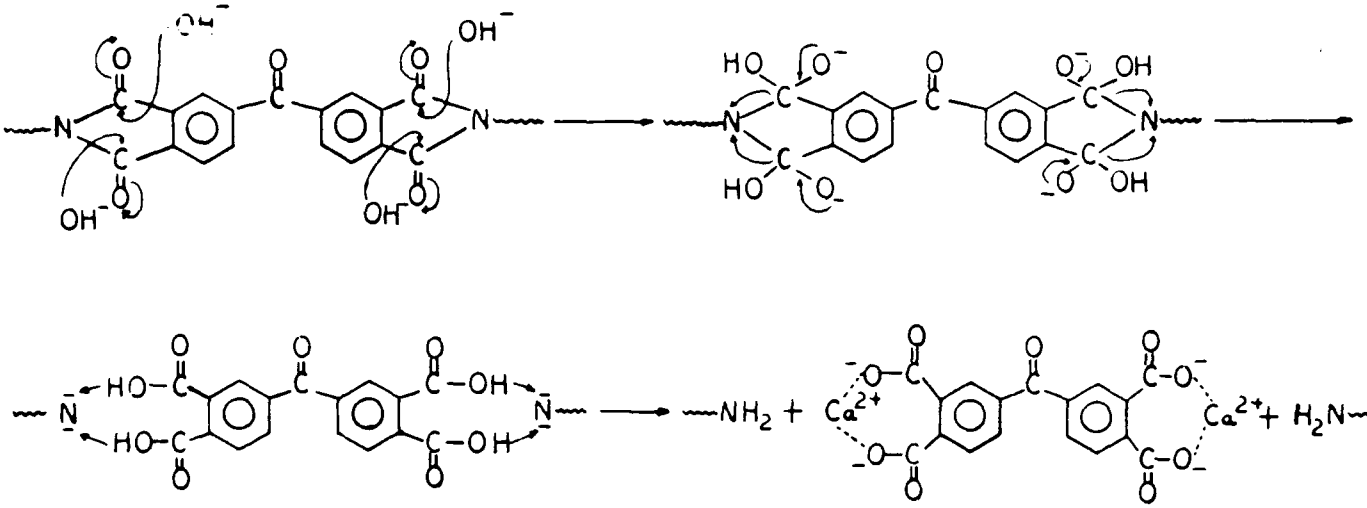

As is clear from the above proposed hydrolysis processes, it appears that the eventual formation of Ca-complexed carboxylate salts results in the disintegration of the composite brought about by the chain scission of a linear PI macromolecule.

D. Conclusions

Microsphere-filled PI lightweight materials having a slurry density of 0.81 g/cc and a bulk density of 0.35 g/cc, displayed a compressive strength of 12 MPa after exposure to hot air at 300°C. Unfortunately, the PI polymer matrix which was transformed by typical <u>in-situ</u> imidization condensation reactions between the carboxylic acid and amide functionaries in the PAA precursor, undergos hydrolysis in hydrothermal environments at temperatures of >150°C.

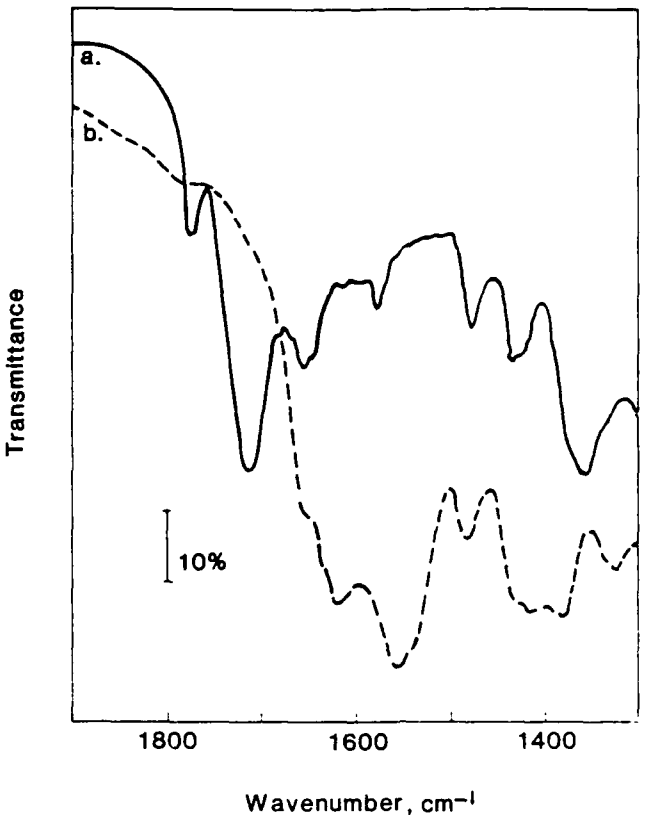

Figure 45. Infrared spectra for cement-filled PI specimens before (a) and after (b) exposure to steam at 300°C.

This is due mainly to the susceptibility of the imide rings in the PI to reaction with moisture at high temperatures. The extent of the hydrolysis was found to increase as partially hydrated cement fillers were incorporated in the PAA slurry. This can be explained by base-catalyzed hydrolysis mechanisms evolving the functional groups in the unreacted PAA and the imide groups in the PI. Hydrolysis of the former occurs principally in the interfacial regions between the PAA and the alkaline cement hydrate at room temperature. In steam at $\geq$150°C, it is initiated by the attack of hydroxide anions on the imide carbon. In these mechanisms, the bond breakage and cleavage of the amide linkages in PAA and the imide rings in PI, brought about by the nucleophilic attack of OH^-, lead to the formation of transitory intermediate compounds containing carboxylate anions and amine compounds. The anionic inter-

mediate organic compounds immediately react with the Ca counterions liberated from the cement surfaces and then form Ca-complexed carboxylate salts. These salt formations not only act to promote the session of polymer chains, but also result in considerable strength retrogression of the PI materials. Therefore, it is concluded that PI lightweight materials not containing any alkaline fillers may be suitable for use in hot air environments at temperatures up to 300°C, but are questionable for use in high pH hydrothermal environments.

Acknowledgements

The authors wish to acknowledge the support and guidance received from Dr. Robert R. Reeber of the U. S. Army Research Office, Research Triangle Park, NC.

References

1. T. Sugama, L. E. Kukacka, N. Carciello, and J. B. Warren, J. Appl. Polym. Sci., 30, 4357 (1985).

2. A. J. Sommer, and H. Leidheiser, Jr., Corrosion, 43, 661 (1987).

3. T. Sugama, L. E. Kukacka, N. Carciello, and J. B. Warren, J. Appl. Polym. Sci., 32, 3469 (1986).

4. R. P. Weny, In: Organic Coatings, Pafitt, G. D. and Patsis, A. V. (Eds.), 6, pp. 373-394. Marcell Dekker, Inc., New York (1984).

5. H. W. Eichner and W. E. Schowalter, Forest Products Laboratory Report No. 1813, Madison, WI (1950).

6. G. S. Kabayaski and D. J. Donnelly, Boeing Corporationg Report No. D6-41517, Seattle, WA, Februrary (1974).

7. Operations in Magnesium Finishing, Dow Chemical U.S.A. Form No. 141-479-86R (1986).

8. R. E. Swanson, "Alloy Design Considerations for Corrosion-Resistant Magnesium." Presentation at Workshop of Viability of Magnesium in Military Hardware, June 16-18 (1987).

9. F. M. Fowkes, In: Treatise on Adhesion and Adhesives, Patrick, R. L. (Ed.), 1, Chapter IX. Marcel Dekker, New York (1967).

10. G. D. Davis, J. S. Ahearn, L. J. Matienzo, and J. D. Venables, J. Mater. Sci., 20, 975 (1985).

11. N. Fin, H. Dodiuk, A. E. Yaniv and L. Drori, Appl. Surface Sci., 28, 11 (1987).

12. R. T. Foley, Corrosion, 42, 277 (1986).

13. J. C. Bolger, "Acid Base Interactions Between Oxide Surfaces and Polar Organic Compounds." In: Adhesion Aspects of Polymeric Coatings, K. L. Mitall (Ed.), pp. 3-18. Plenum Press, New York (1981).

14. T. Sugama, L. E. Kukacka, C. R. Clayton and H. C. Hua, J. Adhesion Sci. and Tech., 1, 265 (1987).

15. C. E. Sroog, J. Polym. Sci., Macromol. Rev. 11, 161 (1976).

16. L. B. Rothman, J. Electrochem. Sco. 127, 2216 (1980).

17. A. M. Wilson, Thin Solid Films, 83, 145 (1981).

References cont.

18. A. K. St. Clair and T. L. St. Clair, in: Polyimide: Synthesis, Characterization and Applications, K. L. Mittal [Ed.] Vol. 2, Plenum Press, New York (1984).

19. W. R. Sorenson and T. W. Campbell, Preparative Methods of Polymer Chemistry, Interscience, New York, (1968).

20. R. J. Cotter and M. Matzner, Ring-Forming Polymerization, Vol. B-2, Academic Press, New York, (1972).

21. R. A. Iezzi and H. Leidheiser, Jr., Corrosion, 37, 28 (1981).

22. R. P. Wenz, Steel surface cleanliness: preparation, characterization, and paint performance, in: Organic Coatings Science and Technology, Vol. 6," G. D. Parfitt and A. V. Patsis, Eds., Marcel Dekker, Inc., New York (1984).

23. D. A. Jones and N. R. Nair, Corrosion, 41, 357 (1985).

24. J. W. Bartha, P. O. Hahn, F. LeGoues, and P. S. Ho, J. Vac. Sci. Technol., 3, 1390 (1985).

25. Joint Committee on Powder Diffraction Standards, Card 30-1491 (1984).

26. E. L. Ghali and R. J. A. Potvin, Corrosion Sci., 12, 583 (1972).

27. M. L. Miller, The structure of polymers, Reinhold Publishing Corporation, New York (1966).

28. J. A. Kargol, D. L. Jordan and A. R. Palermo, Corrosion, 39, 213 (1983).

29. T. Sugama, L. E. Kukacka, N. Carciello, and J. B. Warren, J. Mater. Sci., 22, 722 (1987).

30. Joint Committee on Powder Diffraction Standards, Card 33-667.

31. C. T. Yap, T. L. Tan, L. M. Gan, and H. W. K. Ong, Appl. Surface Sci., 27 247 (1986).

32. T. Sugama, L. E. Kukacka, N. Carciello, and J. B. Warren, J. Mater. Sci., 19, 4045 (1984).

33. H. Leidheiser Jr., R. D. Granata, and R. Turoscy, Corrosion, 43, 296 (1987).

34. T. Sugama, L. E. Kukacka, and N. Carciello, J. Adhesion and Adhesives, 8, 101 (1988).

References cont.

35. T. Sugama, L. E. Kukacka, N. Carciello, and J. B. Warren, J. Mater. Sci. 23, 101 (1988).

36. R. G. Arnold, J. A. Nelson and J. J. Verbanc, "Chemistry of Organic Isocyanates," p. 13. E. I. duPont de Nemours, Wilmington, DE (1956).

37. A. V. Pocius, in: Adhesion Aspects of Polymeric Coatings. K. L. Mittal (Ed.), pp. 173-192. Plenum Press, New York (1983).

38. R. F. Wegman and M. J. Bodnar, "Energetic Materials," Soc. Aerospace Mater. Process Eng., 13th Nat. Sump. Exhibition, Western Periodical Co., North Hollywood, California, pp. 243-52 (1968).

39. T. Smith, J. Appl. Polym. Sci., Appl. Poly. Symp., 32, 11 (1977).

40. J. H. Scofield, Phys. Rev., A.14, 1418 (1976).

41. C. D. Wagner, W. M. Riggs, L. E. Davis and J. F. Moulder, in: Handbook of X-ray Photoelectron Spectoscopy, Muilenberg, G. E. (Ed.), Perkin-Elmer Corporation, U.S.A., pp. 21-23, (1979).

42. C. S. P. Sung and C. B. Hu, J. Biomed. Mater. Res., 13, 161 (1979).

43. B. D. Ratner, in: "Physicochemical Aspects of Polymer Surfaces," V. 2, Mittal, K. L. (Ed.), Plenum Press, New York, pp. 969-83 (1983).

44. D. R. Bauer, "Network Formation and Degradation in Urethane and Melamine - Fermaldehyde Crosslinked Coatings," Proceedings of the ACS Division of Polymeric Materials: Science and Engineering, 56, pp. 91-95 (1987).

45. H. Dodiuk, A. E. Yaniv, I. E. Klein, N. Fin, and L. Drori, Appl. Surface Sci., 21, 137 (1986).

46. Z. A. Foroulis and M. J. Thubrikar, Electrochemica Acts., 21, 225 (1976).

47. J. Sykee and T. Hoar, J. Polym. Sci., Part A-1, 7, 1385 (1969).

48. G. F. L. Ehters, K. R. Fisch and W. R. Powell, J. Polym. Sci., Part A-1, 8, 3511 (1970).

49. H. Ishida, S. Wellinghoff, E. Baer, and J. L. Koening, Macromolecules, 13, 826 (1980).

50. J. R. Salem, F. O. Sequeda, J. Duran, and W. Y. Lee, J. Vac. Sci. Technol., A4, 369 (1986).

References cont.

51. P. L. Buckwalter and A. I. Baise, "Polyimides, Synthesis, Characterization, and Applications," K. L. Mittal (Ed.), Vol. a, Plenum Press, New York (1984).

52. D. Briggs and M. P. Seah, "Practical Surface Analysis by Auger and X-ray Phtoelectron Spectroscopy," John Wiley & Sons, Ltd., New York (1983).

53. T. Sugama, L. E. Kukacka, N. Carciello and N. Hocker, Cem. Concr. Res., (in press).

54. A. Toth, et al. Surf. Interface Anal., 8, 261 (1986).

55. R. Nondberg, et al. Arkiv Kemi, 28, 257 (1968).

56. R. Delasi and J. Russell, J. Appl. Polym. Sci., 15, 2965 (1971).

57. J. O. Punderson and J. F. Heacock, International Wire and Cable Symposium Proceedings, pp. 44-50 (1985).

58. C. A. Pryde, Proceedings of ACS Division of Polymeric Materials Science and Engineering, 59, 219 (1988).

59. J. A. Kreuz and C. M. Hawkins, Proc. Tech. Program - Annual International Electron Packagae Conf. 2nd, 653 (1982).

60. W. P. Pawlowski and D. D. Coolbaugh, Proceeding of ACS Division of Polymeric Materials Science and Engineering, 59, 68 (1988).

Appendix

Program Presentations, Publications, Patents and Awards.

Papers Presented

Sugama, T., Kukacka, L. E., and Carciello, N., Functional Pendent Groups Affecting Chemisorption and Adherent Properties of Polyelectrolyte-Zinc Phosphate Composite Conversion Coatings. Proceedings of the ADPA Corrosion Prevention and Control Conference Sponsored by the U.S. Army Material Command, Williamsburg, VA, April 28-30, 1986.

Sugama, T., Adhesion Properties of Polyelectrolyte-Chemisorbed Zinc Phosphate Conversion Coatings. Proceedings of the American Chemical Society International Symposium and Adhesives, Sealants, and Coatings for Space and Harsh Environments, Denver, CO, April 7-10, 1987.

Sugama, T., Kukacka, L. E., Carciello, N., Polyitaconic Acid Macromolecule Primer for Adhesive Bonding and Corrosion Control of Aluminum. Proceedings of the Tri-Service Conference on Corrosion, U.S. Air Force Academy, Denver, CO, May 5-7, 1987.

Sugama, T., Kukacka, L. E., Carciello, N., Polyacrylic Acid Electrolyte-Modified Zinc Phosphate Conversion Coatings for Corrosion Protection of Steel. Proceedings of the American Chemical Society (ACS) Division of Polymeric Materials Symposium on Corrosion Protective Coatings, Toronto, Canada, June 5-11, 1988.

Kukacka, L. E. and Sugama, T., Polyelectrolyte Macromolecule-Complexed Zinc Phosphate Conversion Coating Systems. Proceedings of 1989 International Congress on Technology and Technology Exchange, New York City, NY, June 28-30, 1989.

Published

Sugama, T., Kukacka, L. E., Carciello, N., and Warren, J. B. Polyacrylic Acid Macromolecule-Complexed Zinc Phosphate Crystal Coatings. Journal of Applied Polymer Science, Vol. 30, 4357-4384 (1985).

Sugama, T., Kukacka, L. E., Carciello, N., and Warren, J. B., Factors Affecting Improvement in the Flexural Modulus of Polyacrylic Acid-Modified Crystalline Films. Journal of Applied Polymer Science, Vol. 32, 3469-88 (1986).

Sugama, T., Kukacka, L. E. Carciello, N., and Warren, J. B., Chemisorption Mechanism and Effect of Polyacrylic Acid on the Improvement in Bond Durability of Zinc Phosphate-to-Polymer Adhesive Joints. Journal of Materials Science, Vol. 22, 722-736 (1987).

Sugama, T., Kukacka, L. E., Clayton, C. R., and Hua, H. C., Effects of Polyacrylic Acid Primers on Adhesion and Durability of FPL-Etched Aluminum/Polyurethane Systems. Journal of Adhesion Science and Technology, Vol. 1, No. 4, 265-280 (1987).

Sugama, T., Kukacka, L. E., Carciello, N., and Warren, J. B., Aspects of the Adhesion and Corrosion Resistance of Polyelectrolyte-Chemisorbed Zinc Phosphate Conversion Coatings. Journal of Materials Science, Vol. 23, 101-11 (1988).

Sugama, T., Kukacka, L. E., and Carciello, N., Failure Modes of Polyurethane/Aluminum Oxide Joints Primed with Hydrophilic Macromolecules. International Journal of Adhesion and Adhesives, Vol. 8, No. 2, 101-106 (1988).

Sugama, T., Kukacka, L. E., Carciello, N. and Warren, J. B., The Use of Polyacrylic Acid Electrolytes Diffused in Zinc Phosphate Conversion Coatings for the Corrosion Protection of Steel. Journal of Coatings Technology, Vol. 61, No. 771, 43-57 (1989).

In Press

Sugama, T., Kukacka, L. E., Carciello, N. and Warren, J. B., Influence of the High Temperature Treatment of Zinc Phosphate Conversion Coatings on the Corrosion Protection of Steel. Journal of Materials Science.

Sugama, T., Kukacka, L. E., and Carciello, N., Cement Hydrate Catalyzed Hydrolysis of Polyimide Lightweight Materials. Journal of Applied Polymer Science.

Issued Patent

Sugama, T., Kukacka, L. E., and Carciello, N., Ductile Polyelectrolyte Macromolecule-Complexed Zinc Phosphate Conversion Crystal Pre-Coatings and Topcoatings Embodying a Laminate. United States Patent Number 4,659,395 on April 21, 1987.

Patents Pending

Sugama, T., Polyacid Macromolecule Primers.

Award

R&D-100 Award for the development of polymer-modified zinc phosphate conversion coatings in 1988.